

# **HASP 2018**

## **Science Report of Payload # 7**



**University of North Florida and University of North Dakota**

# **Measurements of Good and Bad Ozone**

**Students Team:**

**Jesse Lard (UNF) (Team Leader),  
Corrina Yorke (UNF)**

**Faculty Advisors:**

**Dr. Nirmalkumar G. Patel**

**Department of Physics, University of North Florida, Jacksonville, FL 32224  
and**

**Dr. Ron Fevig**

**Department of Space Studies, University of North Dakota, Grand Forks, ND 58202**

<b>Index</b>		
<b>Section</b>	<b>Contents</b>	<b>Page</b>
<b>1</b>	Introduction and Mission Objectives	<b>3</b>
<b>2</b>	Fabrication of Nanocrystalline Thin Film Gas Sensors	<b>14</b>
<b>3</b>	Working Principles of Gas Sensors	<b>18</b>
<b>4</b>	Calibration of Gas Sensors	<b>20</b>
<b>5</b>	Fabrication of Payload Body	<b>24</b>
<b>6</b>	Electronic Circuits	<b>44</b>
<b>7</b>	Integration of Payload and Thermal Vacuum Test	<b>50</b>
<b>8</b>	Launching of Payload	<b>68</b>
<b>9</b>	Results and Discussions	<b>77</b>
<b>9.1</b>	How ozone profile measured?	<b>77</b>
<b>9.2</b>	Uplink commands	<b>79</b>
<b>9.3</b>	Balloon Flight Profile and Response of Pressure Sensor	<b>80</b>
<b>9.4</b>	Power Budget during the Flight	<b>81</b>
<b>9.5</b>	Thermal Stability of the Payload	<b>84</b>
<b>9.6</b>	Measurements of Photovoltage Profile during the Flight	<b>89</b>
<b>9.7</b>	Discussion of Response of Gas Sensors Profiles	<b>94</b>
<b>9.8</b>	Response of Ozone Sensors during the Flight	<b>98</b>
<b>9.9</b>	Measurements of ozone profile in the stratosphere and comparison with the theoretical profile	<b>102</b>
<b>10</b>	Problems, Failure Analysis and Future Plan	<b>108</b>
<b>11</b>	Conclusions	<b>108</b>
<b>12</b>	References	<b>109</b>
<b>13</b>	Acknowledgements	<b>110</b>
<b>14</b>	Presentation of Research Work	<b>110</b>

## 1. Introduction and Mission Objectives

University of North Florida (UNF)-University of North Dakota (UND) team have successfully flown payloads on the HASP balloon flights since 2008 and measured the ozone gas profile in the stratosphere. Based on the success and experience of previous flights and observation of interesting larger ozone peak in troposphere after termination of HASP2017 flight, the UNF-UND team proposed the HASP 2018 flight for the development of new improved version of ozone sensors and payload to measure good ozone profile in the stratosphere and bad ozone in the troposphere. In addition, we are interested to explore the measurements of nocturnal ozone maxima before launching of the flight during early morning as well as in the troposphere after termination of flight at night time. The objectives of proposed HASP2018 flight science experiment were to measure good ozone in stratosphere, bad ozone in troposphere and any possible observation of higher concentration of ozone due to nocturnal ozone maxima after termination of flight at night time. About 90% of ozone is concentrated between 15 and 32 kilometers above the earth's surface (stratospheric ozone). It is also found at ground level in lower concentrations where it is a key component of smog over major cities (tropospheric ozone). The atmospheric layers defined by changes in temperature are shown in fig.1 (a), while the presence of ozone layer in the stratosphere is shown in fig. 1(b).

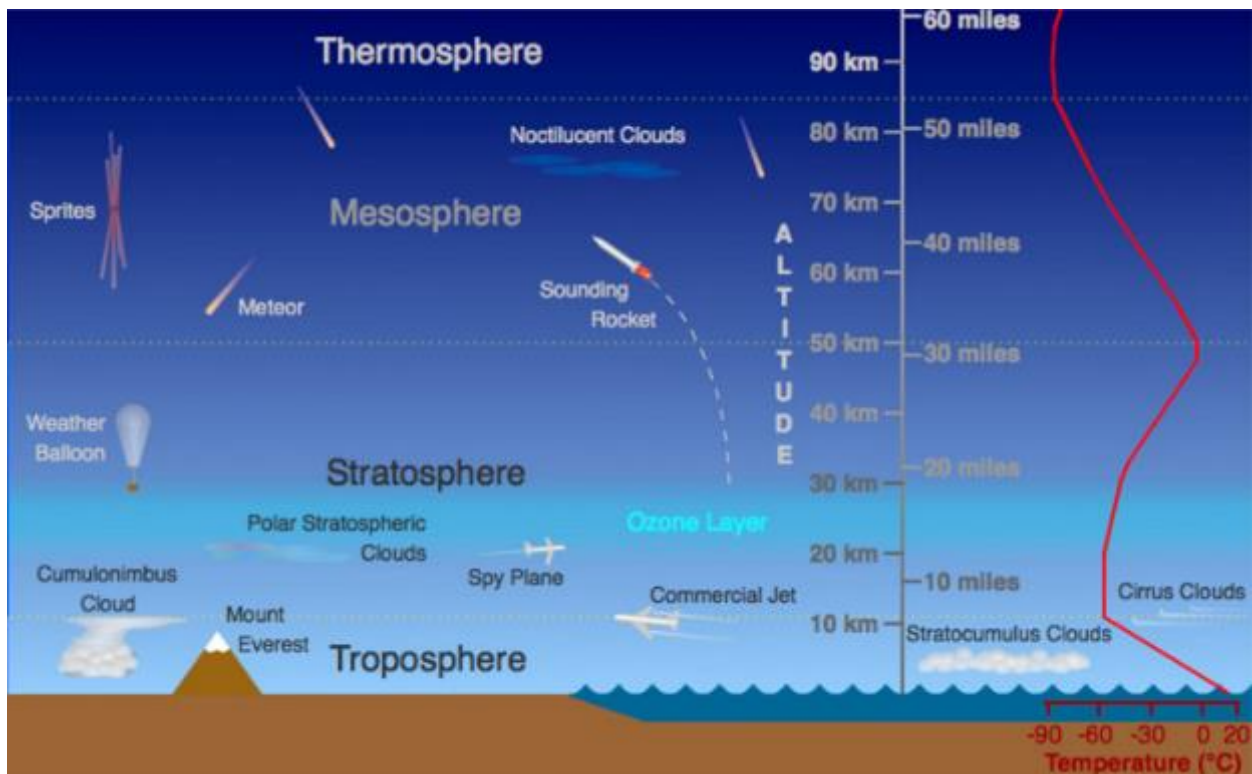


Fig.1 (a) shows the atmospheric layers defined by changes in temperature.

Picture Courtesy: <https://scied.ucar.edu/atmosphere-layers>

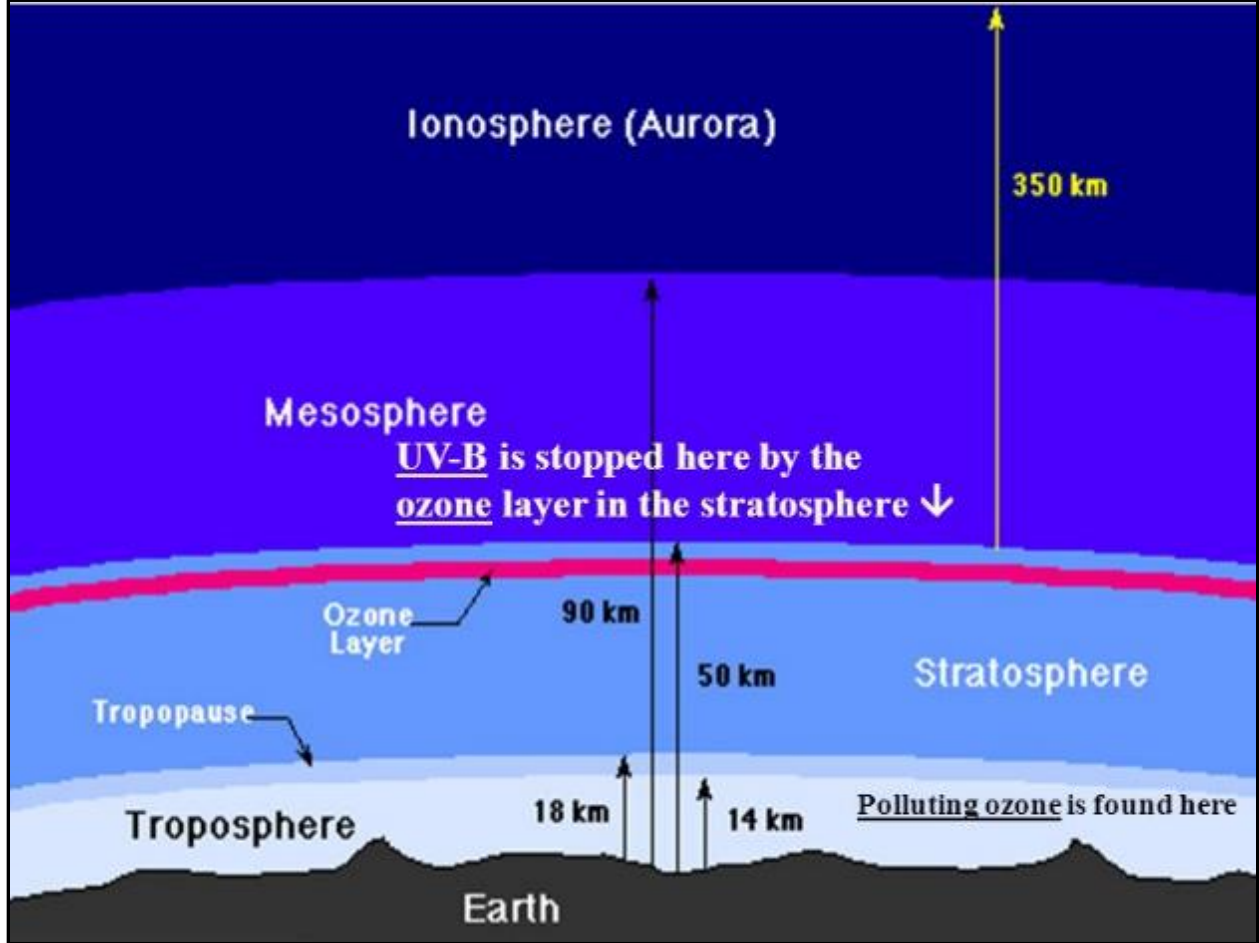
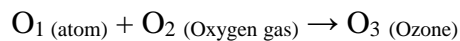
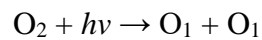
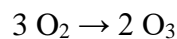


Fig.1 (b) The Ozone layer in the stratosphere.  
 Picture Courtesy: <http://slideplayer.com/slide/9185434/>

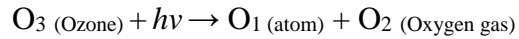
**Generation of Ozone in the Stratosphere:** Oxygen gas ( $O_2$ ) is present in the atmosphere. High energy or shorter wavelength UV light ( $h\nu$ ) collides with the oxygen molecule ( $O_2$ ), causing it to split into two oxygen atoms. These atoms are unstable, and they prefer being "bound" to something else. The free oxygen atoms then smash into other molecules of oxygen, forming ozone ( $O_3$ ).



The overall reaction between oxygen and ozone formation is:



The ozone is destroyed in the process that protects us from UV-B and UV-C rays emitted by the Sun. When ozone ( $O_3$ ) absorbs UV light ( $h\nu$ ), it will split the molecule into one free oxygen atom ( $O_1$ ) and one molecule of oxygen gas ( $O_2$ ). Thus, absorption of UV-B and UV-C leads to the destruction of ozone



Ozone is valuable to us because it absorbs harmful UV radiation during its destruction process (fig.2 (a)). A dynamic equilibrium is established in these reactions. The ozone concentration varies due to the amount of radiation of light received from the sun.

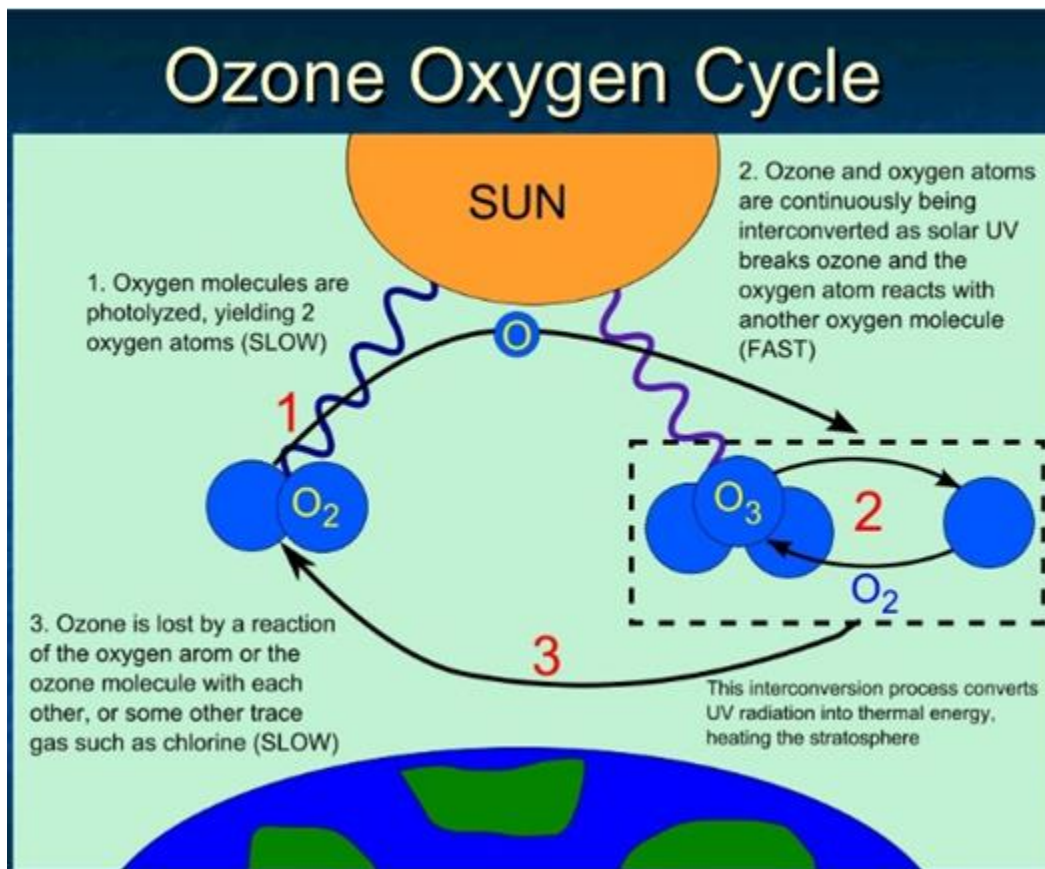


Fig. 2(a) Generation of ozone in the presence of UV light in stratosphere.  
 Picture Courtesy: [https://commons.wikimedia.org/wiki/File:Ozone\\_cycle.svg](https://commons.wikimedia.org/wiki/File:Ozone_cycle.svg)

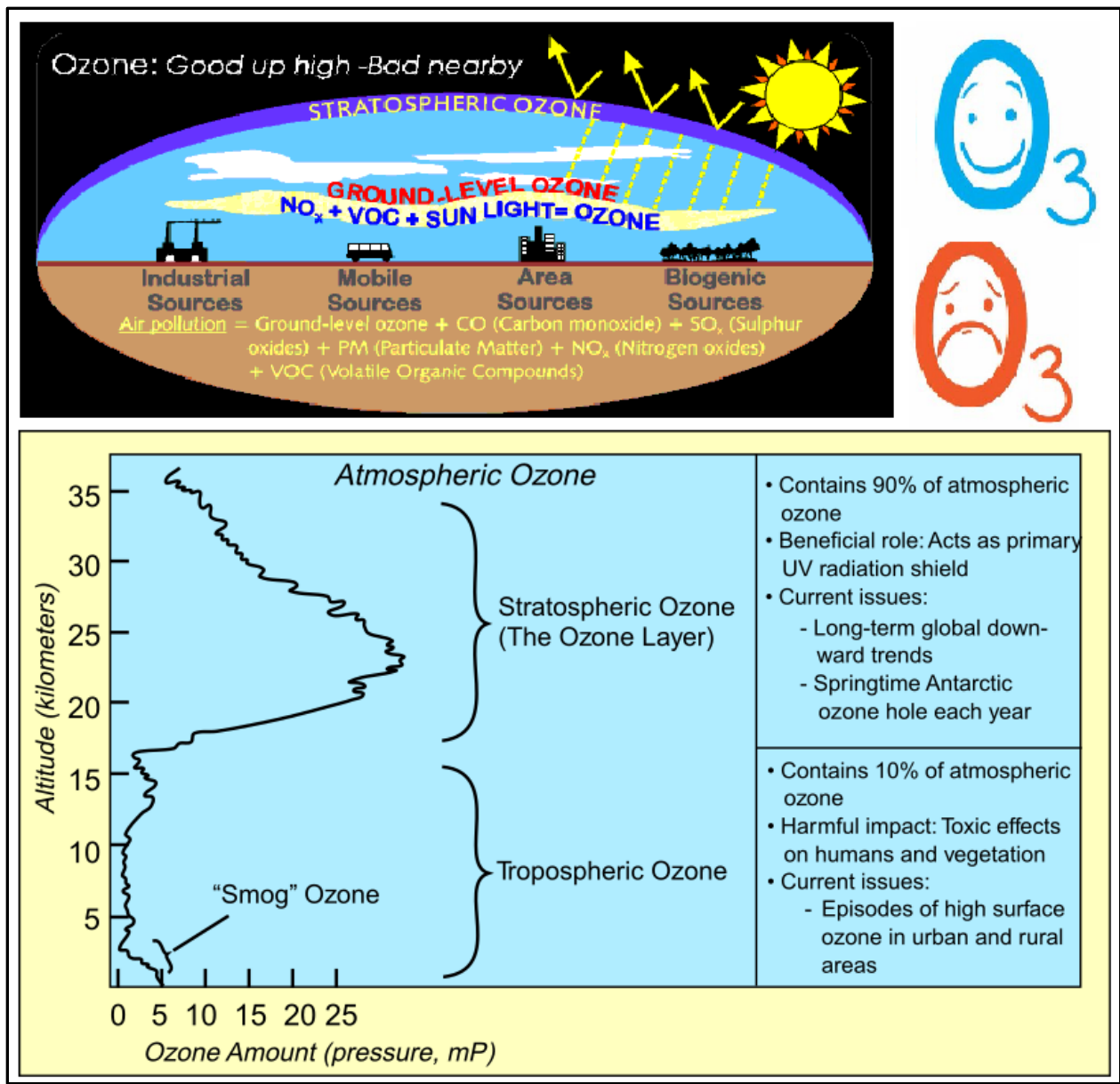


Fig. 2 (b) Good and bad ozone.

Picture Courtesy: [https://commons.wikimedia.org/wiki/File:Atmospheric\\_ozone.svg](https://commons.wikimedia.org/wiki/File:Atmospheric_ozone.svg)

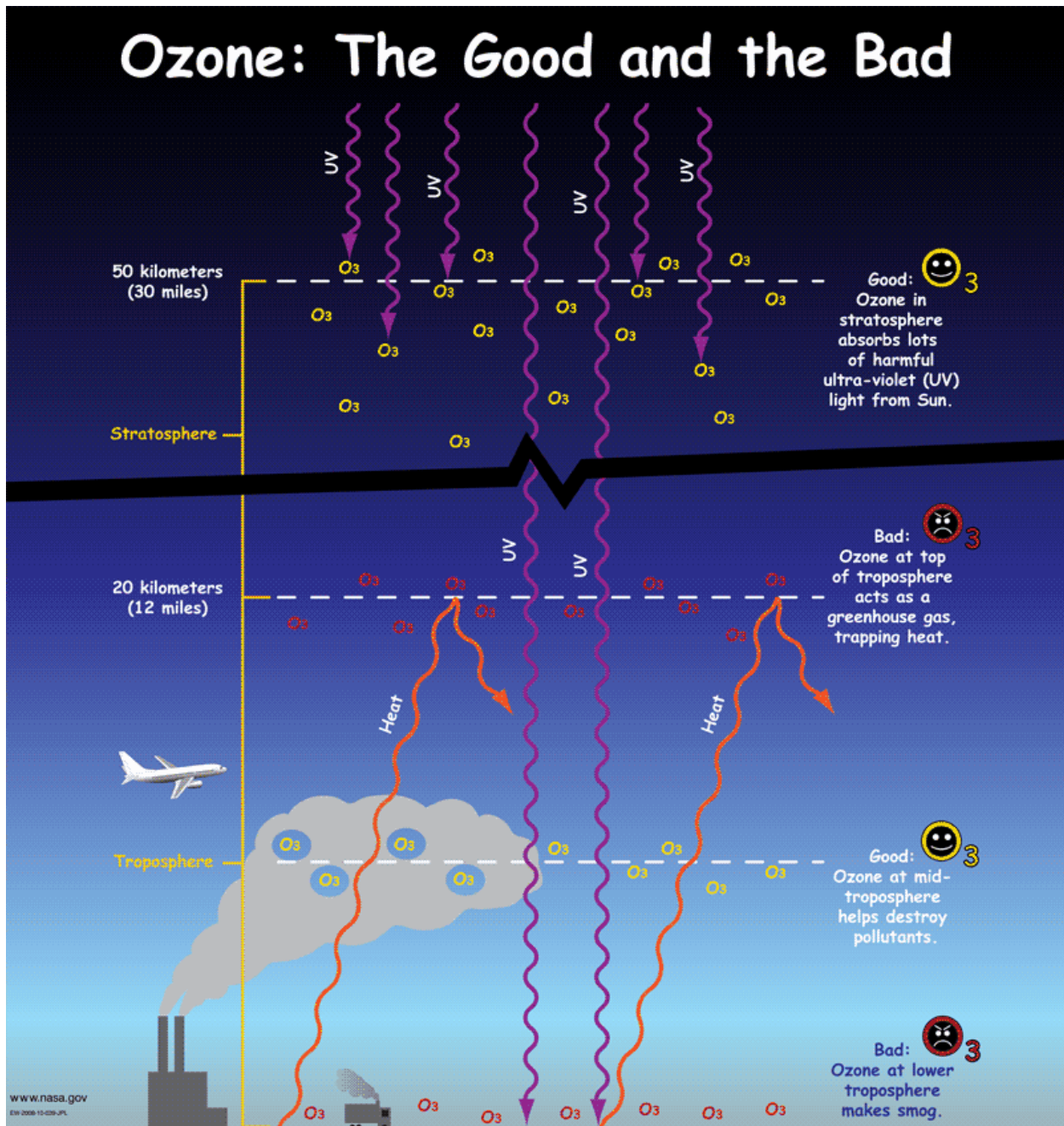


Fig. 2 (c) Good and bad ozone.

Picture Courtesy: <https://spaceplace.nasa.gov/greenhouse/en/>

**Generation of Ozone in the Troposphere:** Ozone in the troposphere is bad. This ozone is contributing to the smog and greenhouse gases created by human activities, which is shown in fig.2 (b) (c)and (d). Ozone close to the ground surface does not exist in high enough concentrations to shield us from UV light.

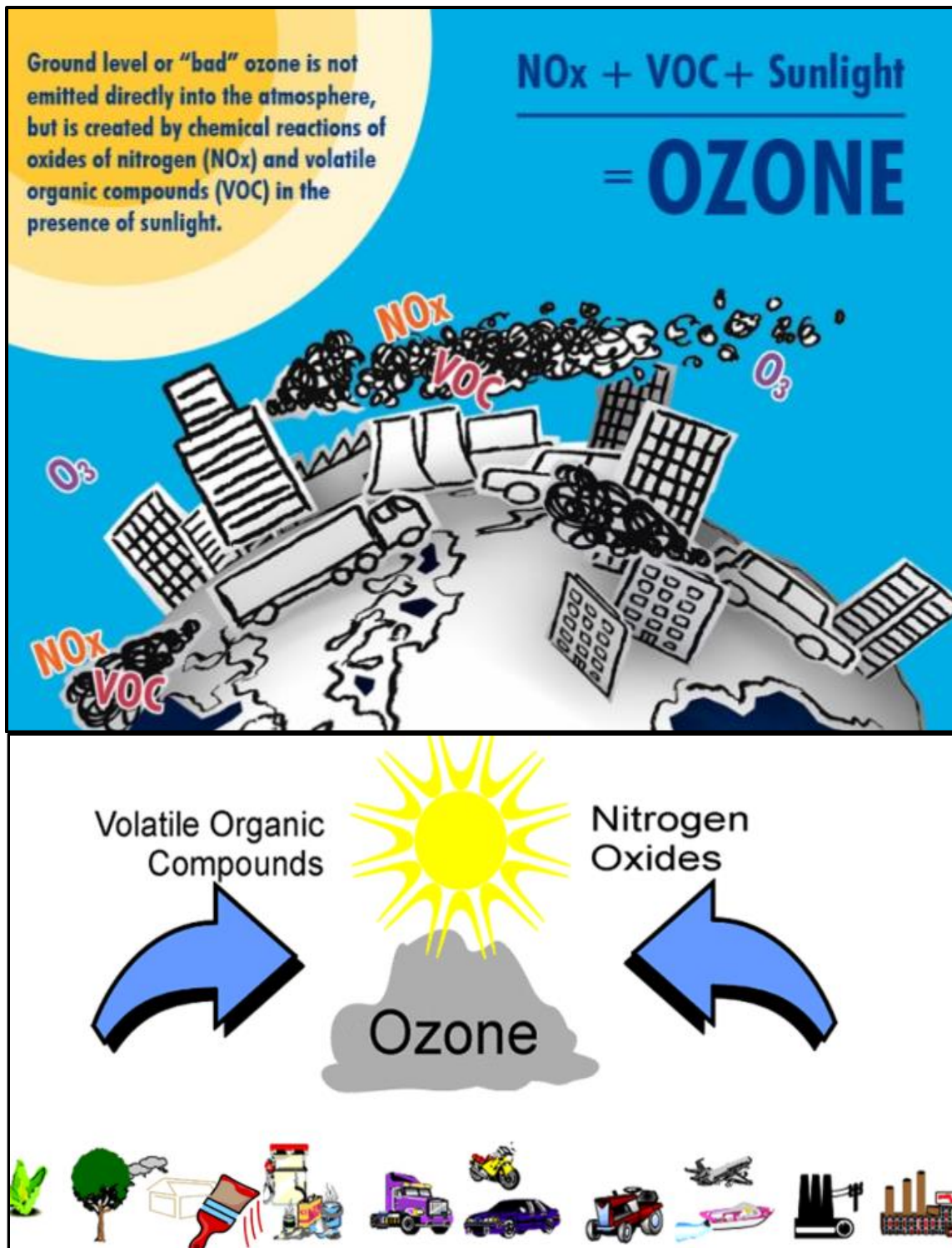


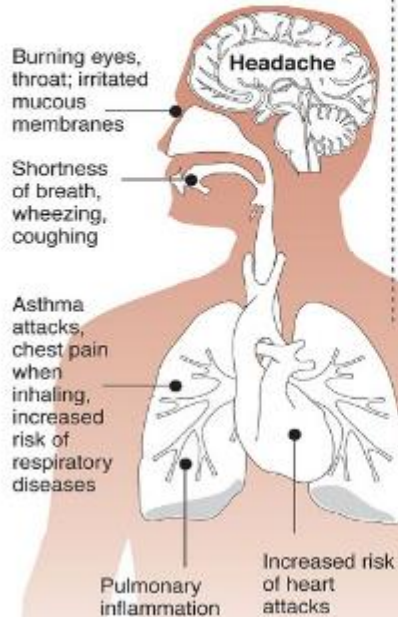
Fig. 2(d) Formation of bad ozone in the troposphere by NO<sub>x</sub>, VOC and sunlight.

Bad ozone creates the respiratory problem, destroys polymers and reduces the plant growth. Fig. 2 (e) shows how bad ozone, the main ingredient in smog, is the most dangerous.

## Why smog is harmful

Ozone, the main ingredient in smog, is one of the most widespread air pollutants and among the most dangerous.

### Effects on health



### How ozone forms

1 Oxygen in the atmosphere  $O_2$

2 Nitric oxide, byproduct of combustion  $NO$

3 Sunlight breaks up nitric oxide



4 Ozone formed by three oxygen atoms



### U.S. ozone limits

In parts per billion

• 1997-2008 **84**

• 2008-present **75**

• New EPA proposal **60-70**

© 2010 MCT  
Source: American Lung Association, State of the Air 2008.  
AP Graphic: Staff

## Smog Effect upon Organisms

- Smog affects the respiratory system of animals, causing irritation to the lining of the lungs.
- Plants when exposed to smog for a long period of time will have their waxy coating of their leaves break down.
  - This will increase the effects of water loss causing greater damage due to pests, diseases, drought and frost.



Fig. 2 (e) why smog is harmful?

## Ozone depletion and Ozone Hole

Pollutant gases, particularly, reactive halogen gases such as chlorine and bromine compounds in the atmosphere are responsible to cause the ozone depletion, which is mainly observed in the 'ozone hole' over Antarctica and over the North Pole. Most of the chlorine, and nearly half of the bromine in the stratosphere, where most of the depletion has been observed, comes from human activities. Fig. 2 (f) and (g) shows the production of ozone and destruction of ozone in the presence of UN light. Fig. 2(h) shows the life cycle of the chlorofluorocarbons (CFCs); how they are transported up into the upper stratosphere/lower mesosphere, how sunlight breaks down the compounds and then how their breakdown products descend into the polar vortex.

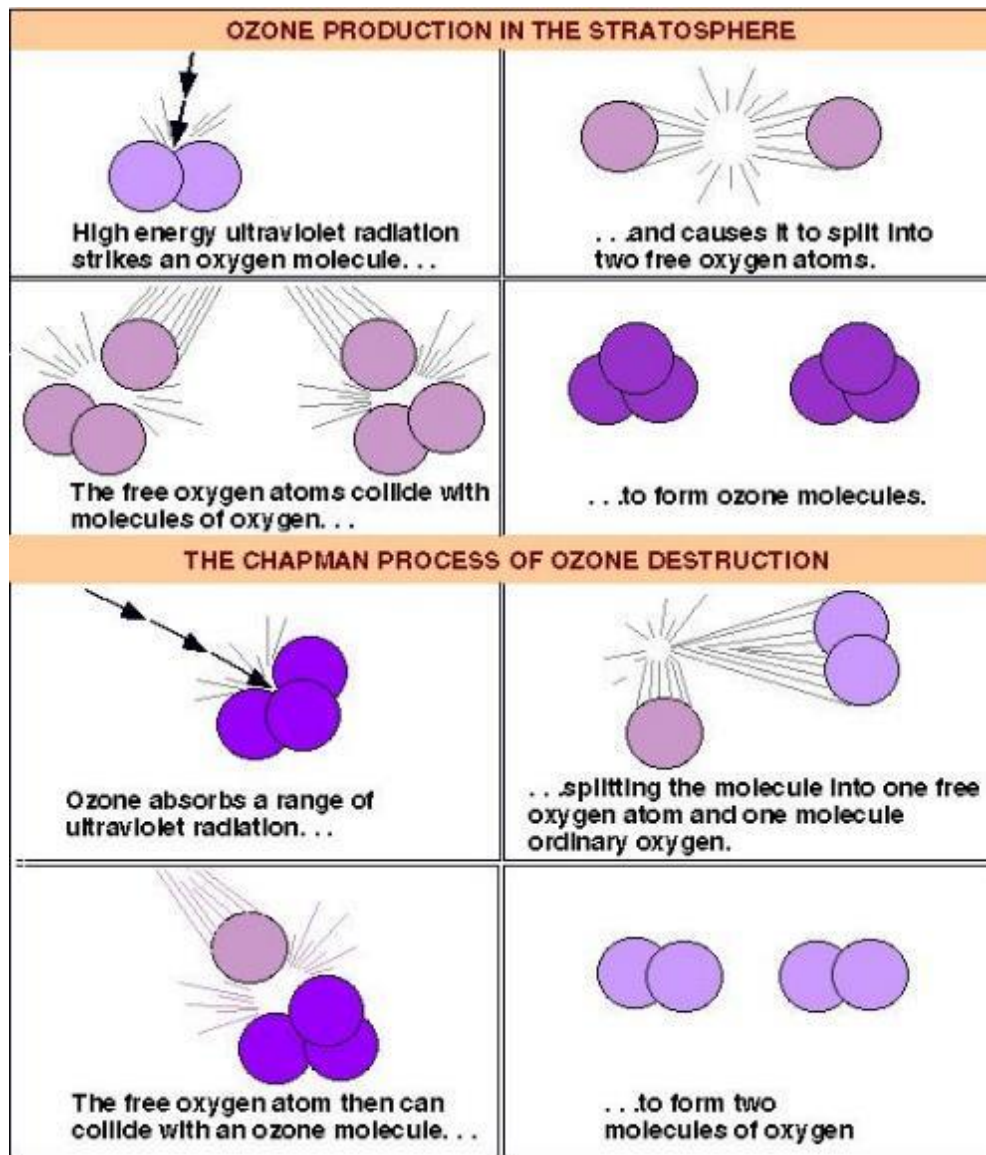


Fig. 2 (f), Production and destruction of ozone.

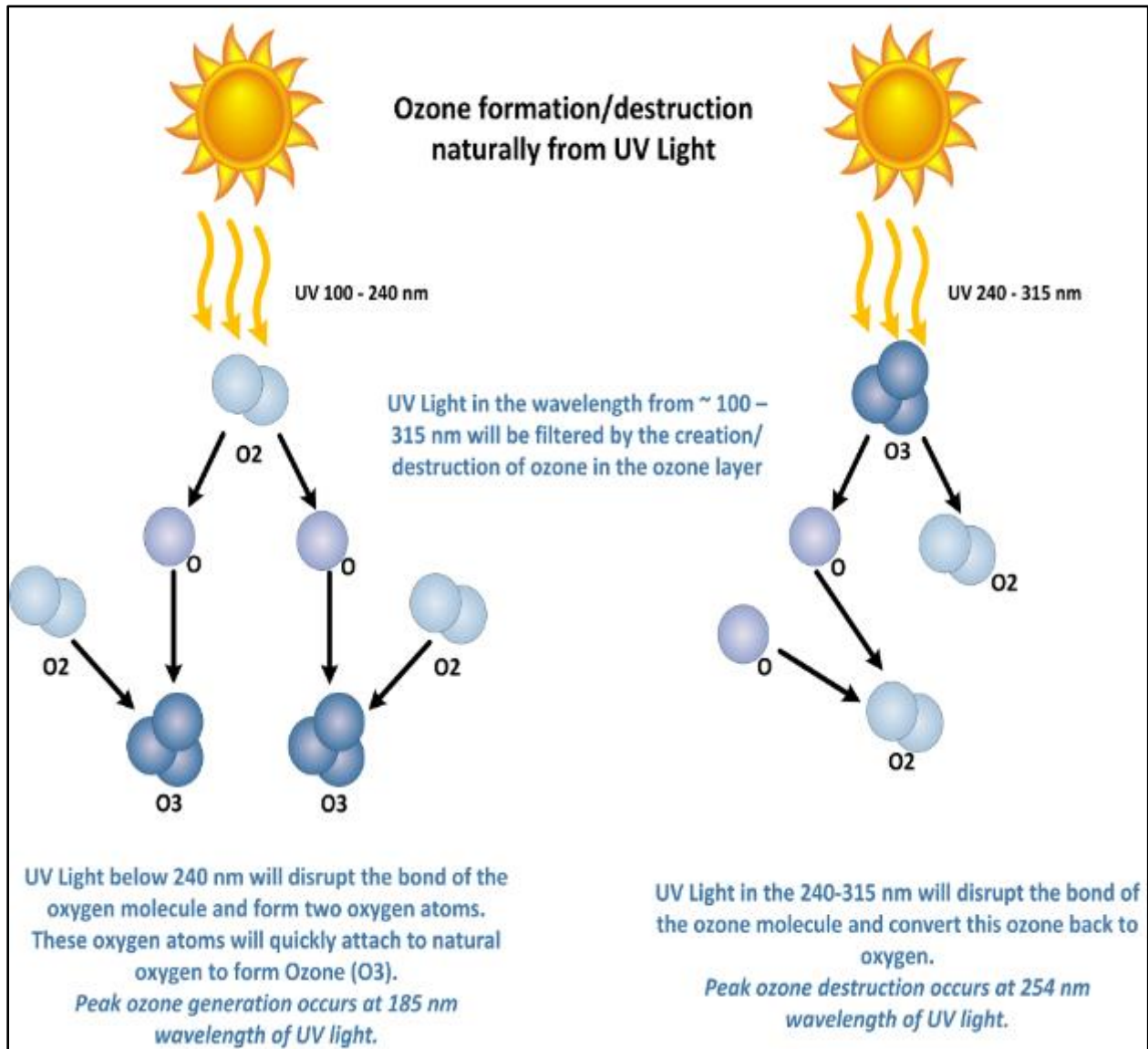


Fig. 2(g) Formation and destruction of ozone from UV light.

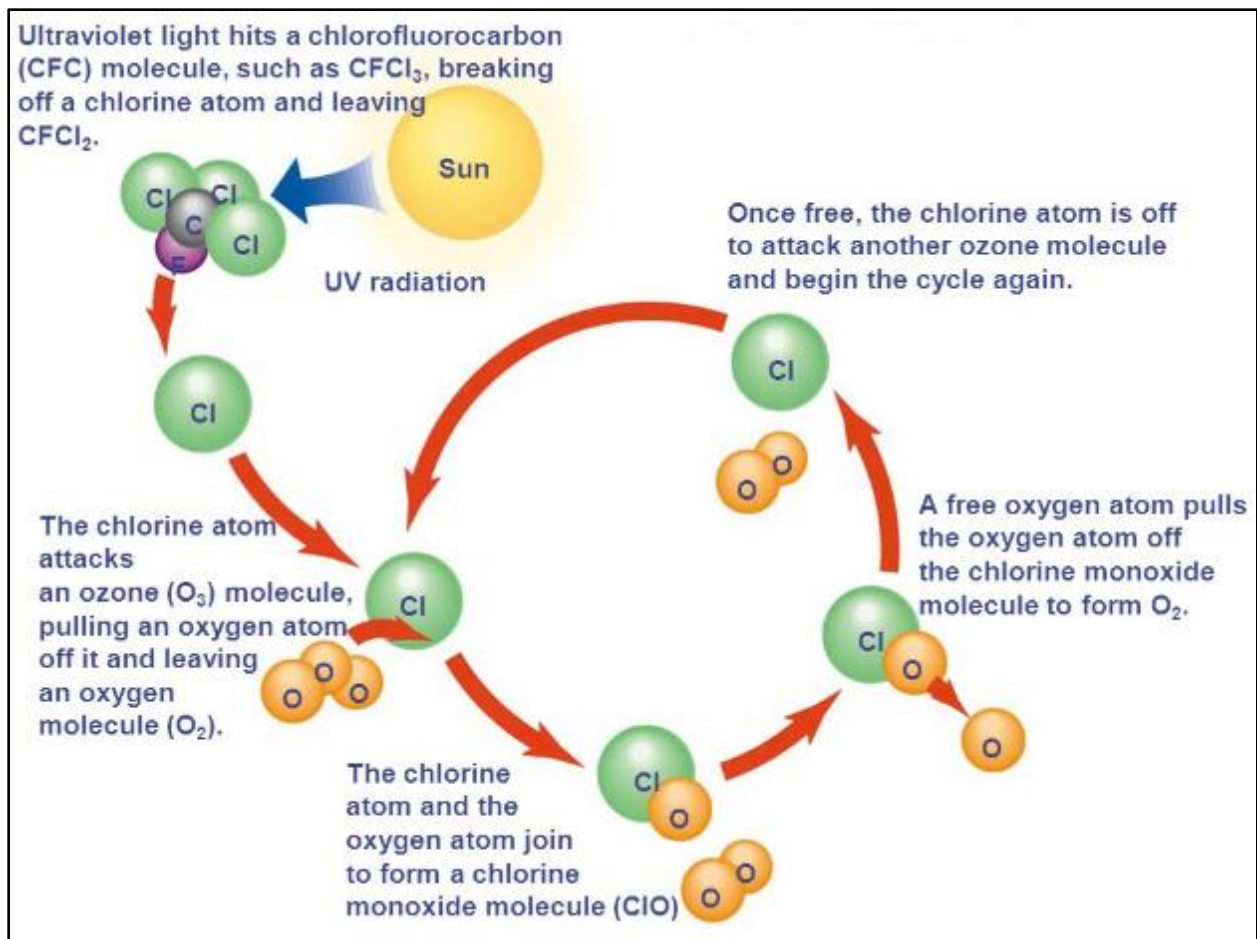


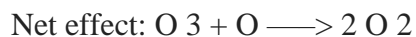
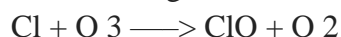
Fig. 2 (e) Chemical processes of ozone depletion and CFCs.

Picture Courtesy: <http://www.yourarticlelibrary.com/speech/ozone-layer-depletion-consequences-and-montreal-protocol/30211>

<http://eco-globe.com/what-destroys-the-earths-ozone-layer/>

Substances such as CFCs, HCFCs, Halons and methyl bromide, that lower the ozone layer do not directly destroy ozone. First they undergo photolysis, forming hydrogen chloride (HCl) or chlorine nitrate ( $\text{ClONO}_2$ ), molecules that do not react with ozone directly, but slowly decompose, giving, among other things, a small number of chlorine atoms (Cl) and Of chlorine monoxide (ClO) molecules that catalyze the destruction of ozone.

The reactions involved in the processes of destruction are more than 100, but can be simplified in the following:



The chlorine atom acts as a catalyst and it is not consumed in the reaction, so it destroys thousands of ozone molecules before disappearing. The bromine atom is even more destructive than chlorine (about 10 or 100 times more). On the other hand, along with this, the chlorine concentrations are very low in the stratosphere and the bromine concentrations are even lower.

**Mechanism of Ozone hole** – The criticality of ozone layer can be understood from the fact that, only 10 or less of every million molecules of air is ozone. The majority of these ozone molecules reside in a layer between 10 and 40 kilometers above the surface of the Earth known as stratosphere. Each spring in the stratosphere over Antarctica (spring in the southern hemisphere is from September through November.), atmospheric ozone is rapidly destroyed by chemical processes. As winter arrives, a vortex of winds develops around the pole and isolates the polar stratosphere. When temperatures drop below  $-78^{\circ}\text{C}$ , thin clouds form of ice, nitric acid, and sulfuric acid mixtures. Chemical reactions on the surfaces of ice crystals in the clouds release active forms of CFCs. Ozone depletion begins, and the ozone “hole” appears (Fig. 2 (f)).

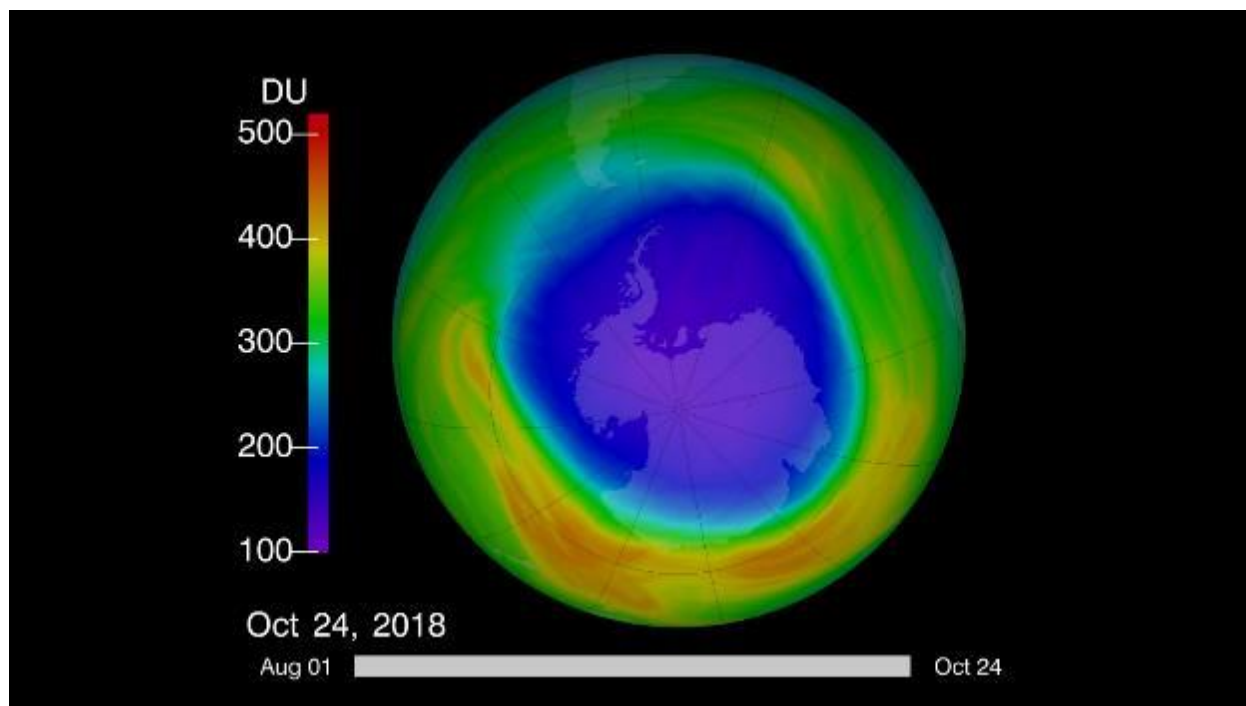


Fig 2 (f) Ozone hole

Picture Courtesy: <https://svs.gsfc.nasa.gov/13103>

About 50% of the total column amount of ozone in the atmosphere disappears during two to three months. At some levels, the losses approach 90%. This has come to be called the Antarctic ozone hole. In spring, temperatures begin to rise, the ice evaporates, and the ozone layer starts to recover. Thus, ozone “hole” is a reduction in concentrations of ozone high above the earth in the

stratosphere. The ozone hole is defined geographically as the area wherein the total ozone amount is less than 220 Dobson Units. The ozone hole has steadily grown in size and length of existence over the past two and half decades. Now, the size of ozone hole over Antarctica is estimated to be about 30 million sq. km. It has been observed that, man-made chlorines, primarily chloroflourocarbons (CFCs), contribute to the thinning of the ozone layer and allow larger quantities of harmful ultraviolet rays to reach the earth.

Looking into this global issue of ozone depletion, we are continuously working on the development and improvement of ozone sensors and low weight sensors payload to measure the ozone profile in the stratosphere on the real time mode using the HASP balloon flight since 2008. HASP-NASA provided a platform for 12 small payloads and 4 large payloads. The maximum mass limit was 20 kg for a large payload and 3 kg for a small payload. UNF and UND jointly had one small payload to measure the ozone profile in the stratosphere. UNF team fabricated the gas sensors system, payload body, microcontroller circuit, software, and electronic communication circuits. The HASP had an onboard computer, power supply batteries, GPS, video camera, and communication link for all payloads.

UNF team was participated the workshop at the NASA-Columbia Scientific Balloon Facility (CSBF) in Palestine, Texas during July 25 to 29, 2018 for the integration of the sensors payload with the HASP. Ozone sensor payload was then integrated with the HASP platform. The UND-UNF payload successfully passed all required thermal vacuum tests and certified for the flight. Then, the HASP2018 flight was launched successfully by NASA-CSBF on Tuesday, September 4, 2018 from Fort Sumner, New Mexico. The flight was terminated on September 5, 2018 near Raso, AZ. The total flight duration was about 09 hours. During the flight, the UNF ozone sensors array detected and measured ozone in the stratosphere. The payload sent out the data files during the flight without any problem. After the termination of the balloon flight, the HASP impacted on the ground using a parachute. The payload got direct impact on ground. Our payload was mounted on corner of the gondola. That side was nosed into the turf pretty hard. Our payload was recovered with lot of mud on all sides. The technical details, pictures and science results of this flight are highlighted in this report.

## **2. Fabrication of Nanocrystalline Thin Film Gas Sensors**

Ozone sensors were fabricated by UNF team at Dr. Patel's Sensors Laboratory at the UNF. Fig.3 (a) and (b) shows thermal vacuum deposition system and electron beam deposition system, respectively, were used to fabricate nanocrystalline nanocomposite thin film gas sensors for the detection of ozone gas.



Fig. 3 (a) Thermal vacuum deposition system and (b) electron beam deposition system.

Fig. 4(a) shows the top view of one typical low magnification scanning electron microscope image of the Indium Tin Oxide (ITO) thin film gas sensor having two gold electrodes for external electrical contacts. Fig. 4 (b) shows a typical array of 8 ITO thin film gas sensors fabricated on an approximately 2.5cm x 2.5cm ultra cleaned glass slide. The glass slides were thoroughly cleaned by the ultrasonic cleaner, detergent, solvent and baked in the oven. The interface of the circuit board to the array is also shown in fig. 4(b).

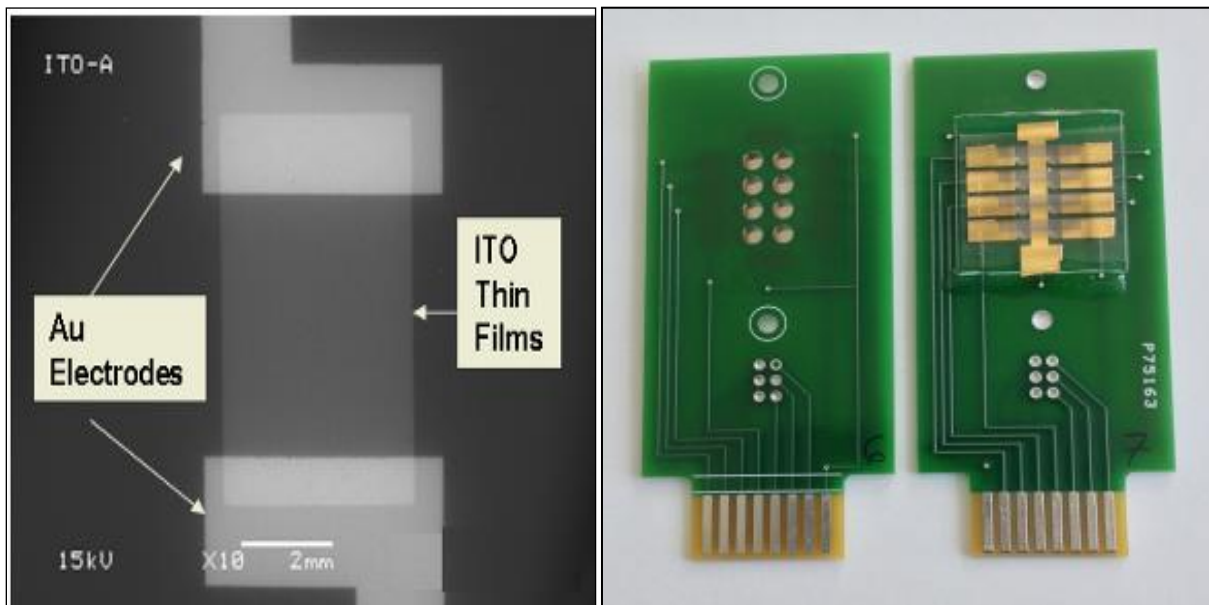


Fig.4 (a) Scanning electron microscope image of top view of one ITO thin film gas sensor (Size: 2 x 2 mm), (b) Top and bottom view of 8 gas sensor array interface with the printed circuit board (Size: 4 x 7 cm) (UNF US Patent 9,606,078).

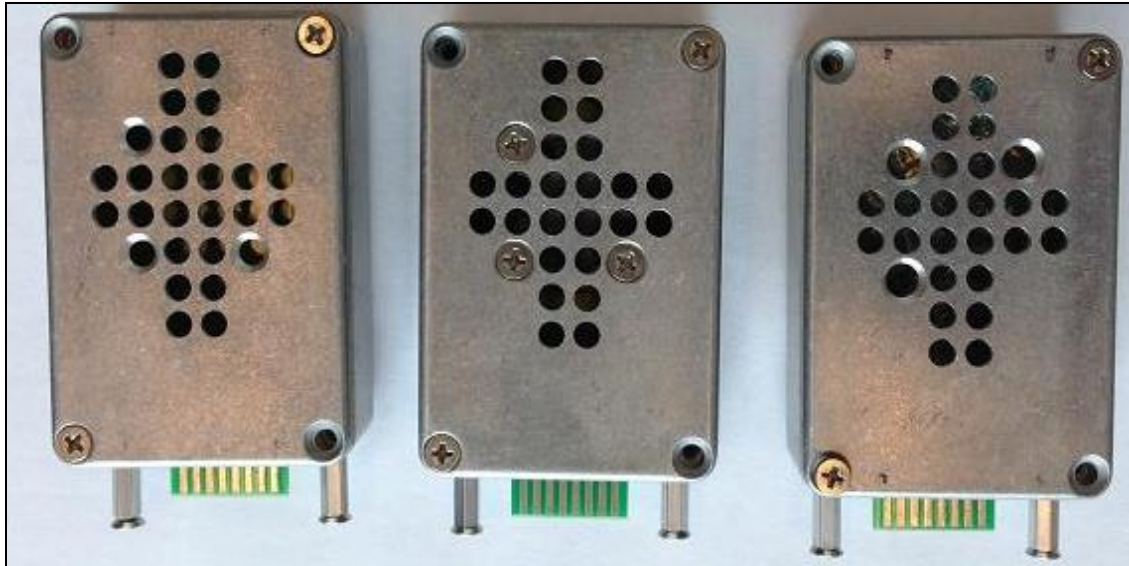


Fig. 4(c) Sensors boxes # 1, 2 and 3. Size of box: 5.5 x 2.5 x 8.0 cm.

Three types of sensor array boxes were fabricated as shown in Fig. 4(c). Each type of sensor array was mounted in a separate box. In addition to the sensors box for the payload, three backup sensors PCB boxes were fabricated. All sensors boxes were calibrated by UNF students' team at different time period and then tested in the thermal vacuum test chamber at CSBF, Palestine, TX.

**We fabricated several new sensors at different growth conditions every year in order to improve the performance and optimization of fabrication parameters such as thickness of film, substrate temperature, deposition rate and doping concentration, etc.**

**Box #1** sensors are nanocrystalline ITO thin film deposited on glass for detection of good ozone.

**Box #2** sensors are ZnO + ITO thin films deposited on glass for detection of good ozone.

**Box #3** sensors are nanocomposite of ITO +SnO<sub>2</sub> thin films deposited on glass for detection of bad ozone and smog in the Atmosphere / Troposphere,

**Backup Box # 4, 5 and 6, Backup PCB # 7, 8 and 9.**

Fig. 5 (a) shows the picture of housing for the UNF sensors, consisting of an array of 8 gas sensors interfaced with a printed circuit board (PCB), flexible Kapton heater (MINCO make HK 5573R30.0 L12BU), temperature sensor (Analog Device TMP36), electrical fan (SUNON, MC25060V2-0000-A99, DC 5V, 0.38W) and a 16 wires flat cable. One end of flat cable has a female card edge connector to connect sensor PCB (Make: 3M, MCS16K-ND), while other end has 16 pin female to connect microcontroller PCB.

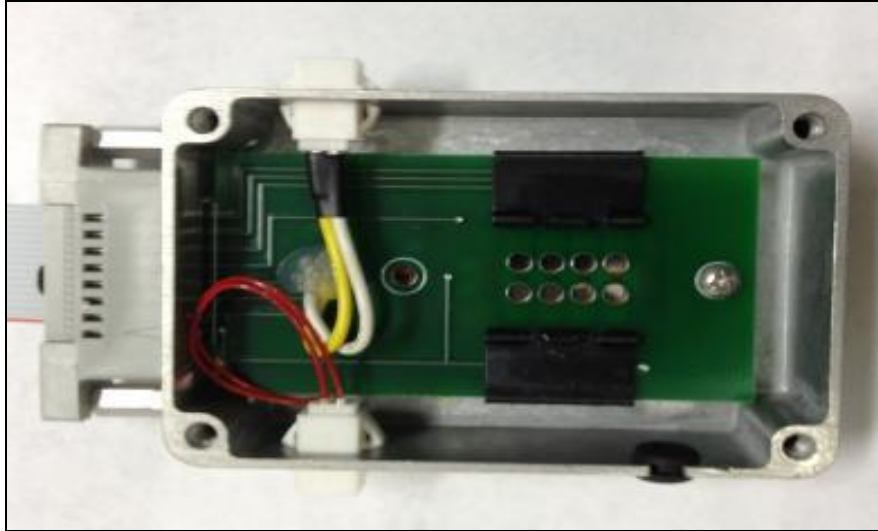


Fig.5 (a) Inner view of UNF Ozone sensors box.

The pin information of sensor PCB and connector are shown in fig. 5(b) and (c), respectively.

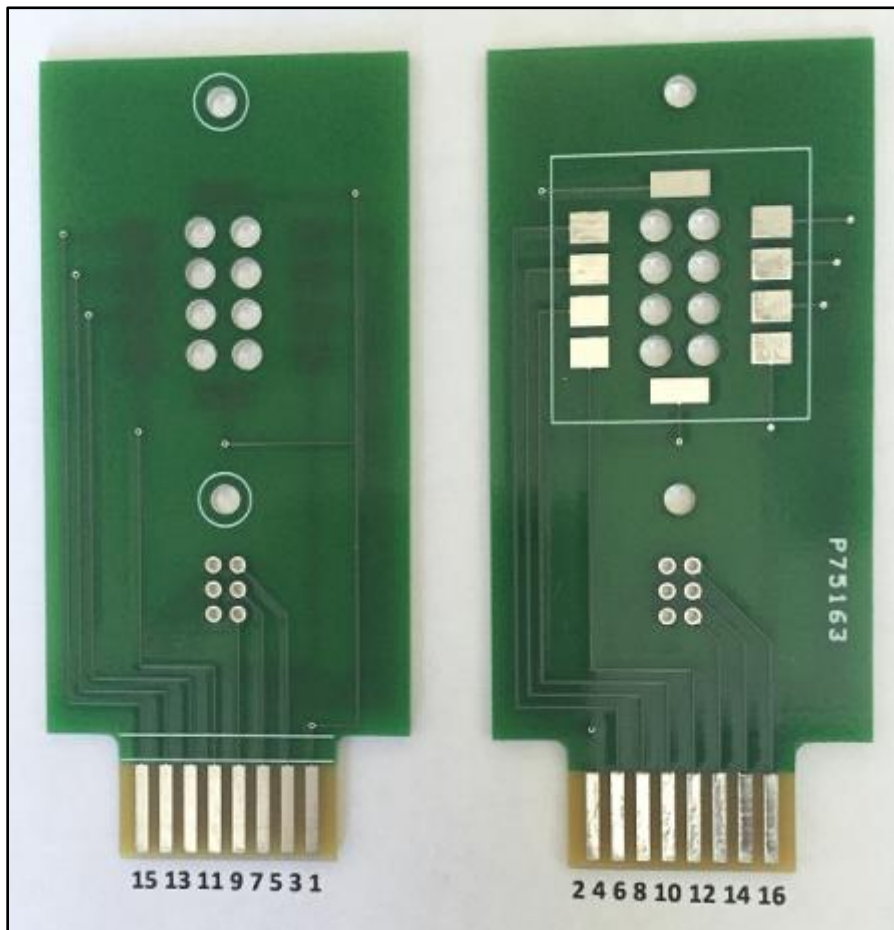


Fig.5 (b) Pin numbers of sensor PCB.

Pin number per connector datasheet							
1	3	5	7	9	11	13	15
Common	Temp Sensor	Temp Sensor	Temp Sensor	Gas Sensor	Gas Sensor	Gas Sensor	Gas Sensor
Open	Gas Sensor	Gas Sensor	Gas Sensor	Gas Sensor	Light Sensor	Light Sensor	Pin not used
2	4	6	8	10	12	14	16
Pin number per connector datasheet							

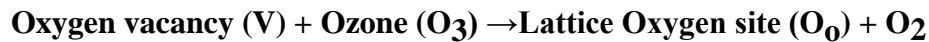
Fig.5 (c) Pin information for connection of 16 pins female card edge connector with sensor PCB

### 3. Working Principles of Gas Sensors

#### Interaction of oxidizing gas on surface of n-type ITO thin film sensor

Upon adsorption of charge accepting molecules at the vacancy sites, namely from oxidizing gases such as ozone (O<sub>3</sub>), these electrons are effectively depleted from the conduction band of ITO. This leads to an increase in the electrical resistance of n-type ITO.

*For ozone gas:*

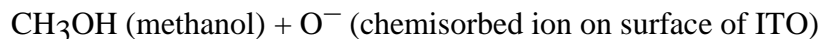


Vacancies can be filled by the reaction with ozone. Filled vacancies are effectively electron traps and as a consequence the resistance of the sensor increases upon reaction with ozone.

#### Interaction of reducing gas on surface of n-type ITO thin film sensor

Oxygen vacancies on ITO surfaces are electrically and chemically active. These vacancies function as n-type donors decreasing the electrical resistivity of ITO. Reducing gases such as CO, H<sub>2</sub> and alcohol vapors result in detectable decreases in the electrical resistance of n-type ITO.

*For reducing gas, e.g. methanol:*



Vapors come in contact with the surface and react with chemisorbed oxygen ions O<sup>-</sup> or O<sup>2-</sup> and re-inject electrons into the conduction band.

In summary, the electrical resistance of ITO increases in the presence of oxidizing gases such as ozone. Upon adsorption of the charge accepting molecules at the vacancy sites, namely oxidizing gases such as ozone, electrons are effectively depleted from the conduction band, leading to an increase in the electrical resistance of n-type ITO. Note that our three different types of sensors boxes have n-type semiconductor gas sensors.

## Dobson Spectrophotometer

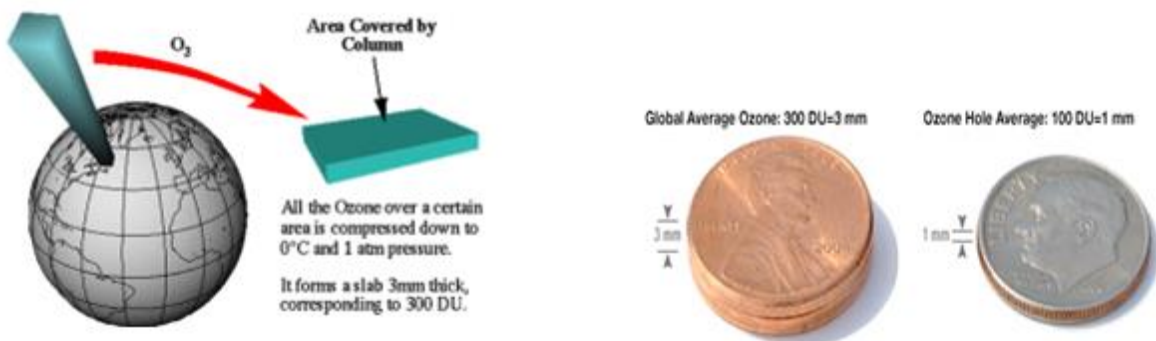
It was invented by Gordon Dobson in 1924. Used to measure both total column ozone and profiles of ozone in the atmosphere. It measures total ozone by measuring the relative intensity of the dangerous UVB radiation that reaches the Earth and comparing to that of UVA radiation at ground level. If all of the ozone were removed from the atmosphere, the amount of UVB radiation would equal the amount of UVA radiation on the ground. As ozone does exist in the atmosphere, the spectrometer can use the ratio between the UVA and UVB radiation on the ground to determine how much ozone is present in the upper atmosphere to absorb the UVC radiation.



## Units for measurement of ozone

In the present study, we used part per million (ppm) units for determination of ozone concentration. We calibrated our sensors in the closed chamber using a digital ozone meter, which has unit in ppm only. Ozone is measured by the Dobson spectrometer in Dobson Units (DU). Our sensors are very cheap, smaller in size, low mass and easy to interface with electronic compared to that of Dobson spectrometer.

1 Dobson Unit (DU) is defined to be 0.01 mm thickness of gas at STP (0°C, 1 atm); the ozone layer represented above is then ~300 DU.



## 4. Calibration of Gas Sensors

The ITO sensors array was first tested and calibrated in the test chamber at UNF. The test chamber was adjusted to the identical conditions of temperature and pressure as in the stratosphere. Fig. 6(a) and (b) shows the pictures of ozone generator and detector used for the calibration of sensors. An ozone generator (Ozone Solutions, Model# OMZ-3400) was used as the source of ozone, which generated 0 to 12 ppm ozone gas.

A digital ozone detector (Eco Sensors, Inc., Model:A-21ZX) was used to measure the concentration of ozone in part per million (ppm). The Keithley digital multimeters and electrometers attached with computer having LabView program were used for the measurements of the ITO sensor's resistance.



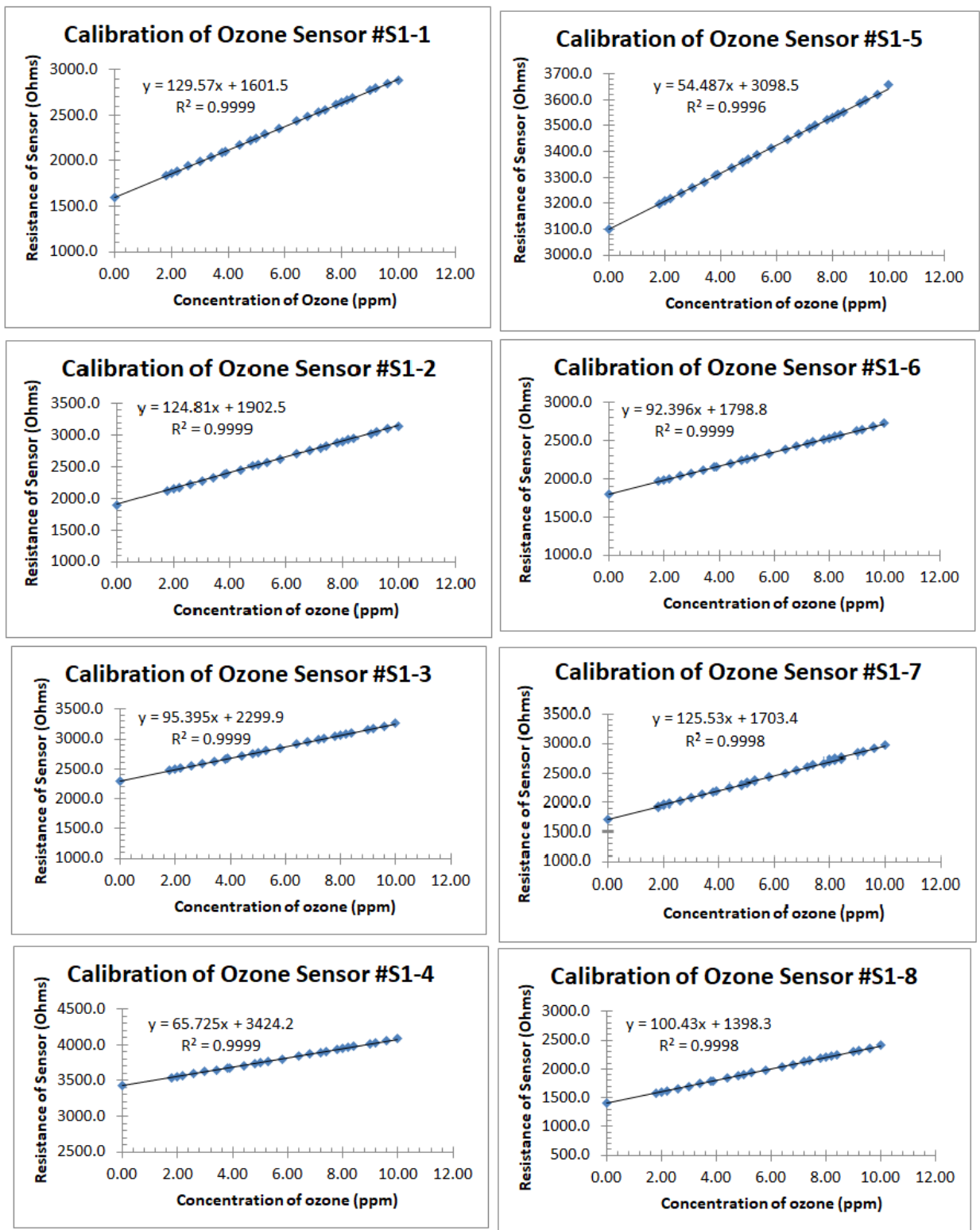
Fig.6(a) Ozone generator and (b) digital ozone detector.

All the 24 sensors of sensors box was calibrated simultaneously under identical conditions of pressure, temperature and concentration of ozone in the test chamber. The sensors were calibrated with ozone gas in the range of 0.02 to about 10.00 ppm in the test chamber in the same run. The usual variation of ozone in the stratosphere is about 3.0 to 10.0 ppm. The measured data fit linearly and trend line equations for each plot were determined.

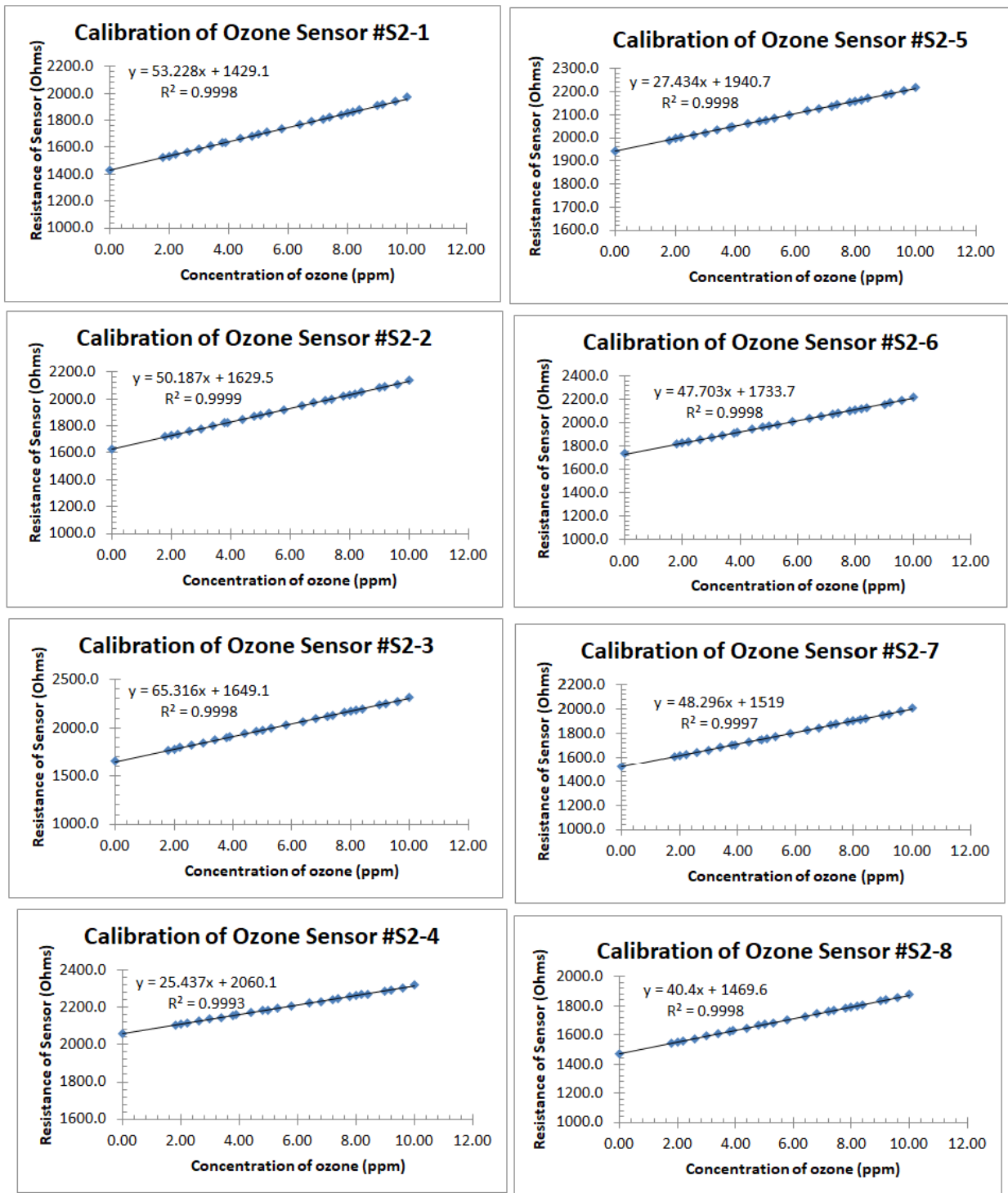
Figs.7 (a) show the calibration plots ozone sensors Box#1 having sensors # S1-1 to S1-8. These sensors were made of nanocrystalline ITO thin film gas sensors fabricated on the glass.

Figs.7 (b) show the calibration plots ozone sensors Box#2 having sensors # S2-1 to S2-8. These sensors were made of nanocomposite of ZnO + ITO thin film and were fabricated on the glass.

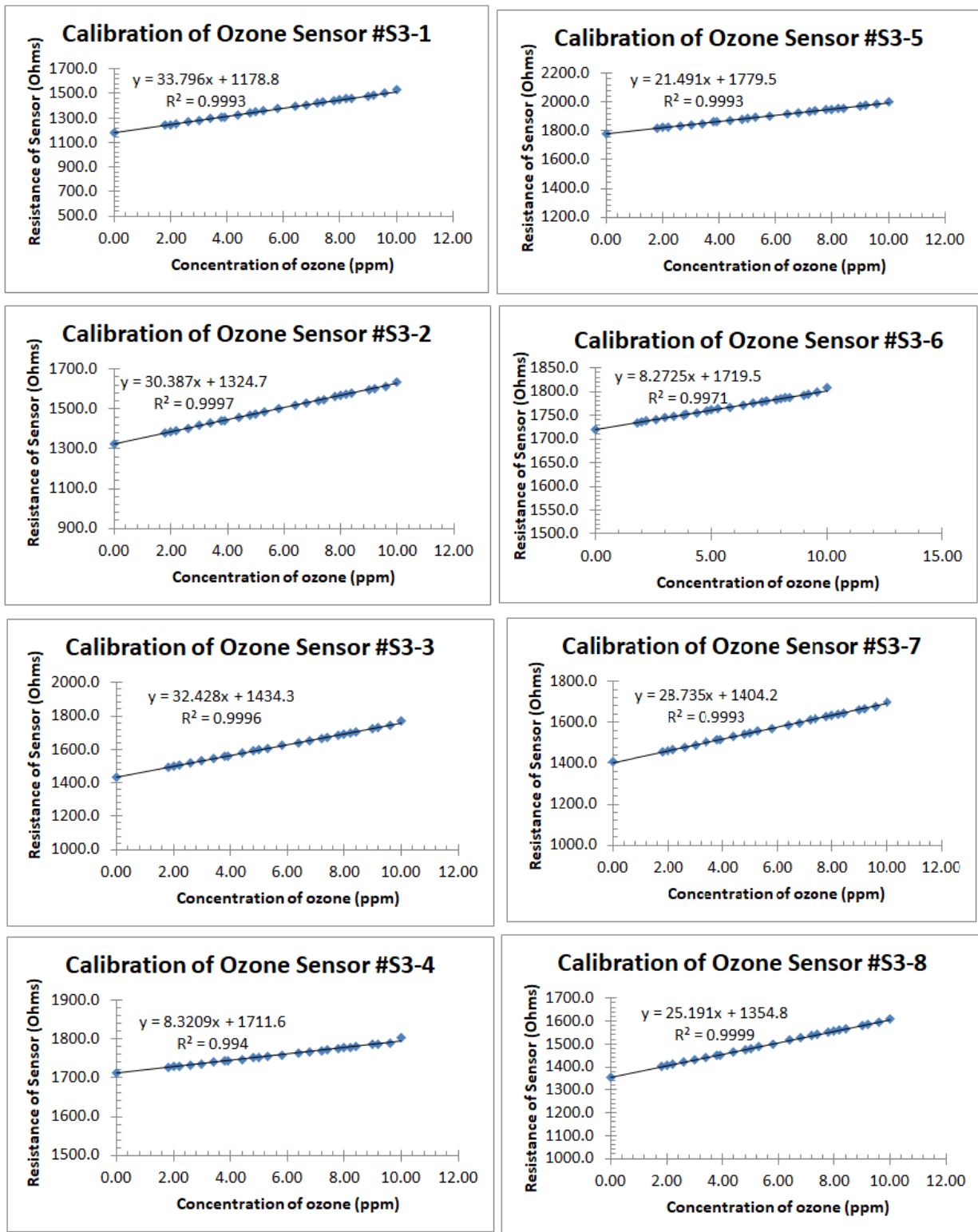
Figs.7 (c) show the calibration plots ozone sensors Box#3 having sensors # S3-1 to S3-8. These sensors were made of nanocomposite of ITO +SnO<sub>2</sub> thin film and were fabricated on the glass.



Figs.7 (a) show the calibration plots ozone sensors Box#1 having ITO thin film gas sensors # S1-1 to S1-8.



Figs.7 (b) show the calibration plots ozone sensors Box#2 having ZnO + ITO thin film gas sensors # S2-1 to S2-8.



Figs.7 (c) show the calibration plots ozone sensors Box# 3 having ITO+SnO<sub>2</sub> thin film gas sensors # S3-1 to S3-8.

All sensors were calibrated at three different times and showed nearly the same nature of response each time. Small variations in the slope and y-intercept values were observed due to the variation of sensor thickness and experimental error.

Note that the calibration algorithm for each layer such as atmosphere, troposphere and stratosphere based on pressure and temperature were applied to determine the concentration of ozone in the entire range of altitude

## 5. Fabrication of Payload Body

The payload retained it's easy to open and close design utilizing the top plate for access to the PCB as well as all sensor boxes. The payload continues to feature a rectangular design due to its robustness as well as for its low rate of outgassing under extreme pressure drops. This design is optimal for the team's goal of a reusable payload body. The details of design and drawing and fabrication work are shown in fig.8 (a) to (s). Corrina Yorke made new design and drawings of the payload body using AutoCAD. UNF students did fabrication work of the payload boy in the UNF workshop. The height of 2018 payload was about 228.6 mm ( $\approx$  about 9 inches).

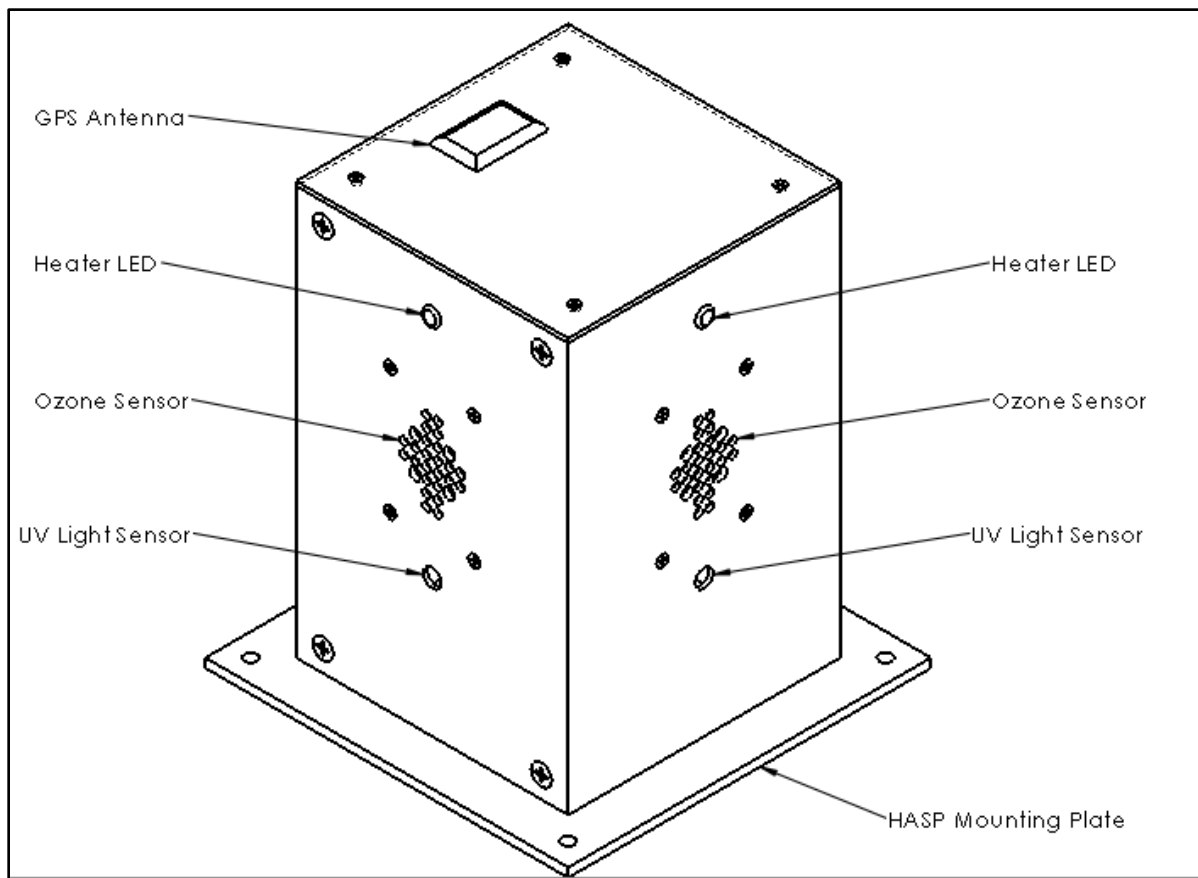


Fig.8 (a) Design of payload body.

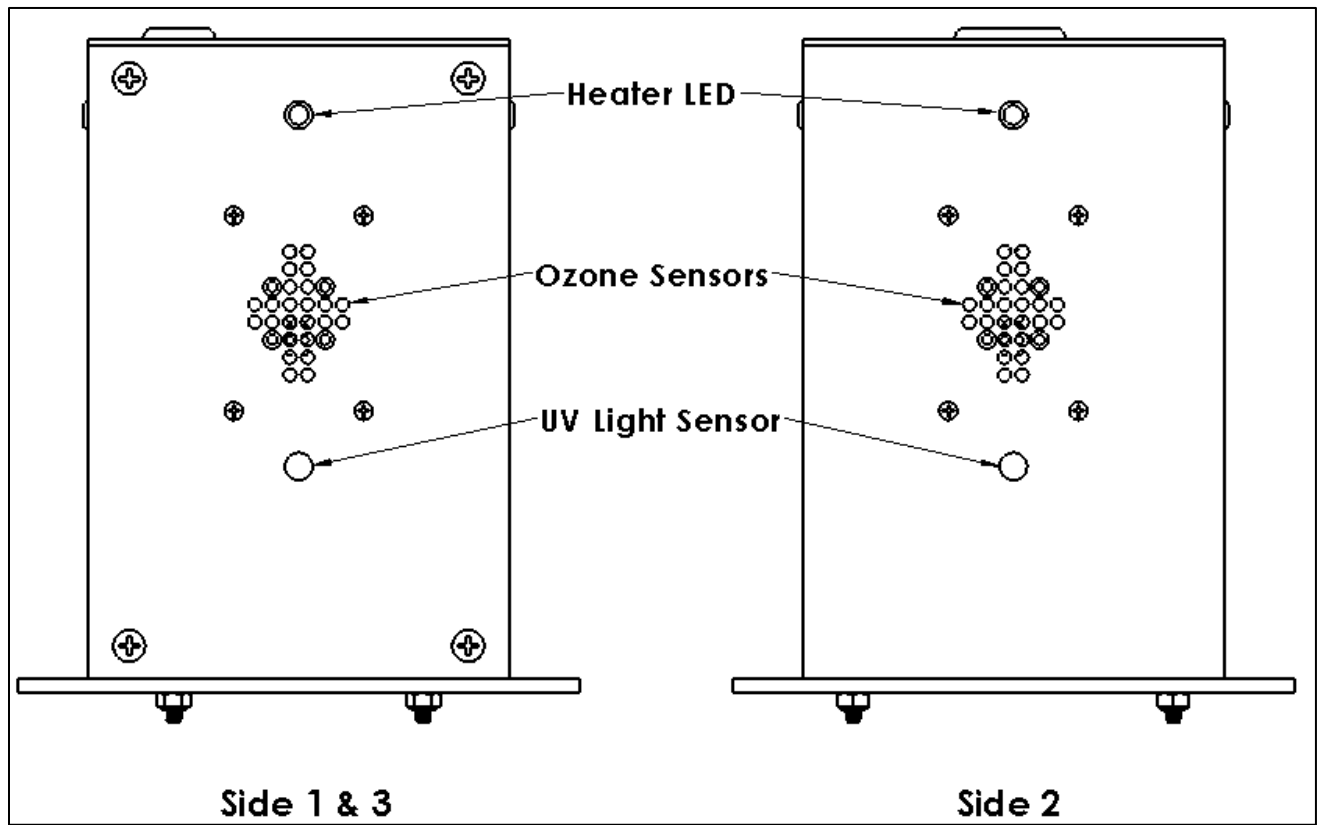


Fig. 8 (b) Side view design of the payload

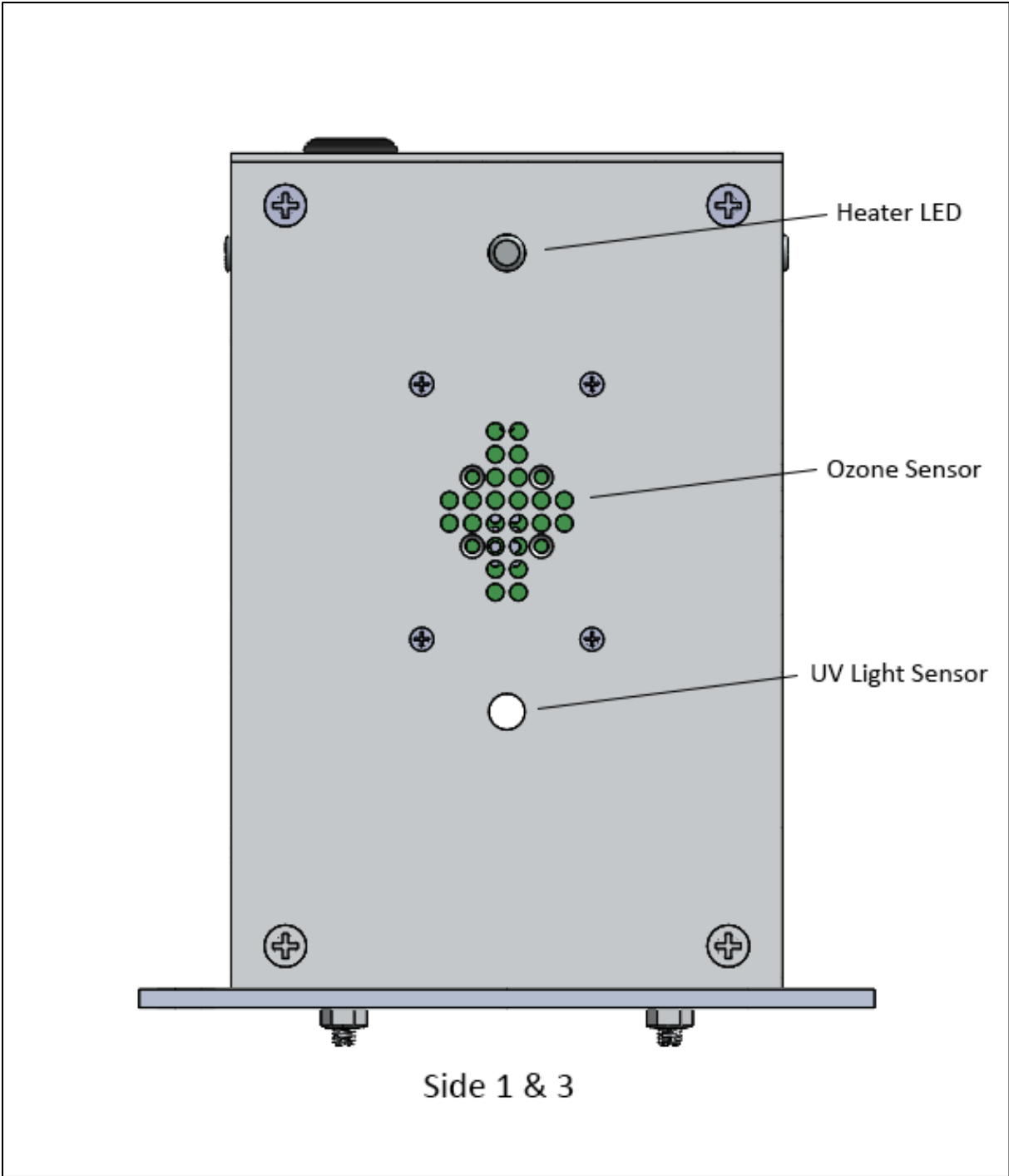


Fig. 8(c) Outer view of design of sides # 1 and 3 of the payload

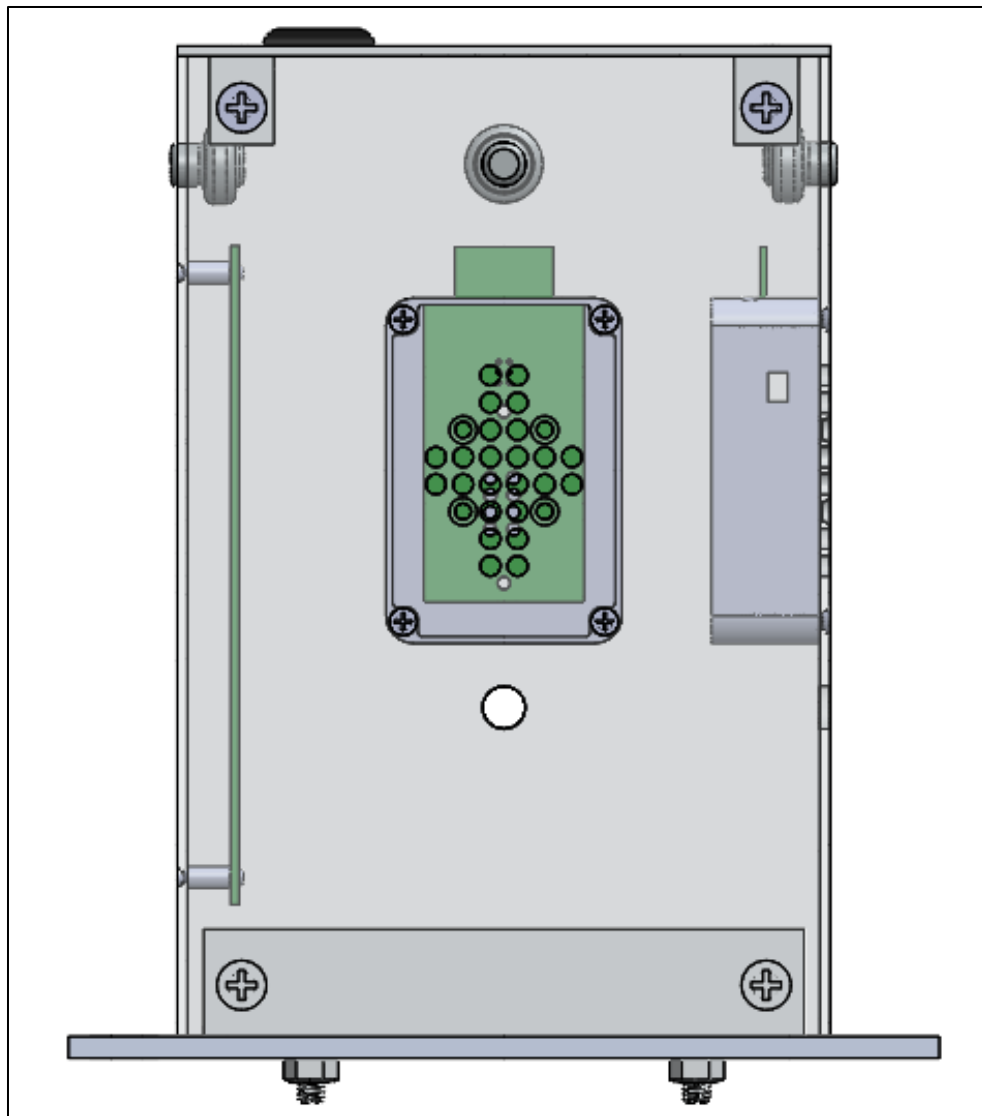


Fig. 8(d) Inside view of design of sides # 1 and 3 of the payload

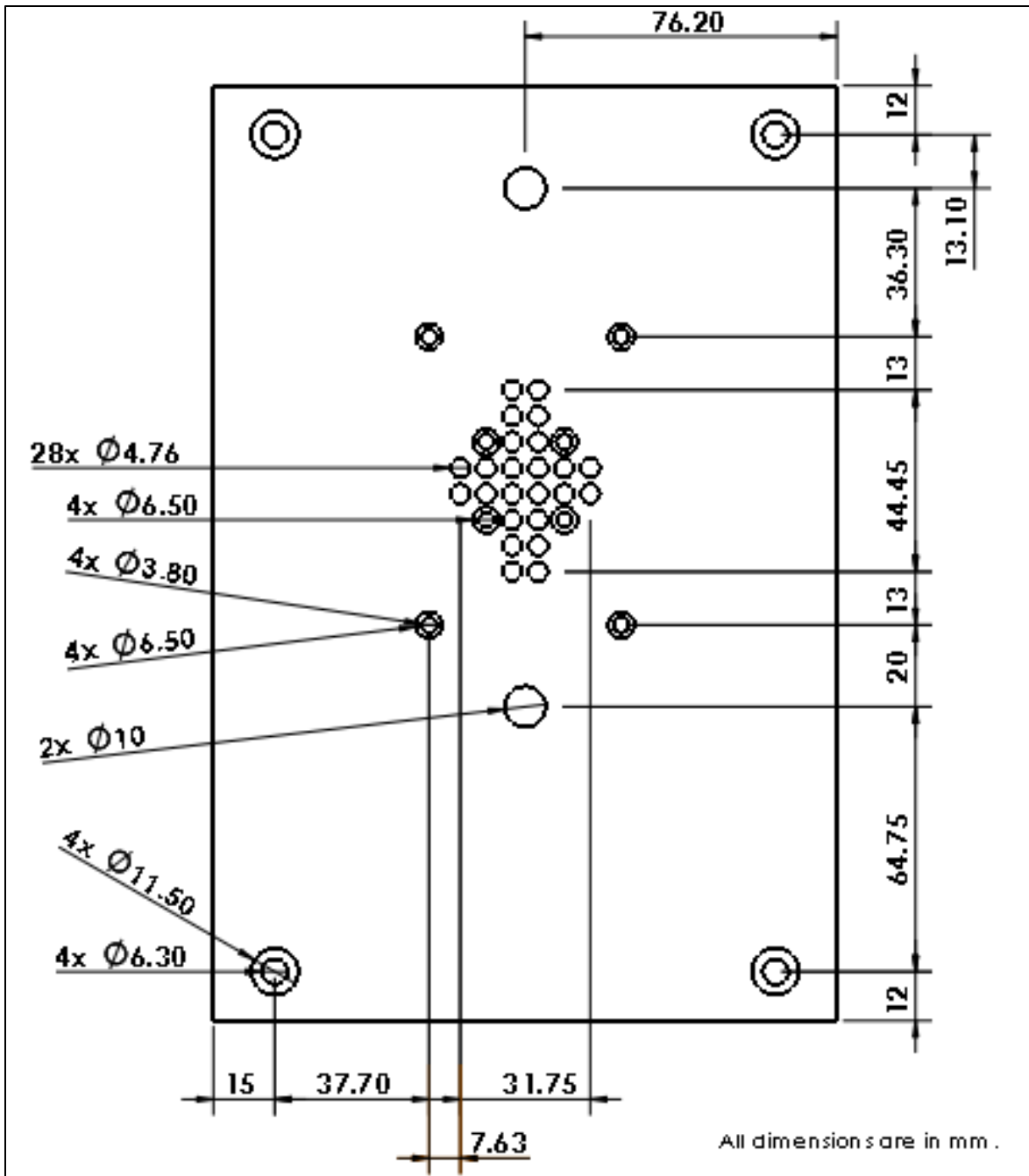


Fig. 8(e) Design with dimensions of sides # 1 and 3 of the payload

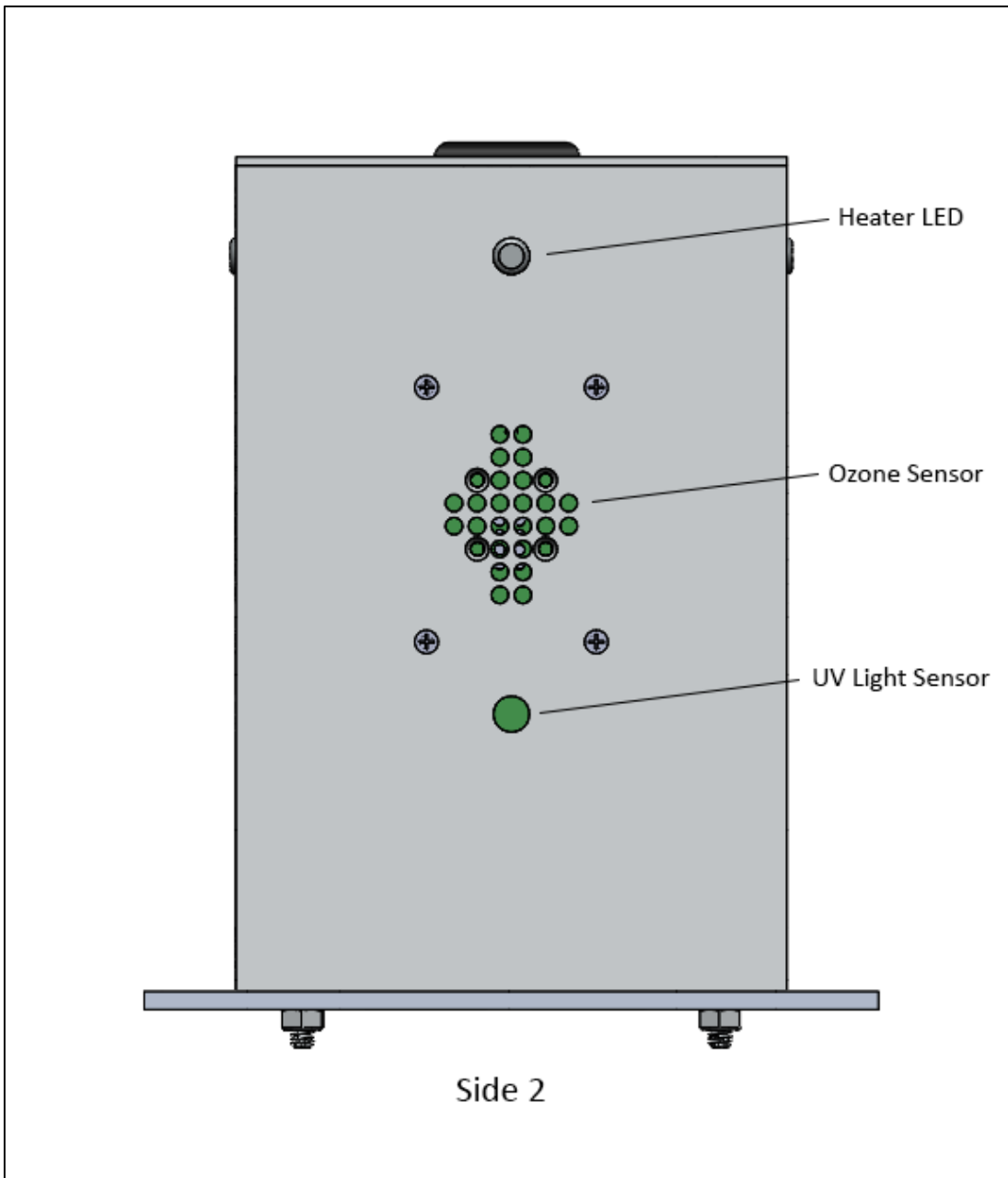


Fig. 8(f) Outer view of design of side # 2 of the payload

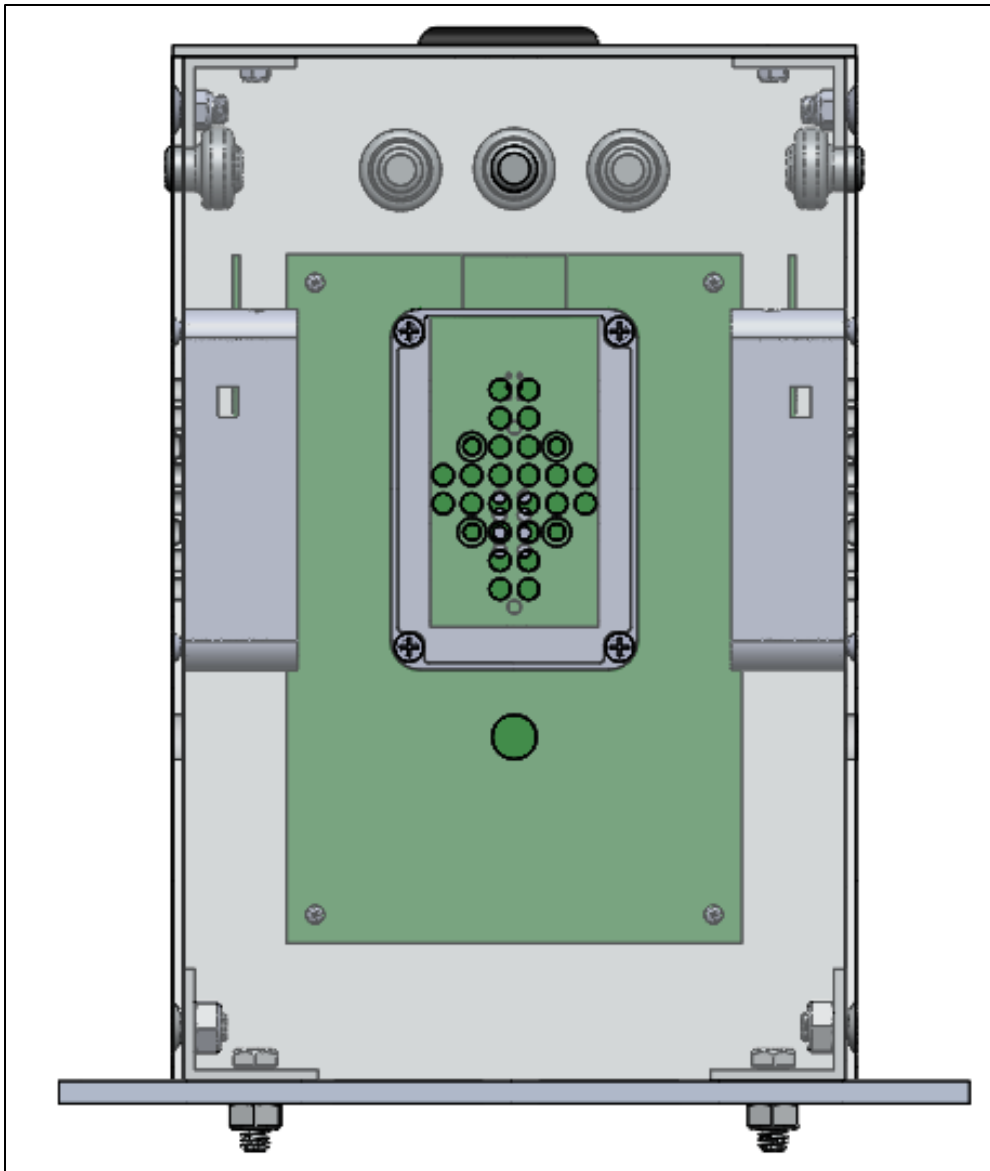


Fig. 8(f) Inside view of design of side # 2 of the payload

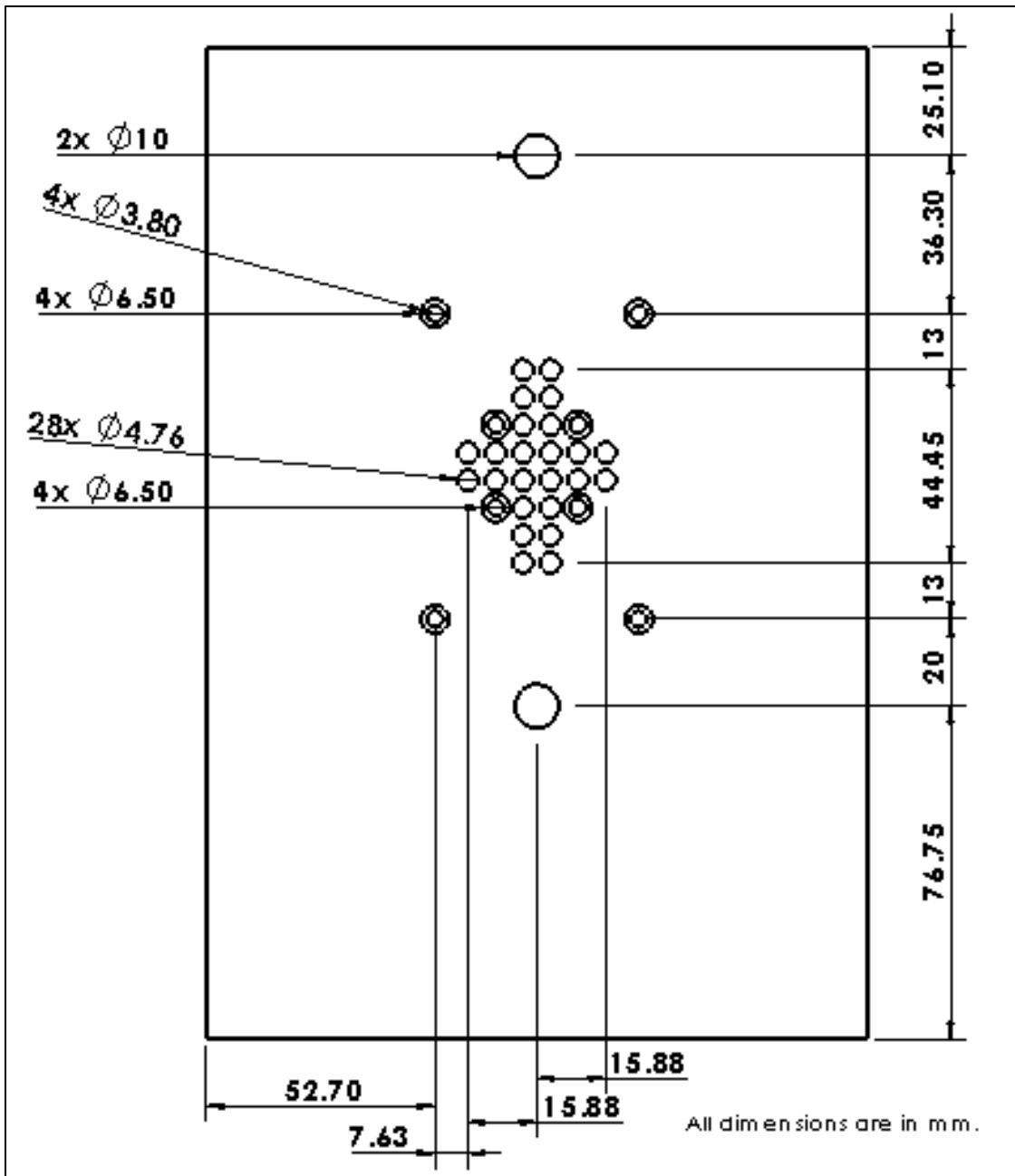


Fig. 8(g) Design with dimensions of side # 2 of the payload

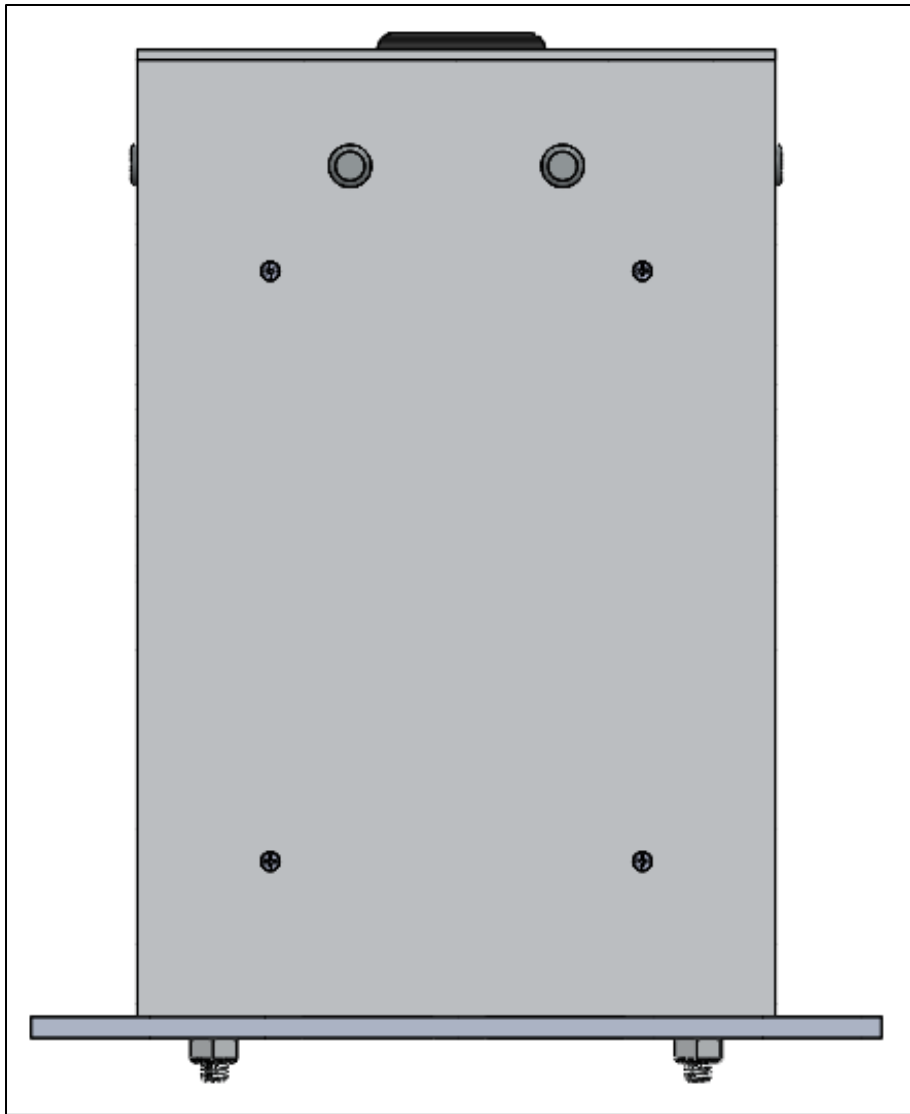


Fig. 8(h) Outer view of design of side # 4 of the payload

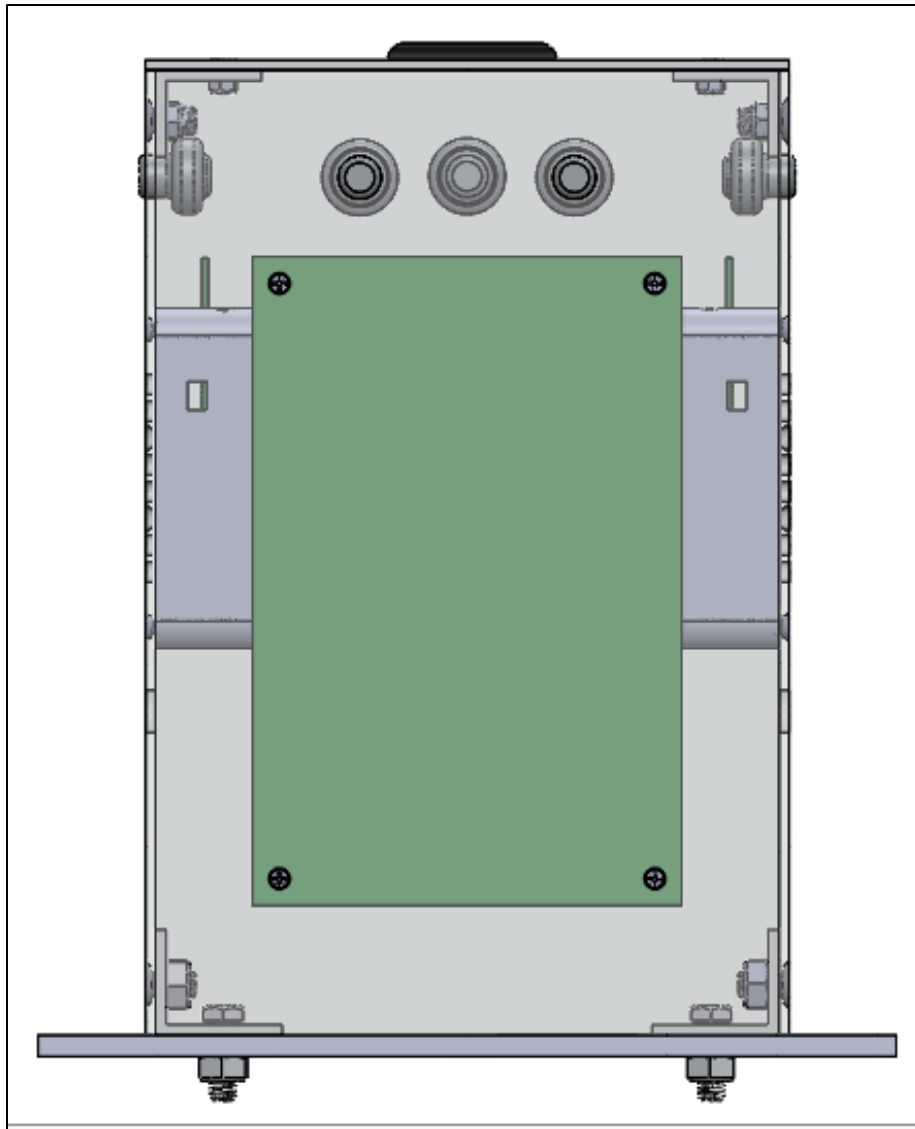


Fig. 8(i) Inside view of design of side # 4 of the payload

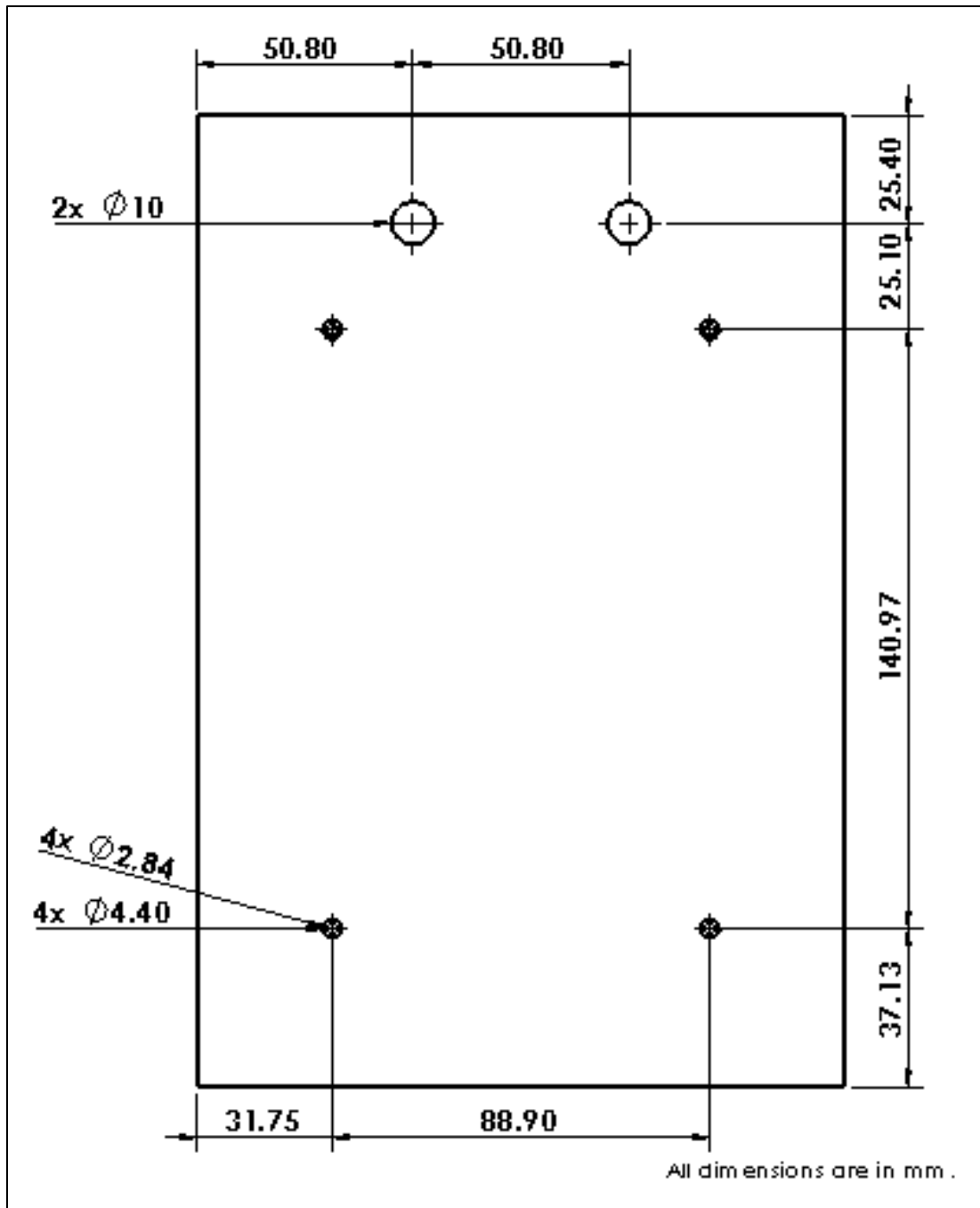


Fig. 8(j) Design with dimensions of side # 4 of the payload

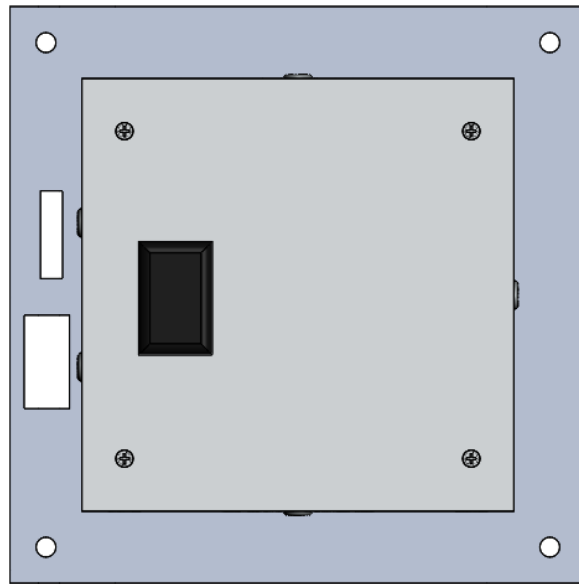


Fig. 8 (k) Design of top plate of the payload

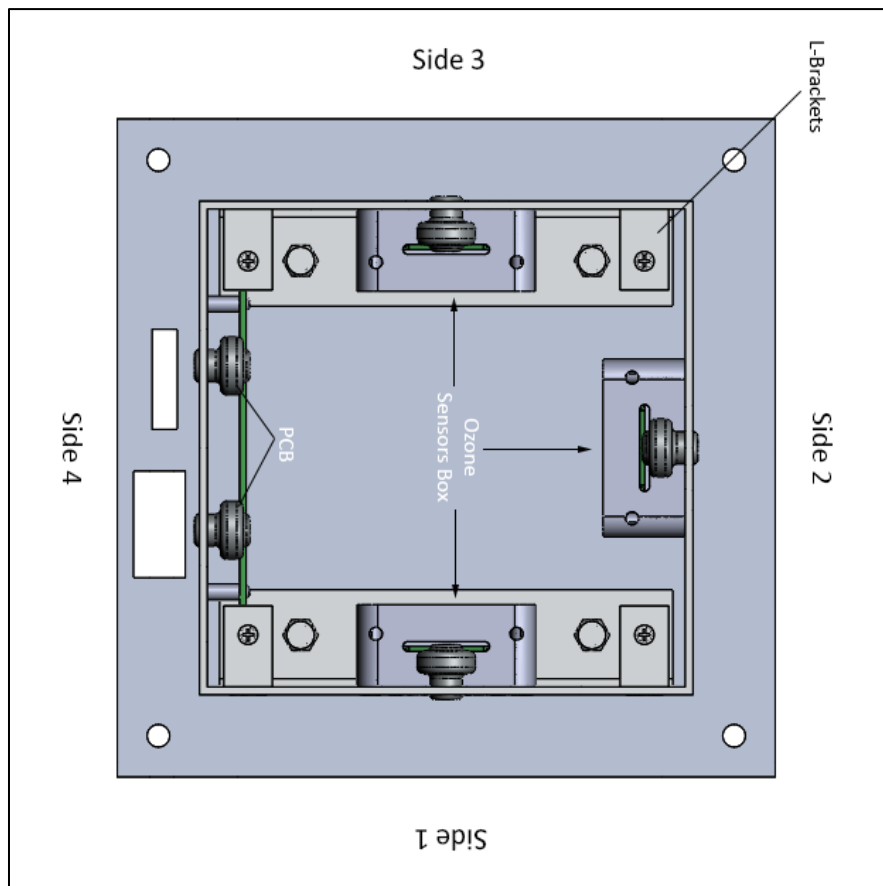


Fig. 8 (l) Top inside view of the payload

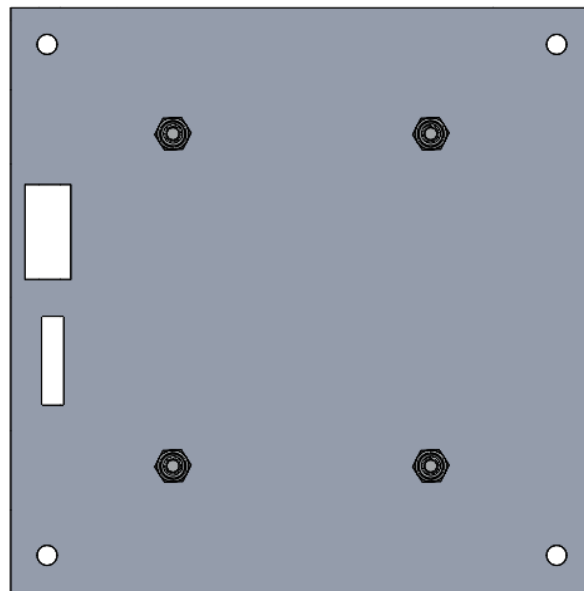


Fig. 8 (m) Bottom outer view of the payload

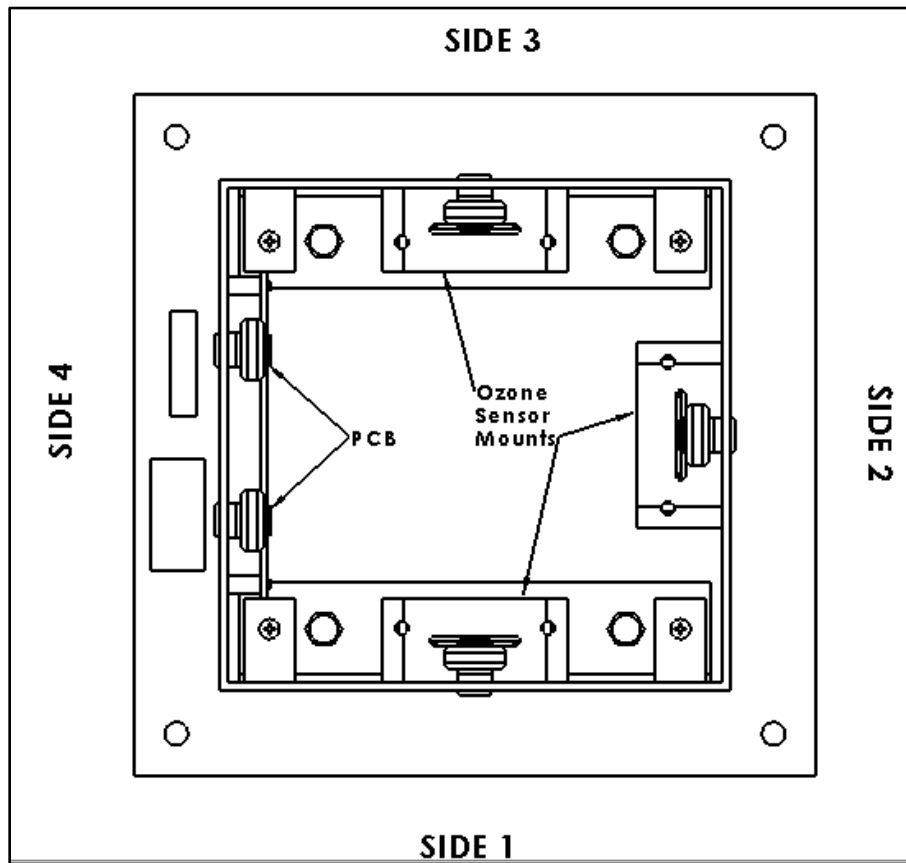


Fig .8 (l) Bottom inside view of the payload

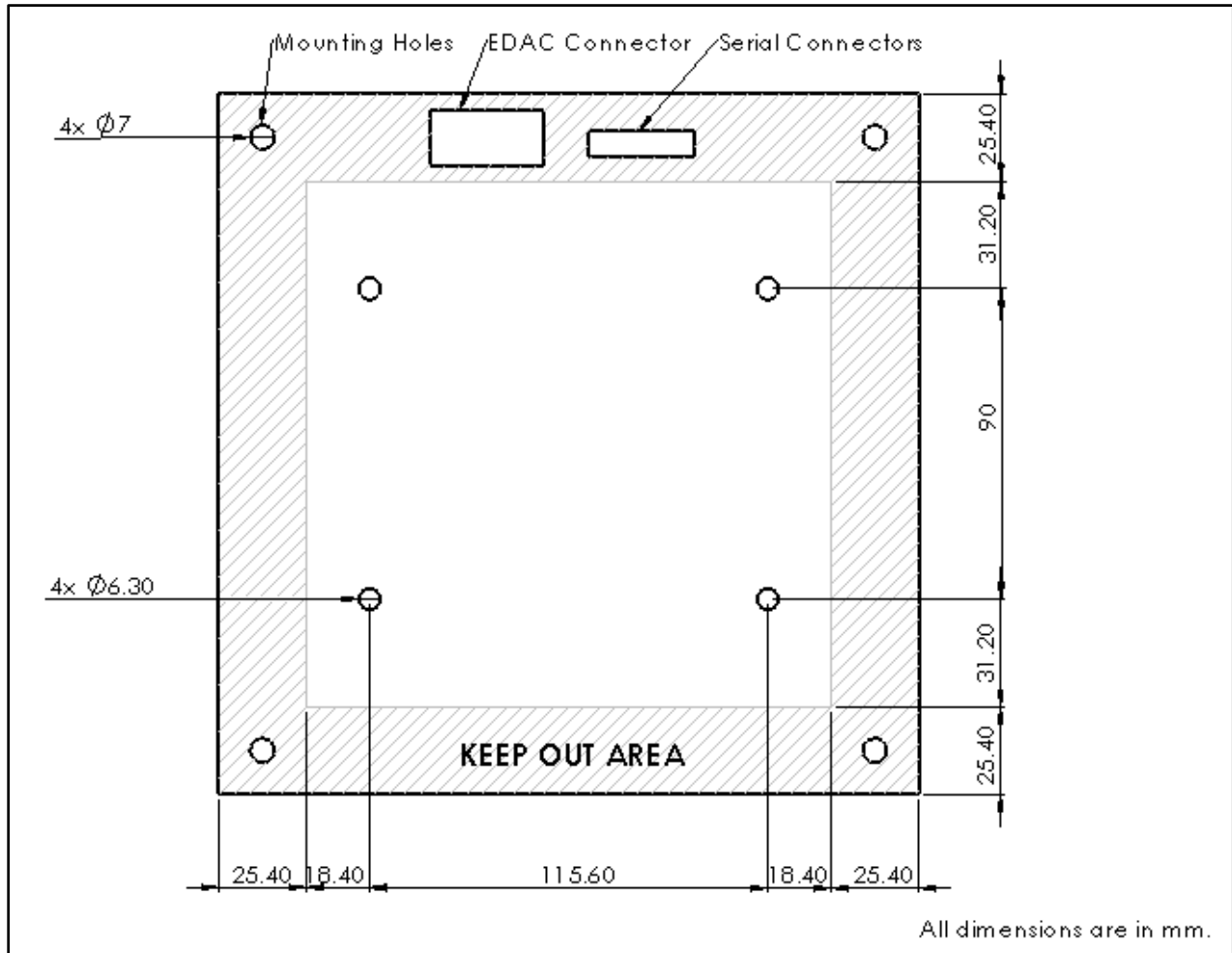


Fig. 8 (m) Design of HASP mounting plate

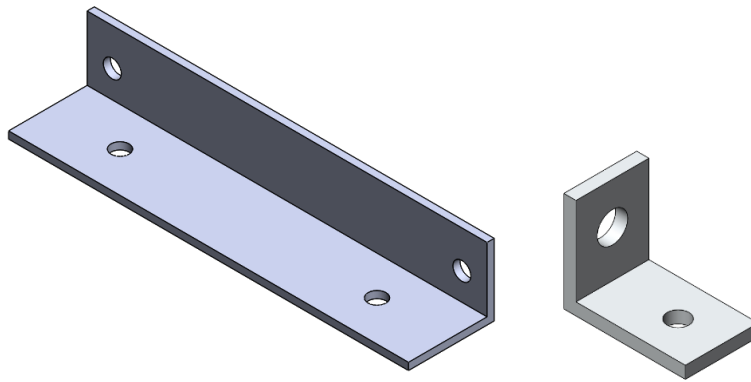
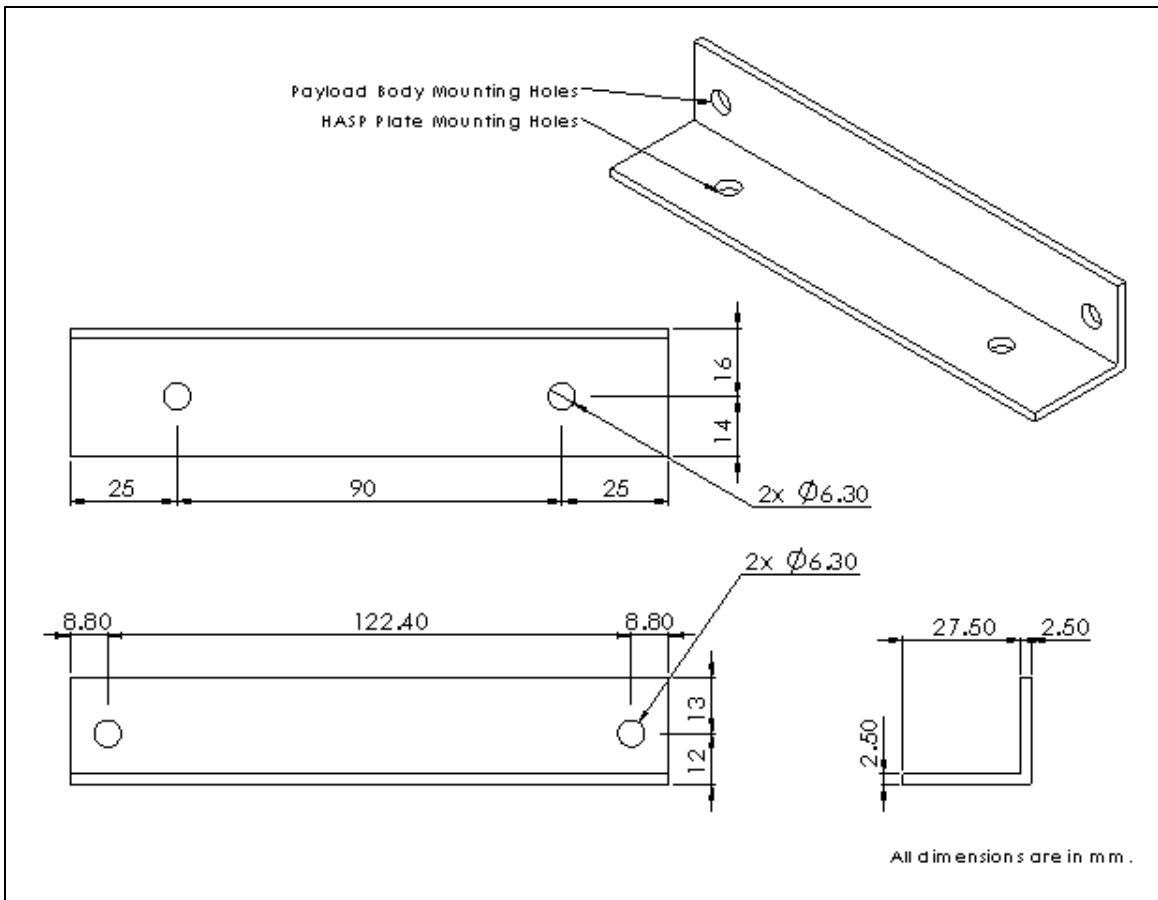


Fig. 8 (n) Design of L-Strip for mounting the HASP plate with payload body and Design of L-Brackets for mounting the top lid on the payload body

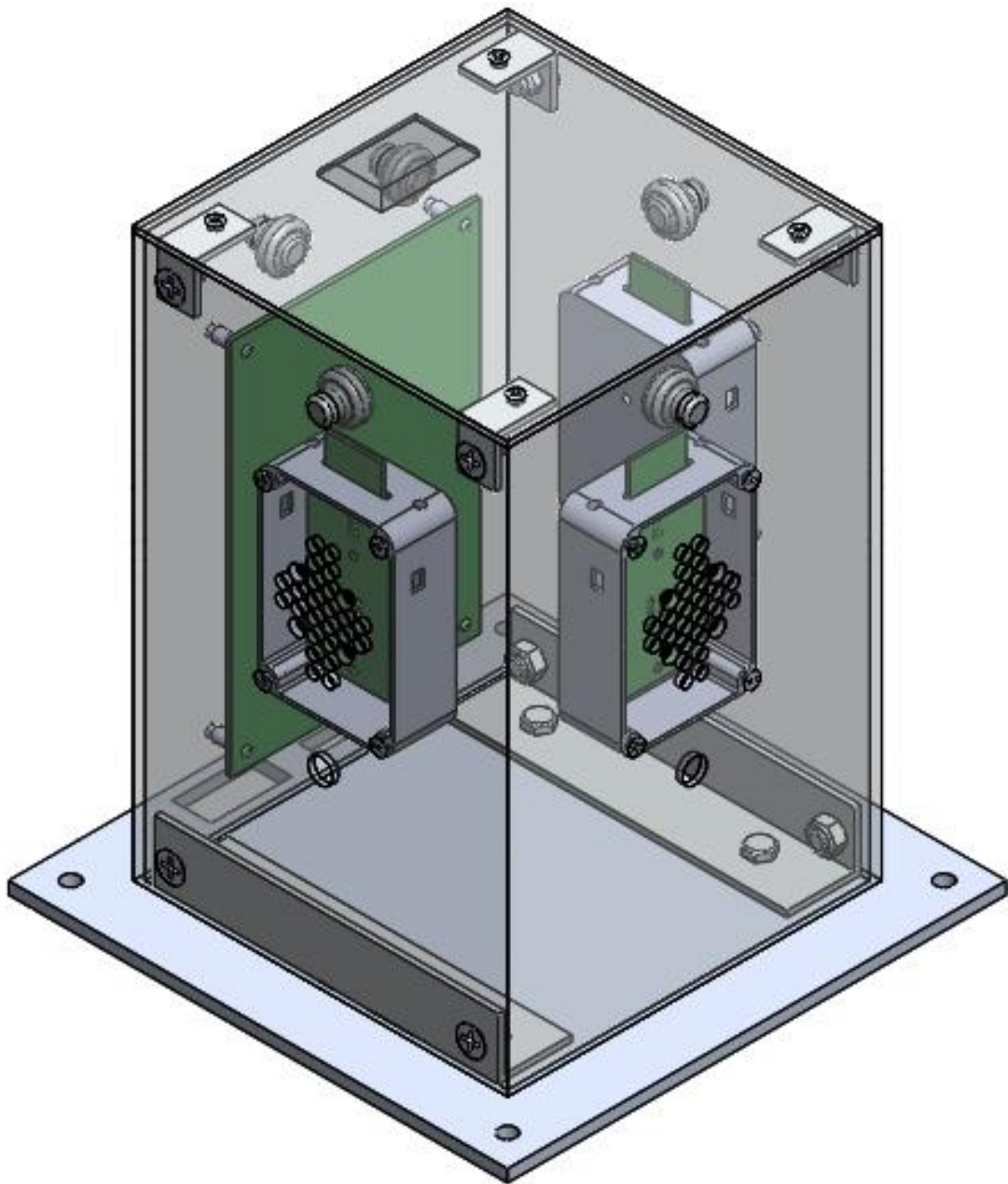


Fig. 8 (o) Design of all sides view of the payload mounted on the HASP plate.

The payload was mounted on the HASP mounting plate using aluminum L-brackets, bolts, washers and nuts.

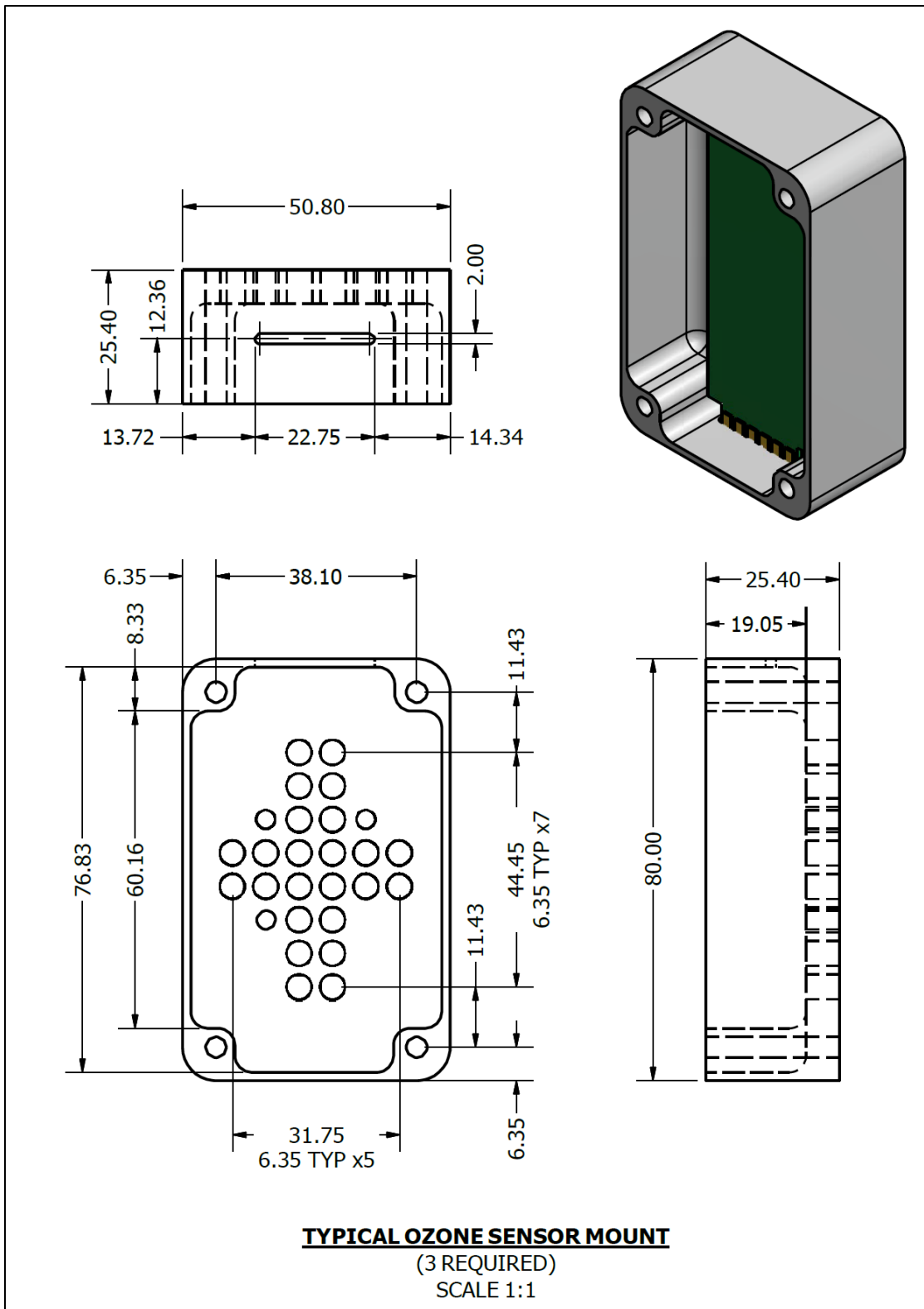


Fig.8 (p) Design of sensor box of the payload  
All dimensions are in mm.

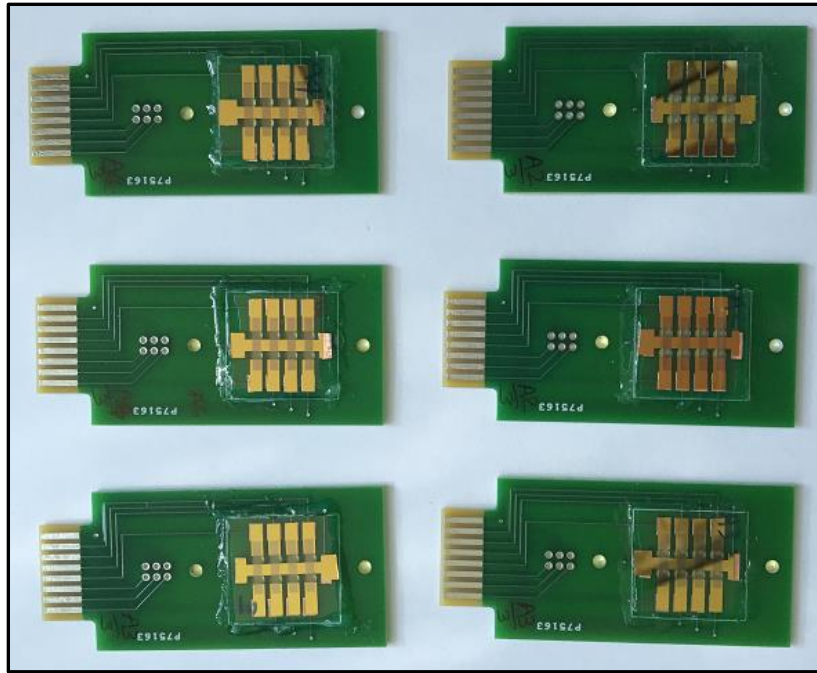


Fig.8 (q) Ozone gas sensor arrays mounted on the PCB

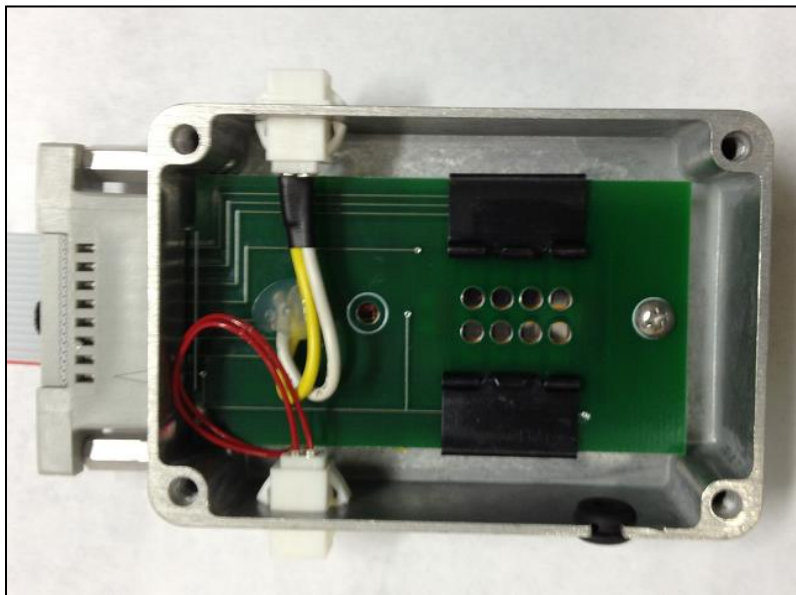


Fig.8 (r) the picture of sensors box of the payload. The sensor box consists of 8 ozone sensors array mounted on the PCB with one heater, miniature fan and a temperature sensor.



Fig.8 (s) Jesse operated the high vacuum systems for the fabrication of thin film gas sensors.

Table-1 shows the parts were procured for the payload body from supplier [www.onlinemetals.com](http://www.onlinemetals.com).

Table-1 Metal parts for the payload body

Name	Size	Purpose
Aluminum Extruded Square Tube Part #6063-T52	height 9" w x d: 6" x6" wall thickness: 0.125"	Payload body
Aluminum Sheet Part#3003-H14	6" X 6" Thickness: 1/8"	Top lid

Table-2 shows weight budget of various parts of the payload. The estimated total mass of payload including its base plate was 2.75 kg, which was less than the limit of 3.00 kg + 0.50 kg mass of base plate (total 3.5 kg)

Table-2. The estimated weight budget of the payload.

Item	Dimension	Mass (g)
8 Ozone sensors box #1 (including fan, heater, box)	Each box	200.0±2.0
8 Ozone sensors box #2 (including fan, heater, box)	3 x 2 x 1 inch	200.0±2.0
8 Pollutant sensors box#3 (including fan, heater, box)	=76.2x50.8x25.4 mm	200.0±2.0
Microcontroller PCB with mounted components	4x 6 inch =101.6 x152.4 mm	300.0±1.0
Payload body, top plate and thermal blanket	9 x 6 x 6 inch =228.6x152.4x152.4 mm	1000±10.0 g
Few Cables, 1 GPS, 2 LEDs, 3 Photodiodes, nuts and bolts		300±5.0 g
HASP mounting plate	7.9 x 7.9 inch =200.6x200.6 mm	550±3.0 g
Total estimated mass of the payload with HASP mounting plate		<b>2750±25.0 g</b>

### Thermal Blanket

The outer surface of payload body was covered by the thermal blanket made of silver color aluminized heat barrier having adhesive backed (Part No. 1828) (Make: [www.PegasusAutoRacing.com](http://www.PegasusAutoRacing.com)) for the improvement of thermal stability. The high reflective surface of the material is capable of withstanding radiant temperatures in excess of 1000°C. Fig. 9 shows the typical plots of % reflectance at different wavelength of light from the silver, gold,

copper and aluminum surfaces. Silver color surface higher reflectance over wide range of wavelength of light compare to gold, copper, and aluminum surfaces.

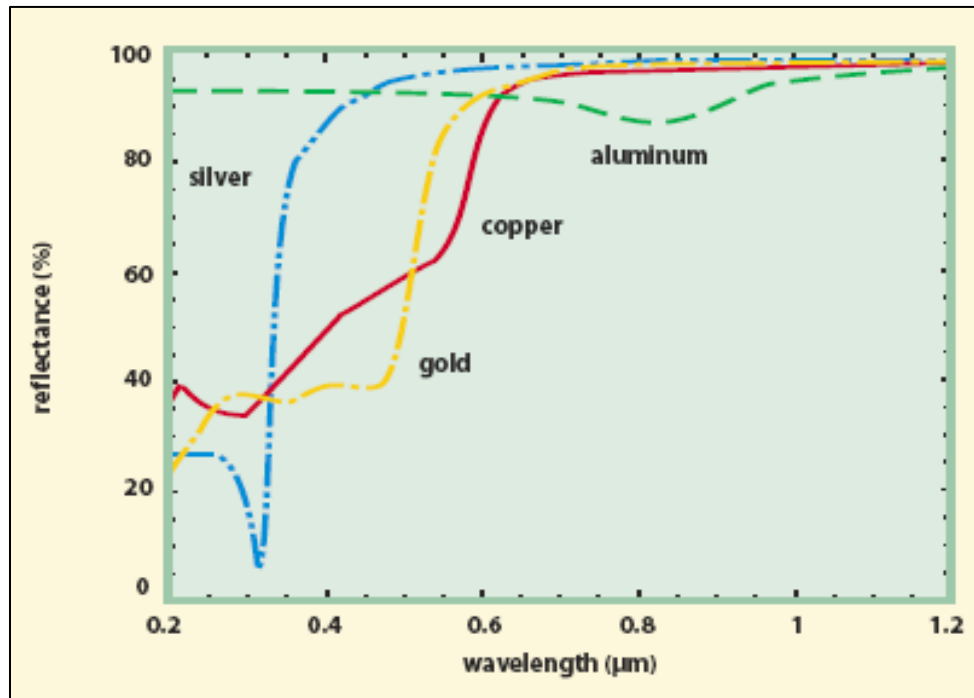


Fig.9. Variation of reflectance with wavelength of light from different color of surfaces.  
Courtesy: <http://www.photonics.com/EDU/Handbook.aspx?AID=25501>

## 6. Electronic Cirucits

The block diagram of circuit is shown in fig. 10 (a), while several sections of circuits are shown in fig. 10 (b) to (h). Two identical microcontroller PCBs were fabricated. The picture of PCB is shown in fig.10 (i). Two identical PCBs were fabricated. One PCB was used for the payload, while for other PCB was used to stimulate software and backup. The original design was made earlier by Jonathan Wade.

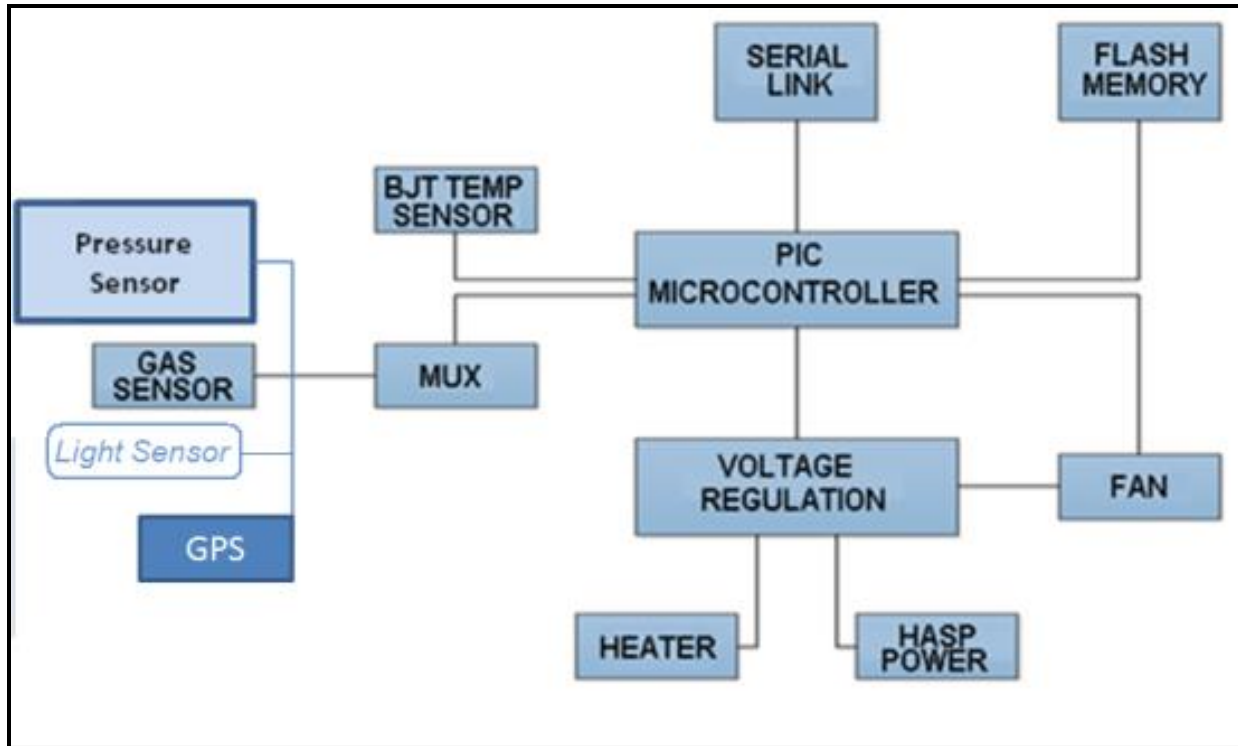


Fig. 10(a) Block diagram of payload circuit

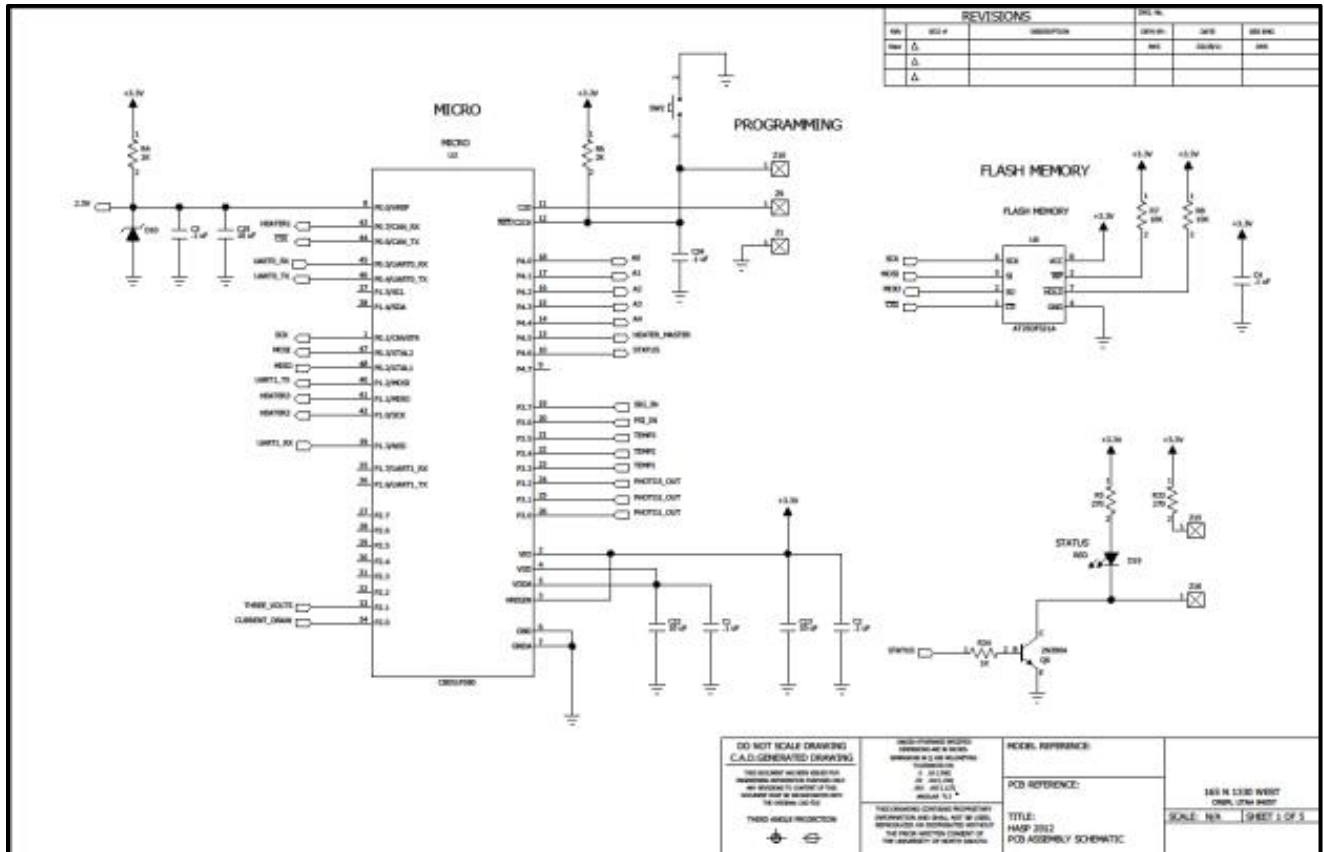


Fig. 10 (b) Circuit for microcontroller and flash memory

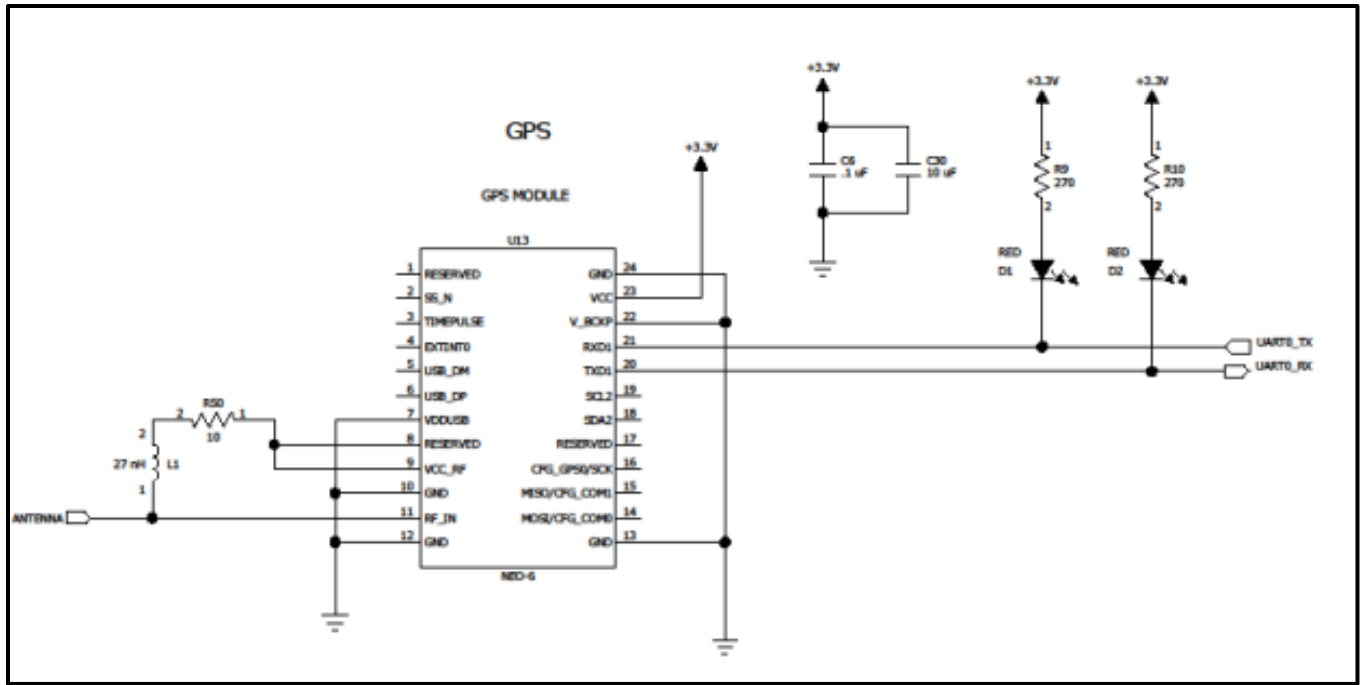


Fig. 10 (c) Circuit for GPS

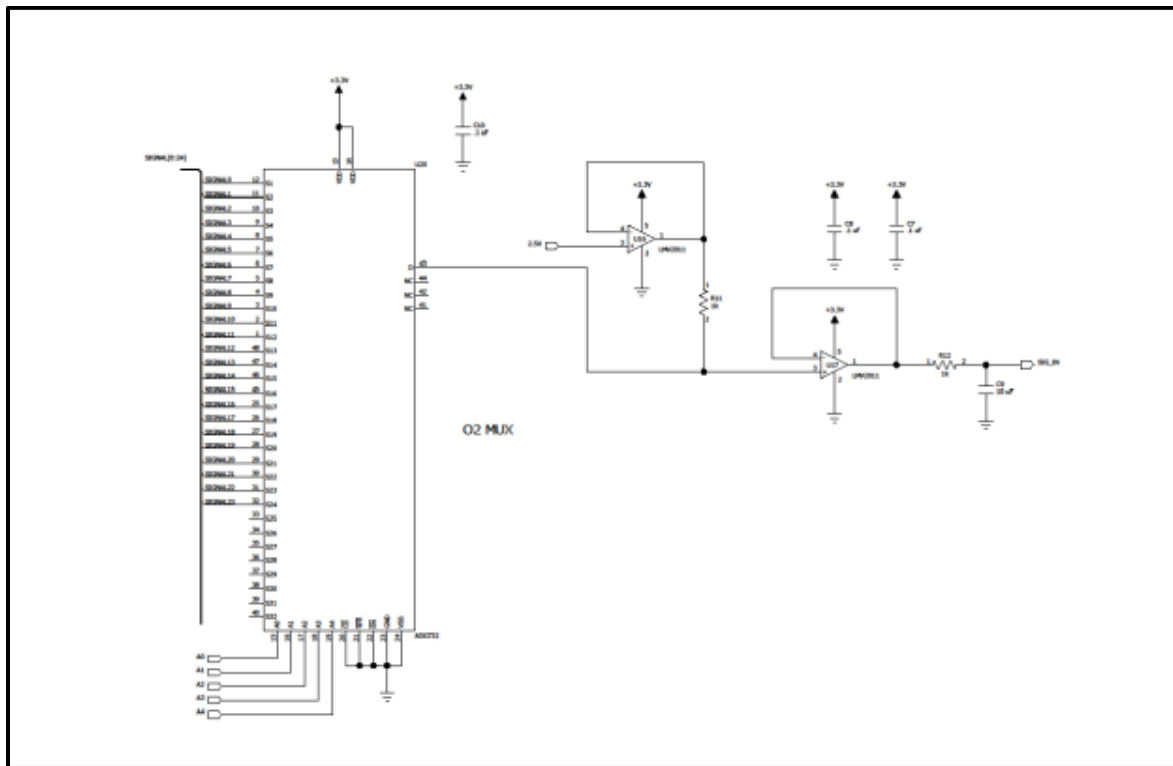


Fig. 10 (d) Multiplexer circuit

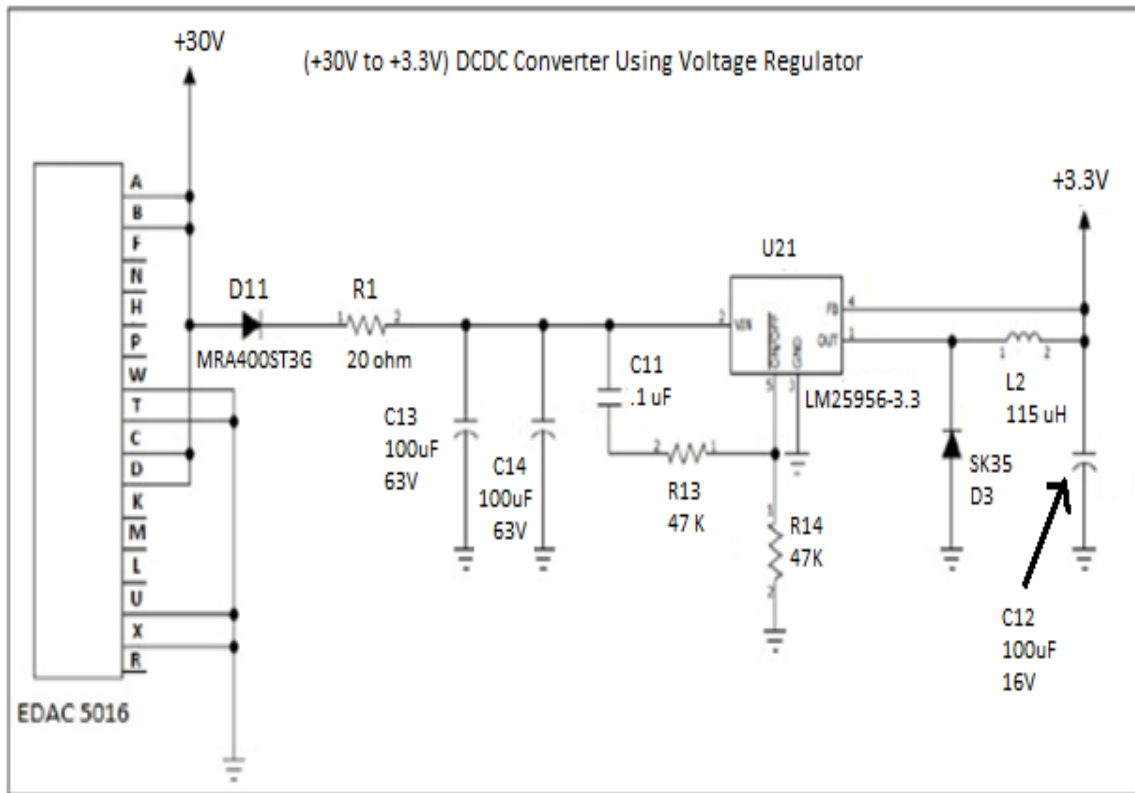


Fig. 10 (e) Voltage regulation circuit

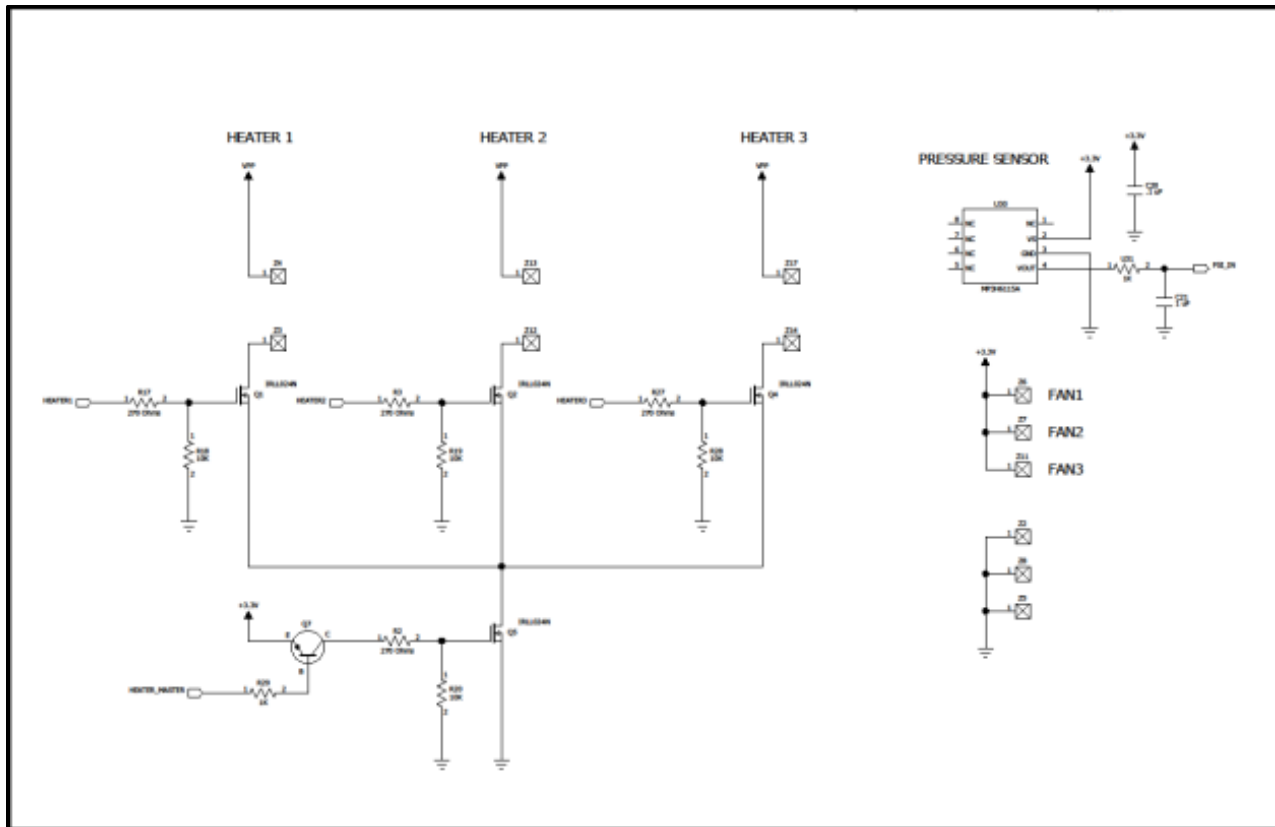


Fig. 10 (f) Circuit for three heaters, three fans and pressure sensor

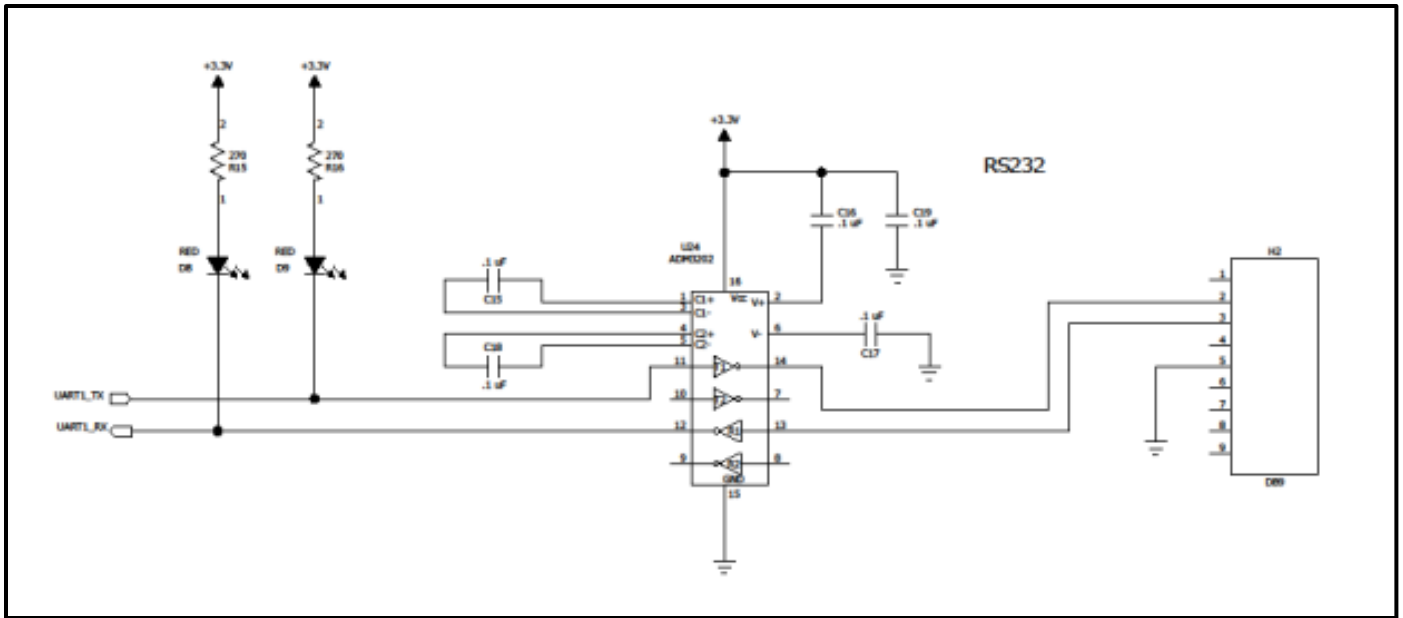


Fig.10 (g) Circuit for RS232

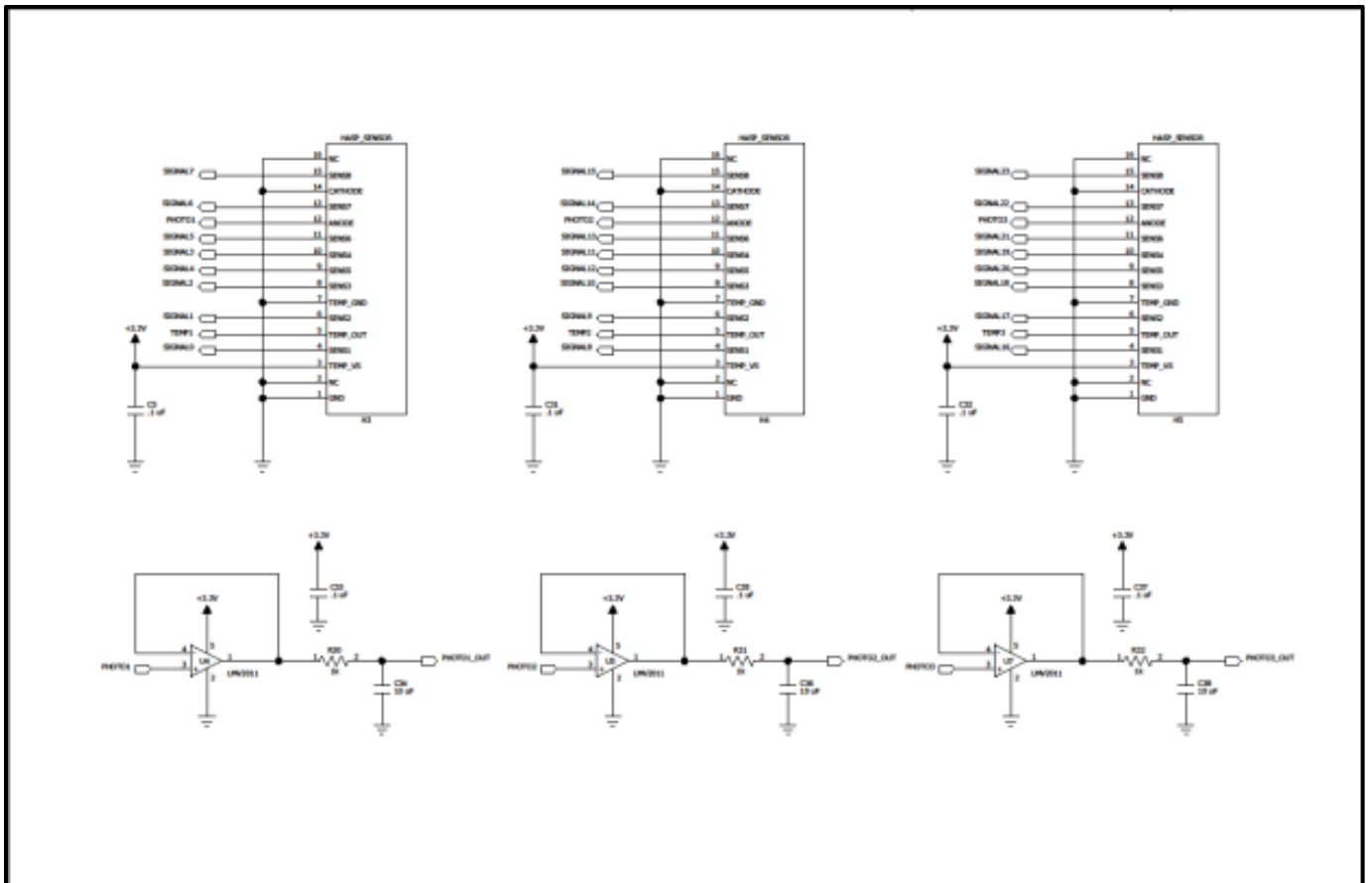


Fig.10 (h) Circuit for three ozone sensors boxes and three photo (light) sensors

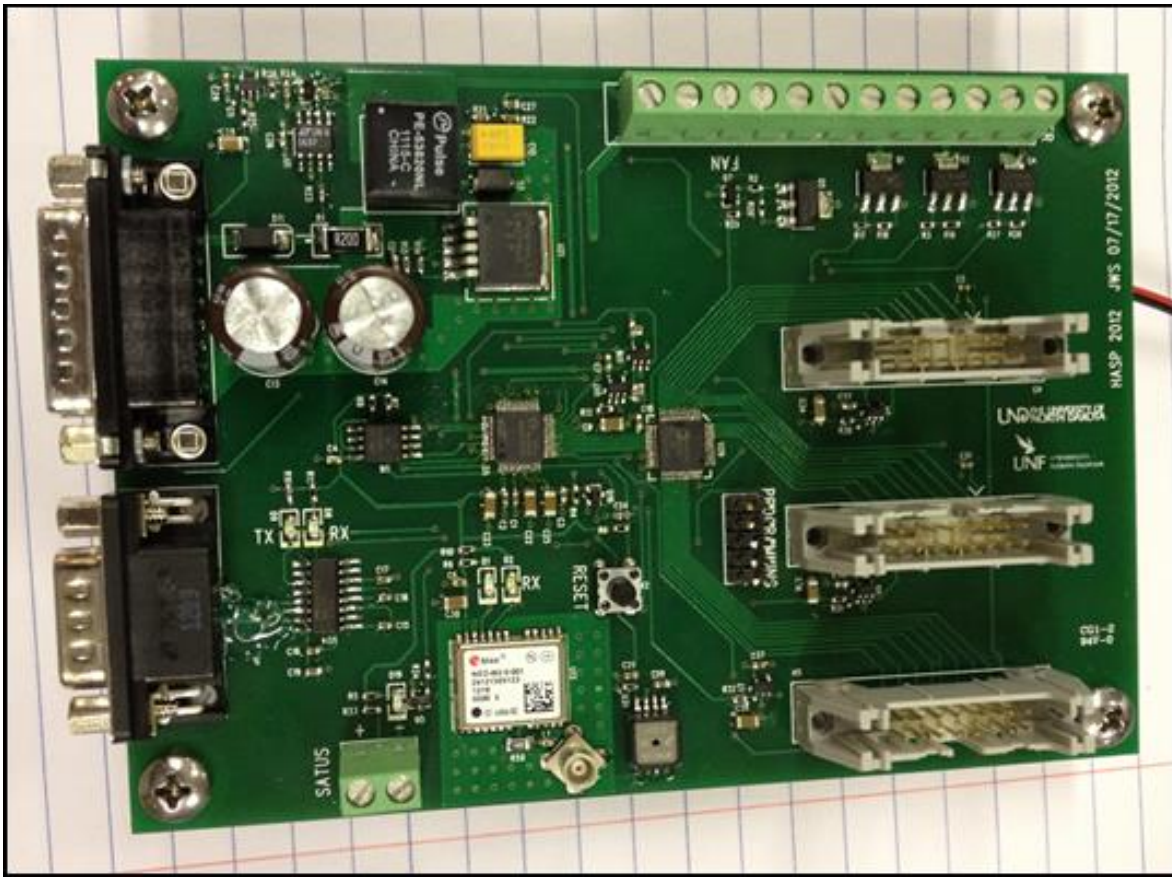


Fig. 10 (i) Picture of microcontroller PCBs

### Predicted Power Budget

The expected current and power drawn by the payload at 3.3 applied voltage are given in the following table-3.

Table-3 Power budget of the payload

Circuit Function	Current Draw (mA) at 3.3 V	Power (W) draw at 3.3 V
Payload Power ON, ALL heaters OFF	$30 \pm 5$	$0.099 \pm 0.017$
Payload Power ON, ONE heater ON	$140 \pm 5$	$0.462 \pm 0.017$
Payload Power ON, TWO heaters ON	$250 \pm 5$	$0.825 \pm 0.017$
Payload Power ON, Three heaters ON	$360 \pm 5$	$1.2 \pm 0.017$

The minimum power drawn by the payload will be about  $0.099 \pm 0.017$  W, while maximum power drawn will be about  $1.2 \pm 0.017$  W. Most of time power drawn by the payload during the float will be less than 1.0 W.

## 7. Integration of Payload and Thermal Vacuum Test

The ozone sensors payload was fabricated, assembled and tested at Dr. Patel's lab. Dr. Nirmal Patel (Faculty), Jesse Lard and Corrina Yorke from University of North Florida were participated the HASP 2018 integration workshop at the NASA-CSBF, Palestine, TX (fig.11 (a)) during July 25 to 29, 2018.



Fig. 11(a) Jesse and Corrina (UNF) at CSBF, Palestine, TX

The payload was initially tested by Mr. Anthony Ficklin and Mr. Joshua Collins and then by Mr. Dough Granger and Dr. Greg Guzik.

Fig.1 (b) shows weighing of the payload using the digital balance. The total mass of payload including its HASP base plate was 2.760 kg, which was less than the limit of 3.00 kg + 0.50 kg mass of the HASP base plate (total 3.5 kg).



Fig.11 (b) weighing of the payload

The measured current draw at 30 VDC was measured about 45 mA nominal running (all three heaters OFF) and 387 mA maximum (all three heaters ON) at full load. The current limit was tested for determination of value of a safety fuse. Fig. 12 (a) shows testing of current by Anthony and Joshua ( HASP-LSU), integration of payload with HASP (Fig. 12(b)) and then tested by Dr. Guzik (HASP\_LSU)(Fig. 12(c)).



Fig.12 (a) Mr. Anthony Ficklin and Mr. Joshua Collins are testing of maximum current drawn by the UNF payload.



Fig.12 (b) Integration of payload with HASP by Jesse and Mr. Dough Granger.



Fig.12 (c) Dr. Greg Guzik, Director, LSGC & HASP during testing of UNF payload.

The payload was tested in the BEMCO chamber, which is shown in Fig. 3(a) for high temperature (about 54 °C), low temperature about (-52 °C), high pressure (about 950 mbar), and low pressure (about 1 mbar). Fig. 3(b) shows the picture of participants of various teams, Fig.3(c) shows UNF team members during the thermal vacuum test and fig 3(c and d) shows pictures of UNF team with the payload during thermal vacuum testing and after successfully clearing all the thermal vacuum test and getting certified of the payload for the HASP balloon flight 2018.

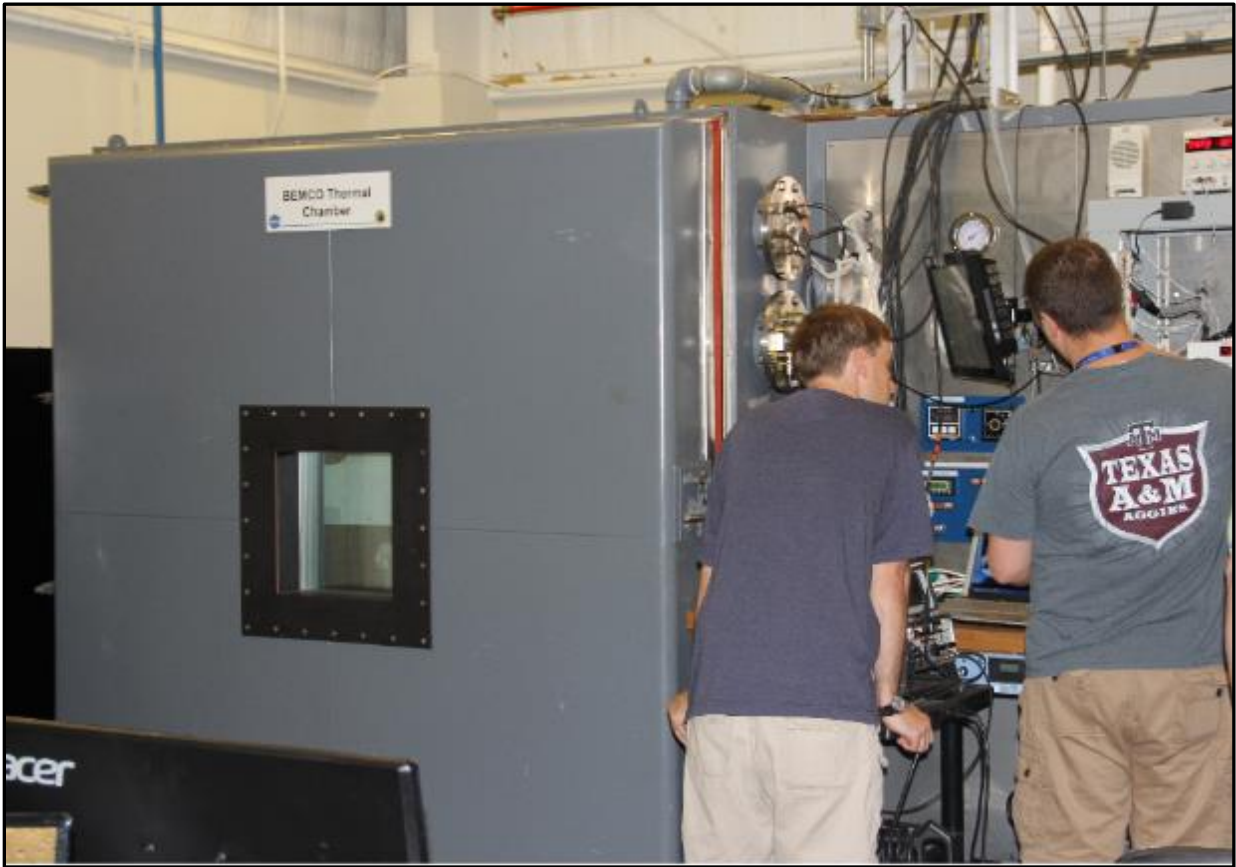


Fig. 13 (a) BEMCO thermal vacuum test chamber



Fig. 13 (b) HASP 2018 Participants from various teams.



Fig.13 (c) UNF team- Corrina, Nirmal, and Jesse (from Left to right) during thermal vacuum testing

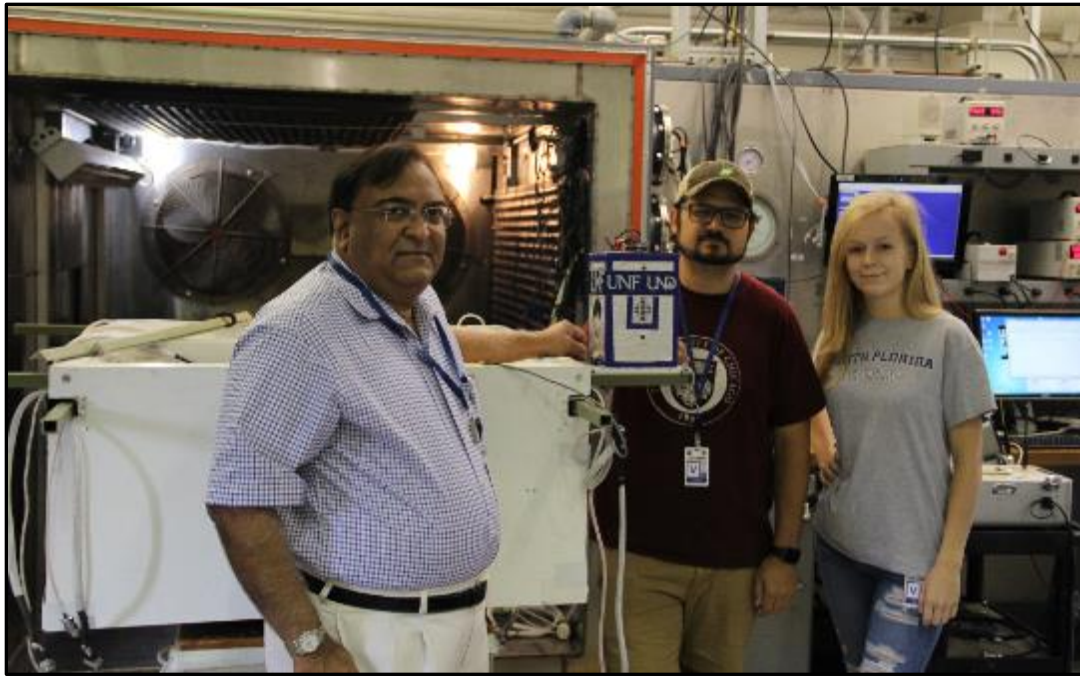


Fig. 13 (d) UNF team- Nirmal, Jesse and Corrina (from Left to right) disintegrating the payload from HASP after successful thermal vacuum test.

During the thermal vacuum test, all sensors data, pressure transducer, UV light sensors, temperature on sensors, heaters, GPS, data communication and uplink commands were tested and verified several times. The payload was certified for the HASP 2018 balloon flight after successful completion of the thermal vacuum test.

Fig.14 shows the variation of voltage with time during thermal vacuum test. The voltage level was nearly constant during test time period. It was found that the average voltage level was 3337.5 mV with standard deviation of 27.0 mV.

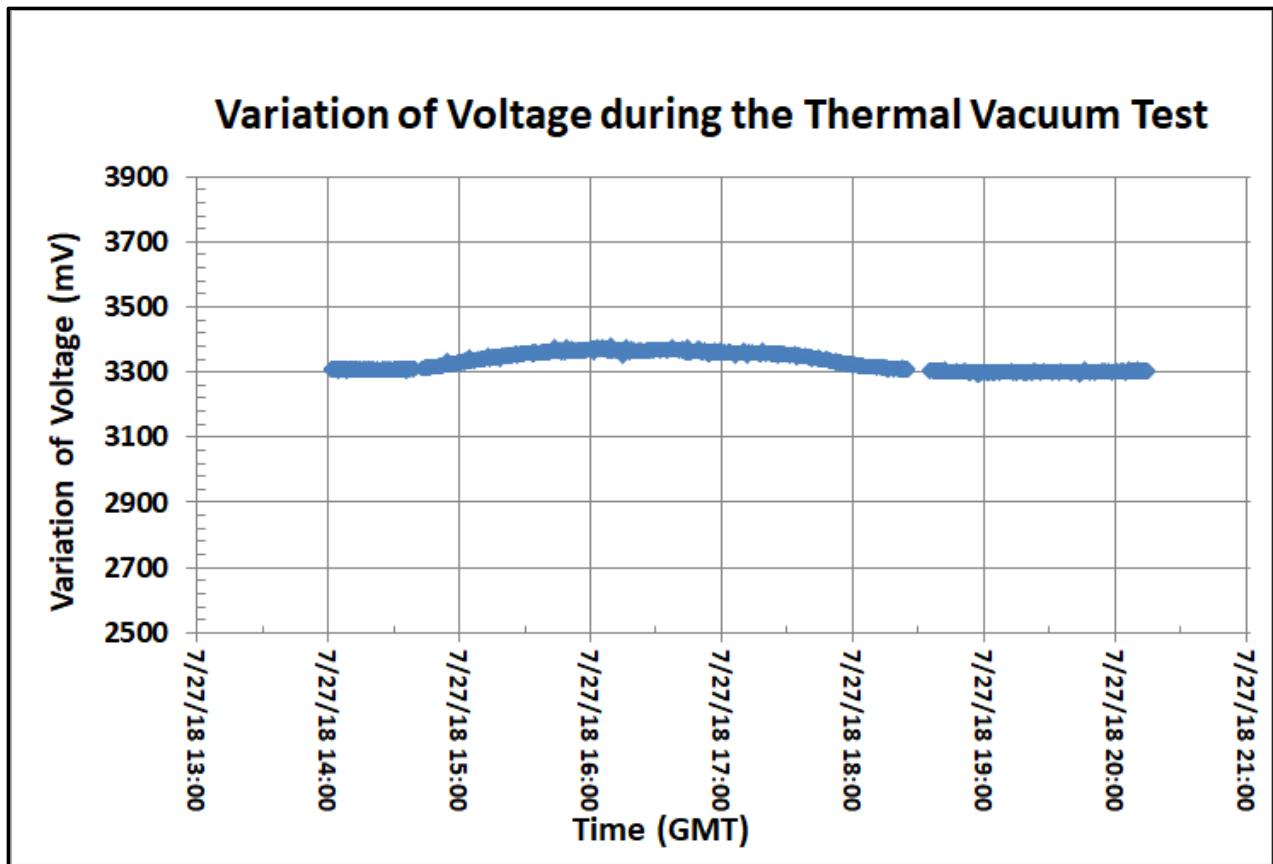


Fig.14 Variation of voltage applied to the payload with time

The current drawn by the payload during the thermal vacuum test is shown in fig. 15 (a). Payload draw (i)  $34 \pm 3$  mA when all three heaters were off, (ii) about  $147 \pm 4$  mA when heater #1 was on, (ii) about  $250 \pm 6$  mA when heaters # 1 and 2 were on, and (iv) about  $356 \pm 6$  mA when all the three heaters #1, 2, and 3 were on. Total time duration for all three heaters on is very small compared to one or two heaters on.

Fig. 15(b) shows variation of voltage and current of the payload during thermal vacuum test measured by HASP (Data courtesy: Mr. Doug Granger, HASP- LSU). These data and plot for voltage and current (fig. 15(b) are nearly match with our measured value of voltage and current (fig.14 and 15(a)).

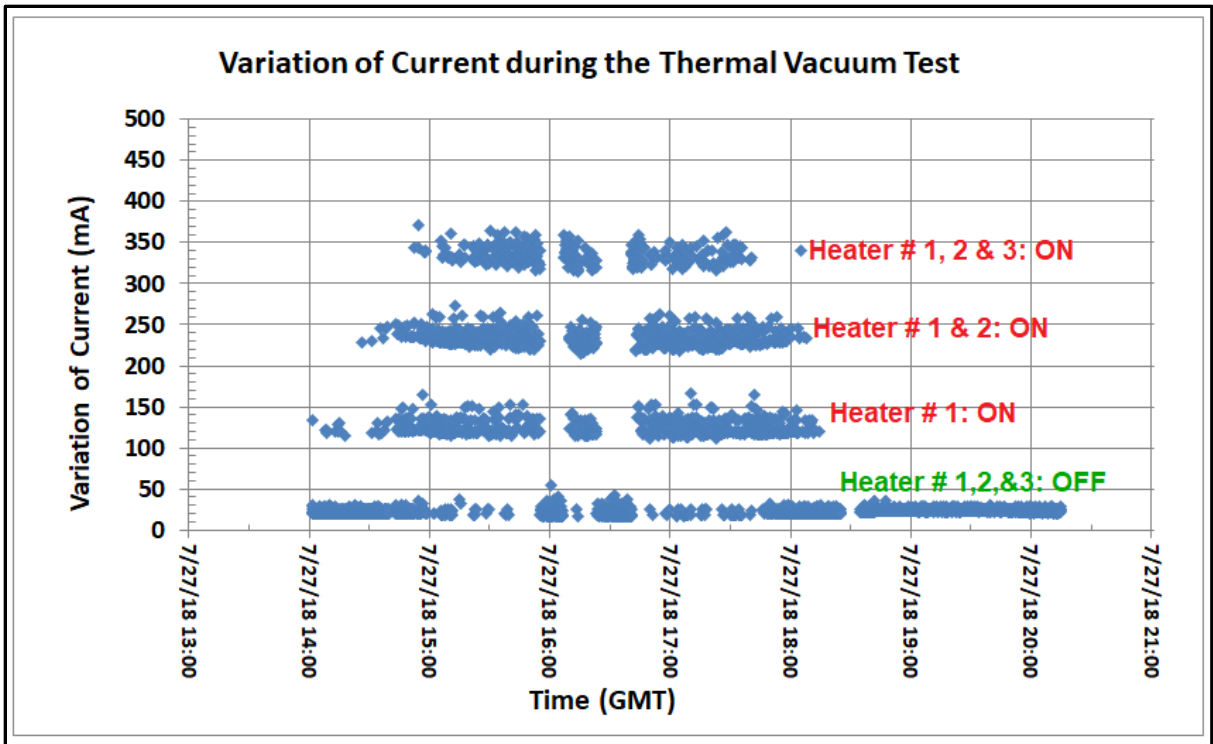


Fig.15 (a) Variation of current consumed by the payload with time.

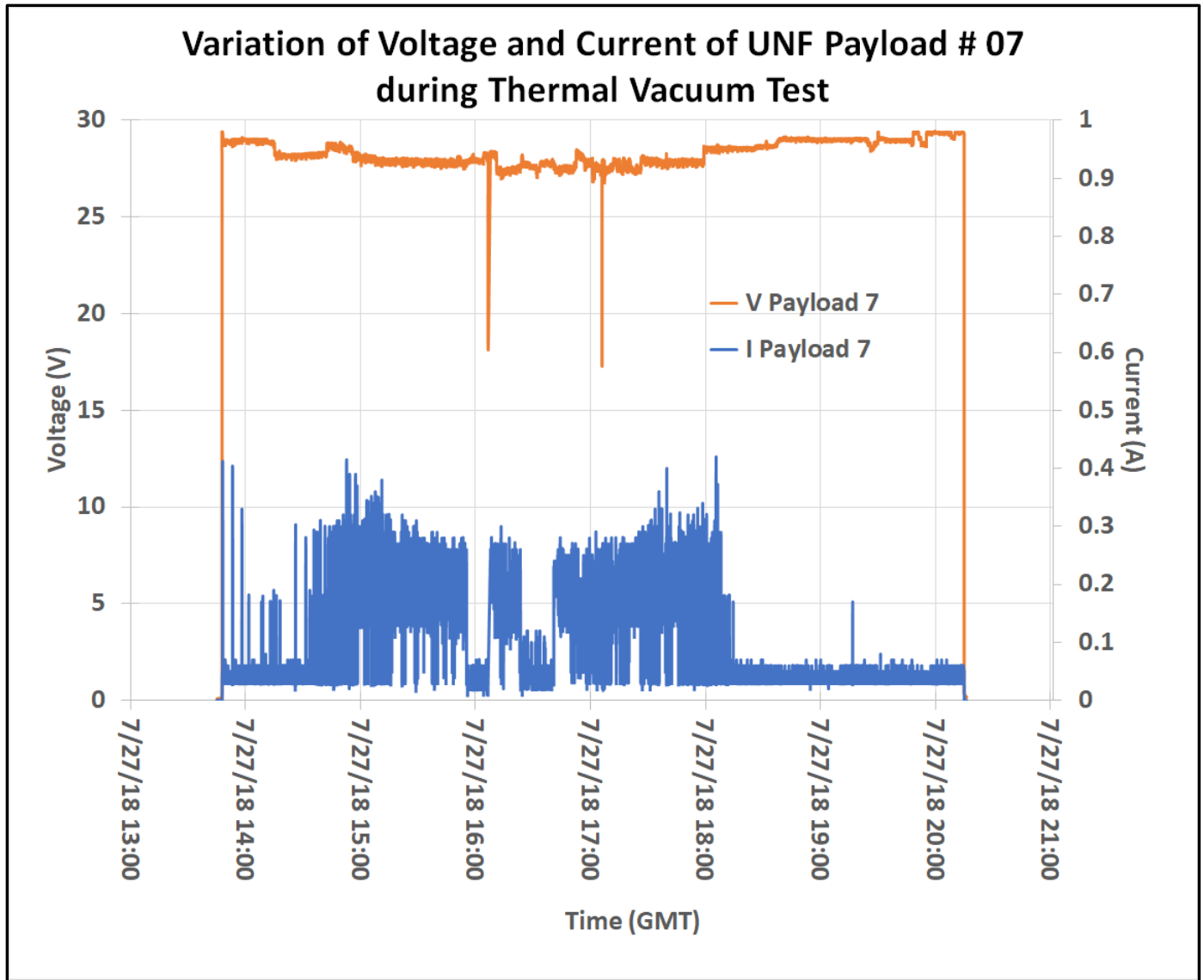


Fig. 15(b) Variation of voltage and current of the payload during thermal vacuum test measured by HASP (Data courtesy: Mr. Doug Granger, HASP- LSU).

The variation of pressure measured by the payload during the thermal vacuum test is shown in the fig.16(a). Our pressure transducer did not measure the pressure below 100 mbar due to its technical limitation and hence saturated. The measured pressure data were nearly matched with the data measured by the HASP pressure transducer, which is shown in the fig. 16(b). In addition, fig. 16(b) also shows the variation of temperature measured on the outer surface of the payload -7 body with time during the thermal vacuum test.

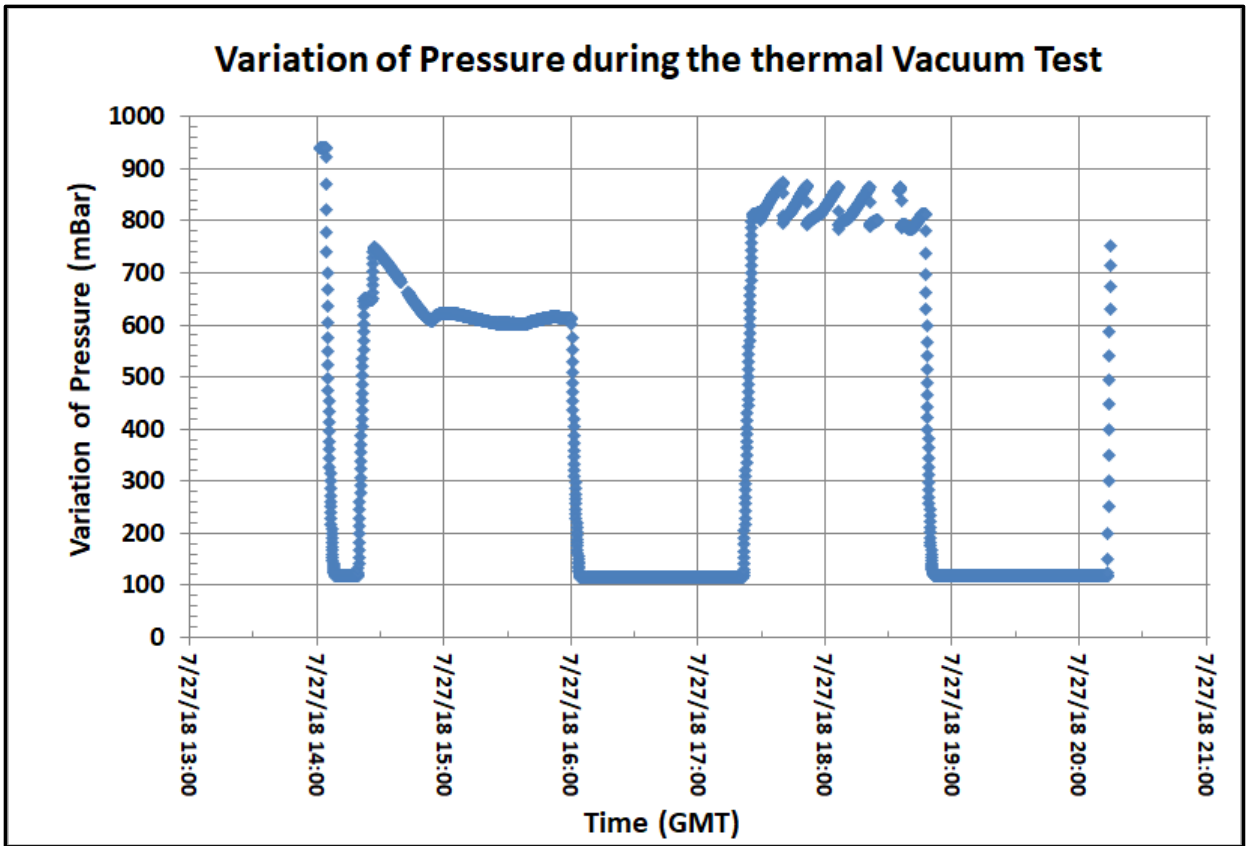


Fig.16 (a) Variation of pressure in the thermal vacuum chamber with time measured by the pressure transducer of UNF payload

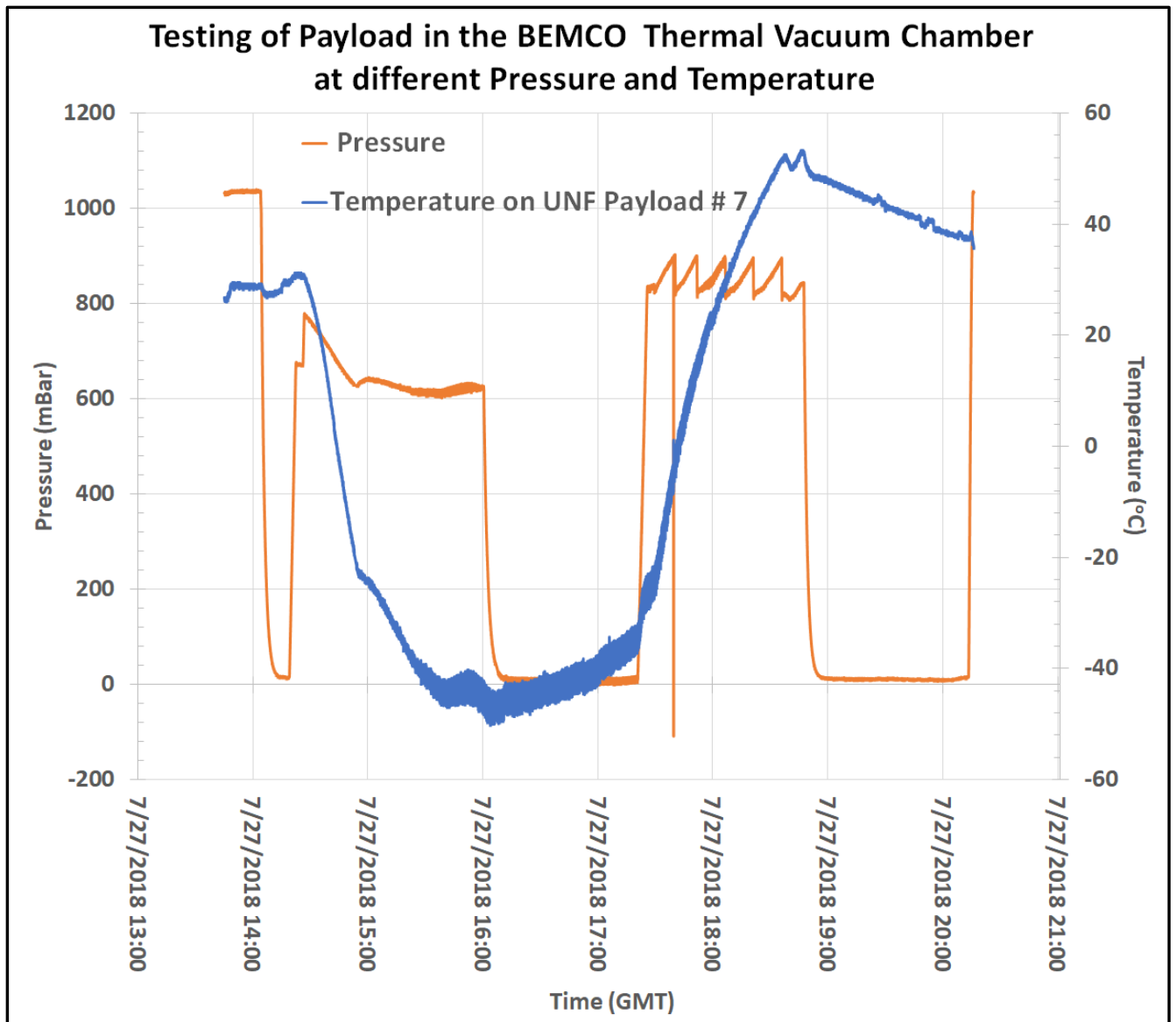


Fig.16 (b) Variation of pressure and temperature in the chamber with time measured by HASP (Data courtesy: Mr. Doug Granger, HASP- LSU).

The resistance of 8 sensors in box #1, 2 and 3 was measured during the thermal vacuum test and are shown in the fig. 17 (a), (b) and (c), respectively. It was observed that the resistance of all sensors was nearly constant during the test. It was also found that the resistance was slowly decreasing with time after 17:00 GMT. The ambient temperature in the chamber was set to increase at 17:00 GMT for about 3:15 hours. Due to the semiconducting properties of the sensor materials, it was expected that its electrical resistance should decrease with increasing of the ambient temperature as well outgassing from chamber wall, surface of hardware of platform and all payloads. However, that variation was reasonably small.

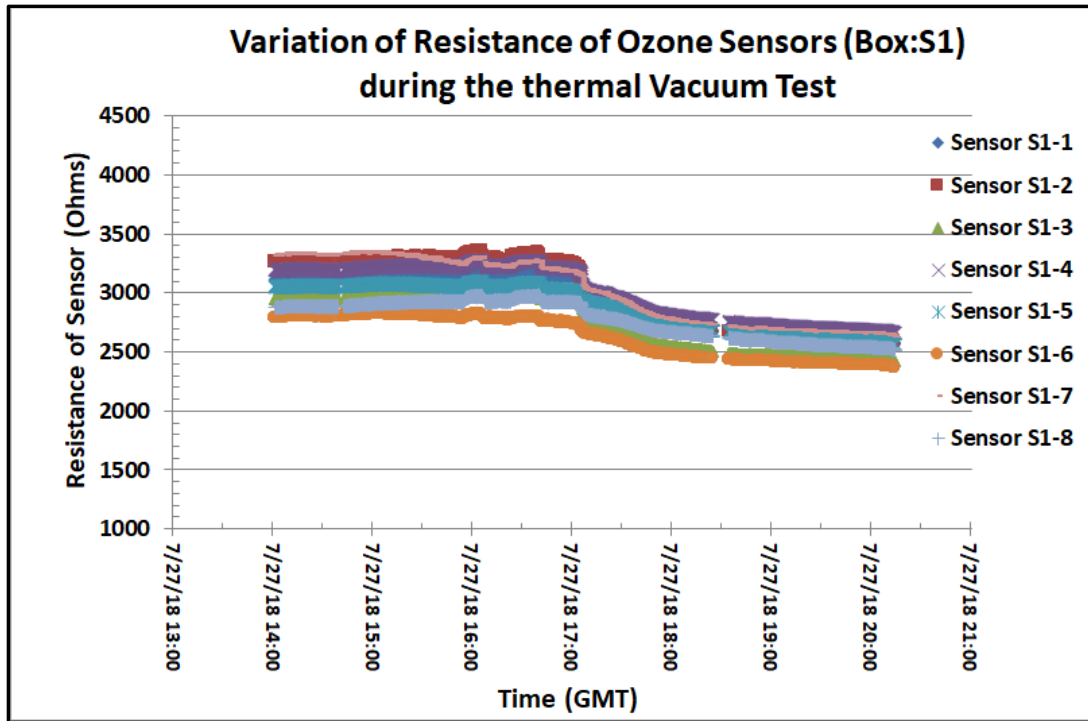


Fig.17 (a) Variation of resistance of gas sensors of sensors box #S1 with time during the thermal vacuum test

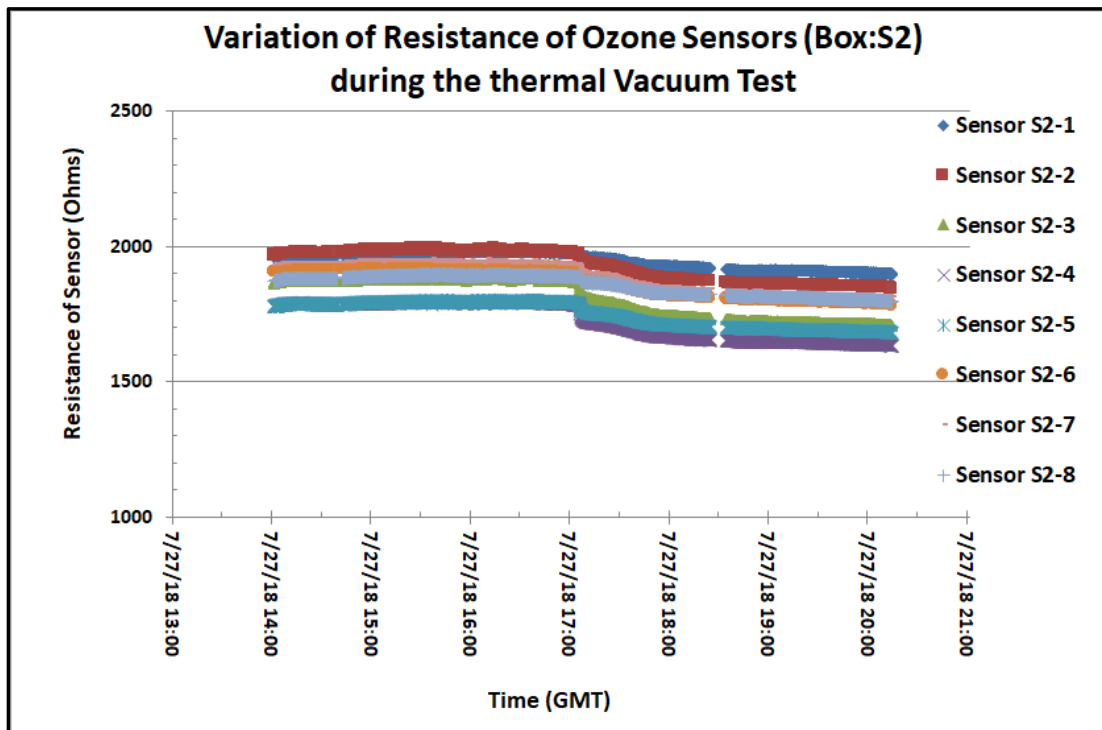


Fig.17 (b) Variation of resistance of gas sensors of sensors box #S2 with time during the thermal vacuum test

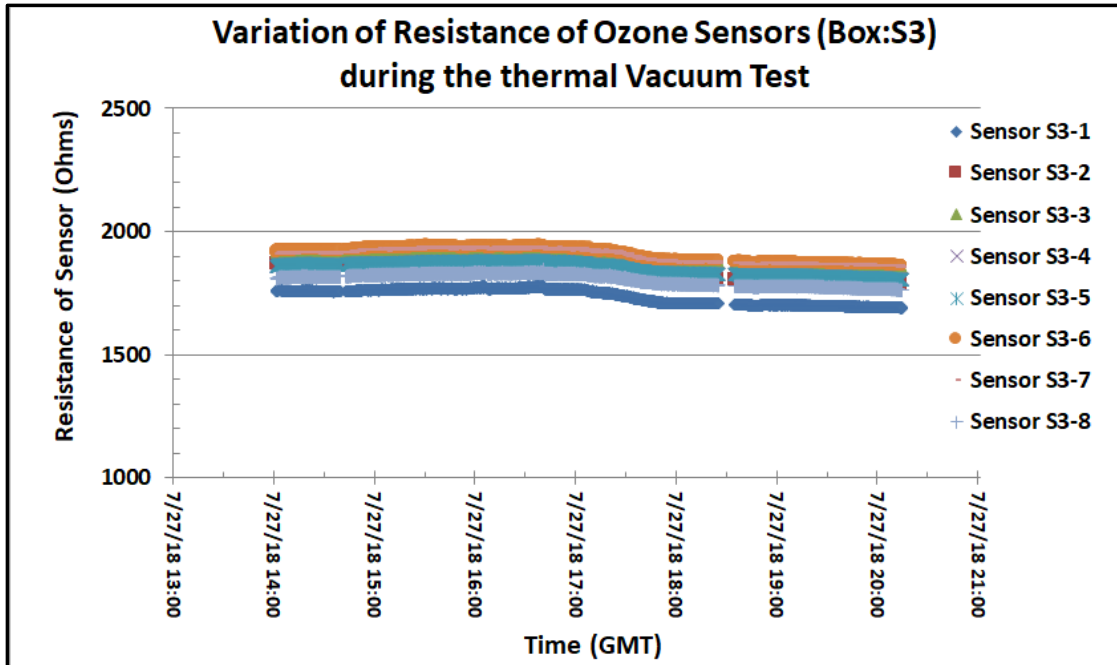


Fig.17 (c) Variation of resistance of gas sensors of sensors box #S3 with time during the thermal vacuum test

It was found that the sensors resistance was quite stable during the low temperature test cycle. A heater mounted on the back side of the sensors array was controlled by the on-off controller and maintained the temperature of sensors array constant during the low temperature test cycle.

Fig.18 shows the variation of temperature of all three sensors arrays with time. It shows all three arrays remain at the constant temperature during the test. Two small spikes of decrease in temperature were observed around 16:05 to 17:00 GMT due to intentionally turned off all three heaters and then turned on for testing of the uplink command two times as a part of testing procedure.

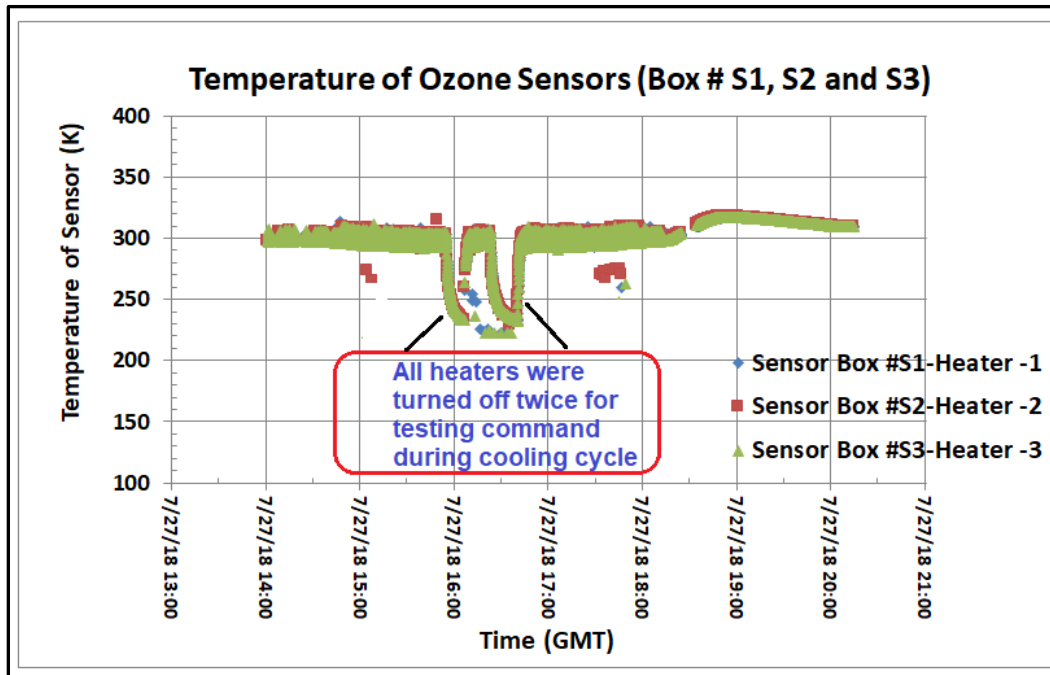


Fig.18 Variation of temperature of gas sensors of sensors box #S1, S2 and S3 with time during the thermal vacuum test

Fig. 19 (a) shows the response of photo diode sensors mounted on sensors boxes with time. It was observed that all three photodiode sensors were in working condition. The variation of photo voltage with time was due to stray light in the chamber, radiation heaters mount in the test chamber (Fig. 19 (b)).

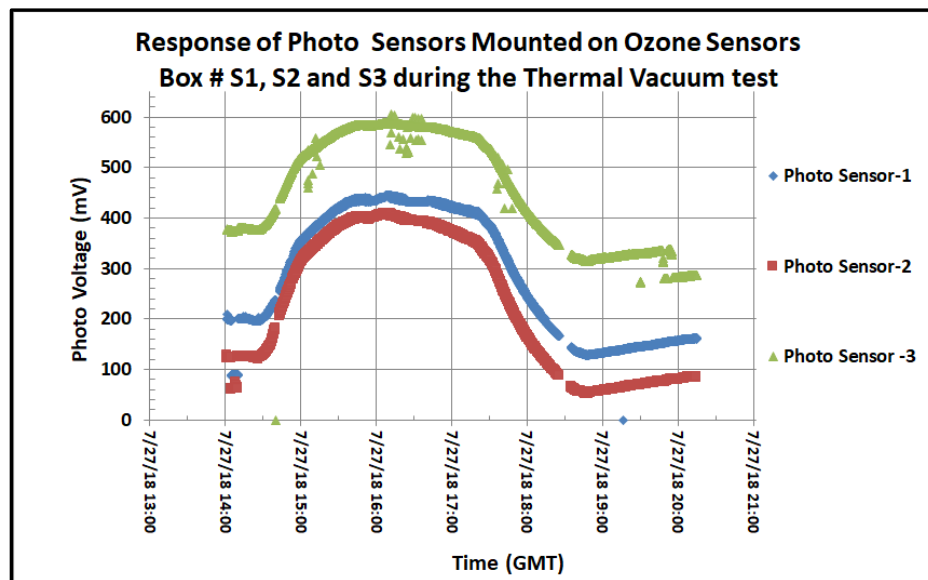


Fig.19 (a) Response of photo sensors mounted on Sensors box #S1, S2 and S3 with time during the thermal vacuum test



Fig. 19 (b) Inner view of a thermal vacuum test chamber shows stray light in the chamber and radiation heaters.

During the thermal vacuum test, we have successfully tested five uplink commands. These commands were mainly for rest payload system, switching the payload GPS to HASP GPS, switching HASP GPS to the payload GPS, switching OFF all heaters and switching ON all heaters switch. Fig.20 (a) shows how our data were changed in the EXCEL worksheet due to execution of the uplink commands.

HASP2018 Thermal Vacuum Test # 1, Friday, July 27, 2018									
Payload # 7, Testing of Uplink Commands									
<b>Turn Master Heater Switch OFF</b>									
Command: HEAT_ON Hex Code: 7535									
GPS Stamp	Time (UNIX/GMT)	Time (CST)	Time (GMT)	PHOTO3 (mV)	VOLT (mV)	CURRENT (mA)	PRESSURE (mBar)	Heater Status	
HASP2013 UBLOX	155500	10:55 AM	15:55:00	582	3367	340	614	111	
HASP2013 UBLOX	155505	10:55 AM	15:55:05	583	3366	230	614	110	
HASP2013 UBLOX	155510	10:55 AM	15:55:10	583	3367	230	614	110	
HASP2013 UBLOX	155515	10:55 AM	15:55:15	582	3368	340	614	1111	
→ HASP2013 UBLOX	155520	10:55 AM	15:55:20	583	3366	19	614	1111	
HASP2013 UBLOX	155525	10:55 AM	15:55:25	583	3367	19	614	1111	
HASP2013 UBLOX	155530	10:55 AM	15:55:30	583	3366	25	614	1111	
<b>Turn Master Heater Switch ON (Default)</b>									
Command: HEAT_OFF Hex Code:7636									
HASP2013 UBLOX	160620	11:06 AM	16:06:20	588	3373	17	115	1111	
HASP2013 UBLOX	160625	11:06 AM	16:06:25	588	3373	18	115	1111	
→ HASP2013 UBLOX	160710	11:07 AM	16:07:10	589	3372	360	115	111	
HASP2013 UBLOX	160715	11:07 AM	16:07:15	589	3372	331	115	111	
HASP2013 UBLOX	160745	11:07 AM	16:07:45	588	3372	337	115	111	
<b>"Reset System" shown by "Hello" in the data string</b>									
Command: RESET Hex Code: 7131									
GPS Stamp	Time (UNIX/GMT)	Time (CST)	Time (GMT)		1(Ohm)	S1-2(Ohm)	S1-3(Ohm)	S1-4(Ohm)	
HASP2013 UBLOX	180515	1:05 PM	18:05:15	2715	2732	2539	2802	2709	
HASP2013 UBLOX	180520	1:05 PM	18:05:20	2719	2736	2539	2802	2709	
→ HELLO									
HASP2013 UBLOX	180530	1:05 PM	18:05:30	2726	2732	2542	2802	2709	
HASP2013 UBLOX	180535	1:05 PM	18:05:35	2709	2729	2536	2795	2705	
HASP2013 UBLOX	180540	1:05 PM	18:05:40	2709	2726	2536	2798	2705	
<b>Changing our payload GPS (HASP UBLOX) to HASP GPS (HASP)</b>									
Command: HASP_STREAM Hex Code: 7A3A									
GPS Stamp	Time (UNIX/GMT)	Time (CST)	Time (GMT)						
HASP2013 UBLOX	182505	1:25 PM	13:25:05						
HASP2013 UBLOX	182510	1:25 PM	13:25:10						
→ HASP2013	1532715916	1:25 PM	13:25:16						
HASP2013	1532715921	1:25 PM	13:25:21						
<b>Changing HASP GPS (HASP) to our payload GPS (HASP UBLOX) (Default)</b>									
Command: UBLOX_STREAM Hex Code: 7939									
GPS Stamp	Time (UNIX/GMT)	Time (CST)	Time (GMT)						
HASP2013	1532716486	1:34 PM	13:34:46						
HASP2013	1532716491	1:34 PM	13:34:51						
→ HASP2013 UBLOX	183455	1:34 PM	13:34:55						
HASP2013 UBLOX	183500	1:35 PM	13:35:00						

Fig.20 (a). Testing of uplink commands during the thermal vacuum test

Our GPS has also measured the altitude during the thermal vacuum test. The measured values of altitude with time is shown in the Fig.20(b). It shows that the plot having average value of  $131 \pm 18$  m. The measured of values may **not be correct** as it was measured in side the chamber. We can conclude that our GPS as well as HASP GPS both were worked well. There was some noise or minor data communcation issue. We performance of GPS was checked by measurement of the altitude data during the hang test and before launching of the payload.

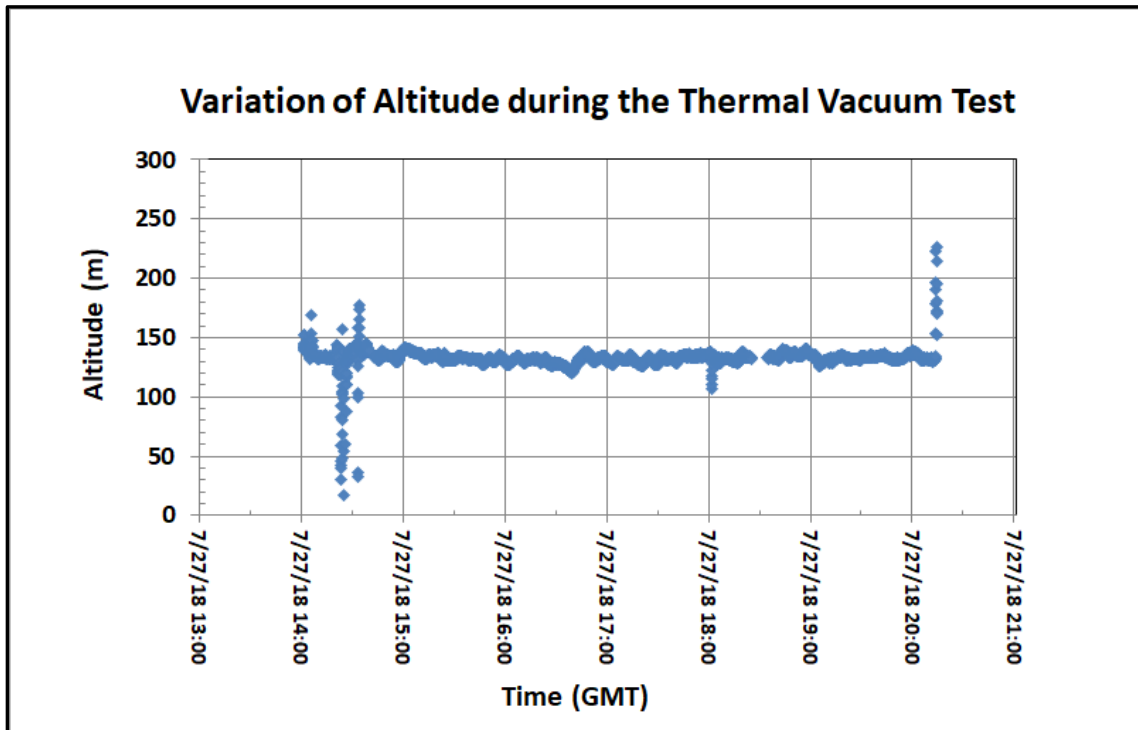


Fig. 20 (b) Measured altitude with time during the thermal vacuum test.

After successful completion of the thermal vacuum test, the payload was disintegrated from the HASP platform. The payload was packed in the shipping box having FedEx prepaid shipping label (Fig. 20 (c)). The payload box was transported to the CSBF, Fort Sumner, NM by HASP-LSU.



Fig. 20 (c) Jesse and Corrina packed the payload.

The payload was again mounted on the HASP platform and power ON test at the CSBF, Fort Sumner. The HASP with all payloads were undergone the hang test and FRR before launching of the balloon flight during first week of September 2018.

## 8. Launching of Payload

The payload was again mounted on the HASP platform and performed the power ON and data communication tests at the CSBF, Fort Sumner. Fig. 21 (a) to (f) shows the pictures of testing of all payloads, hang test, launch preparation, inflating of balloon and launching of balloon at the CSBF, Palestine, TX.



Fig. 21(a) Rolling HASP out to in front of hanger for compatibility testing at CSBF, Palestine  
(Picture Courtesy: Doug Granger, HASP-LSU)



Fig. 21(b) Hang Test of payload at CSBF, Palestine, NM  
(Picture Courtesy: Doug Granger, HASP-LSU)



Fig. 21(c) HASP on “BIG BILL” vehicle.  
(Picture Courtesy: Doug Granger, HASP-LSU)



Fig.21(d) Inflating the balloon with helium gas.  
(Picture Courtesy: Doug Granger, HASP-LSU)



Fig.21(e) Final count down for launch.  
(Picture Courtesy: Doug Granger, HASP-LSU)



Fig.21(e) Launching of balloon.  
(Picture Courtesy: Doug Granger, HASP-LSU)

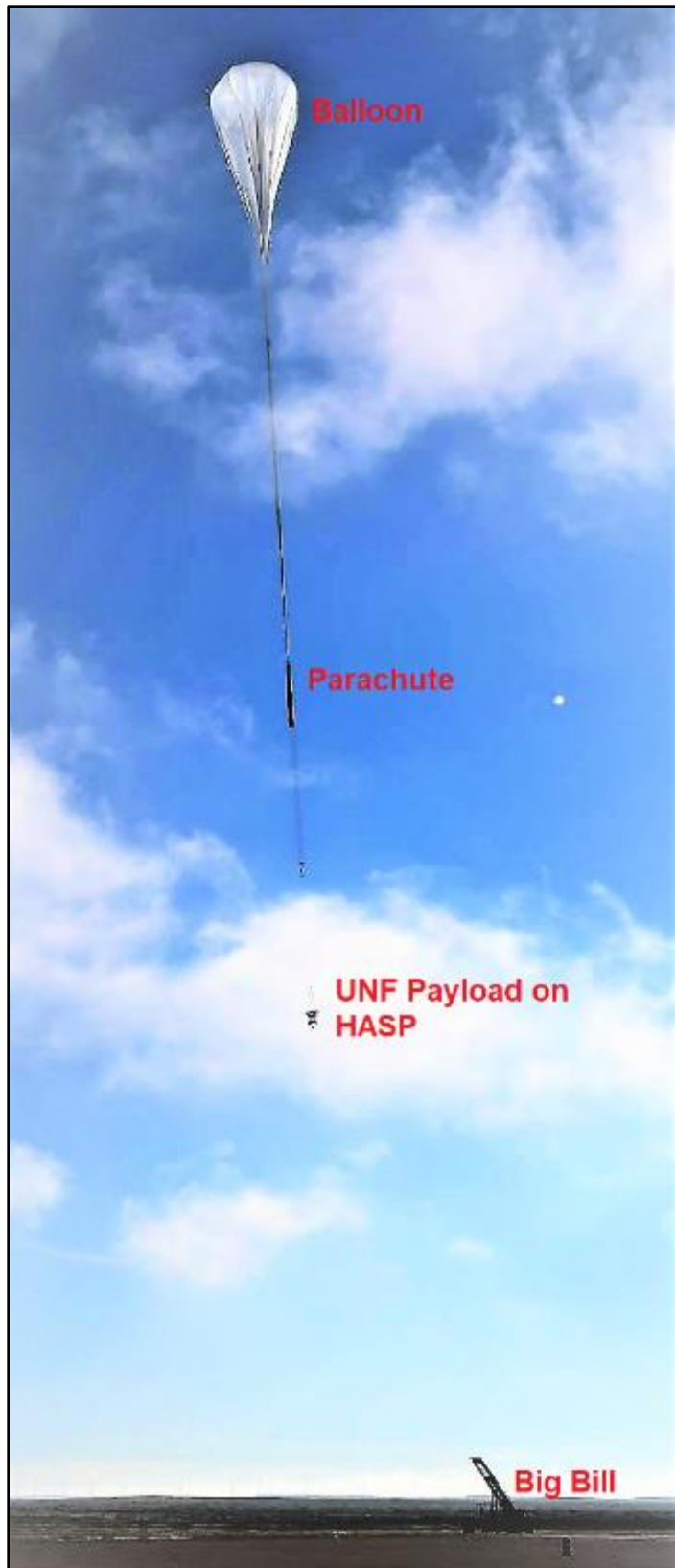


Fig. 21(f) Lift up of HASP.  
(Picture Courtesy: Doug Granger, HASP-LSU)

HASP2018 flight was successfully launched into the stratosphere at an altitude of about 120,000 feet from the NASA- CSBF, Fort Sumner, NM on Monday, September 4, 2018 at 14:03:22 UTC. HASP 2018 balloon flight system typical information is shown in fig.22 (a).

	<b>Balloon Manufacturer</b>	Winzen
	<b>Balloon Type</b>	Zero pressure, 1 cap (W11.82-1E-37 CSBF #979)
	<b>Balloon Size</b>	11.82 million cubic feet
	<b>Parachute Diameter</b>	79 feet
	<b>HASP Weight</b>	411 pounds
	<b>SIP Weight</b>	589 pounds
	<b>Balloon Systems</b>	458 pounds
	<b>Ballast</b>	542 pounds
	<b>Altitude with Ballast</b>	122,500 feet
	<b>Altitude without Ballast</b>	126,000 feet
	<b>Ballast for Drive-Up</b>	140 pounds
	<b>Ballast for Sunset</b>	259 pounds

Fig. 22 (a) Flight system information

(Picture Courtesy: <http://laspace.lsu.edu/hasp/Flightinfo.php>)

A video camera mounted on HASP delivered video stream during the flight. HASP in stratosphere is shown in fig. 22 (b).



Fig. 22 (b) HASP in stratosphere during day time

Fig. 22 (c) shows the flight path of the balloon on the Google map.

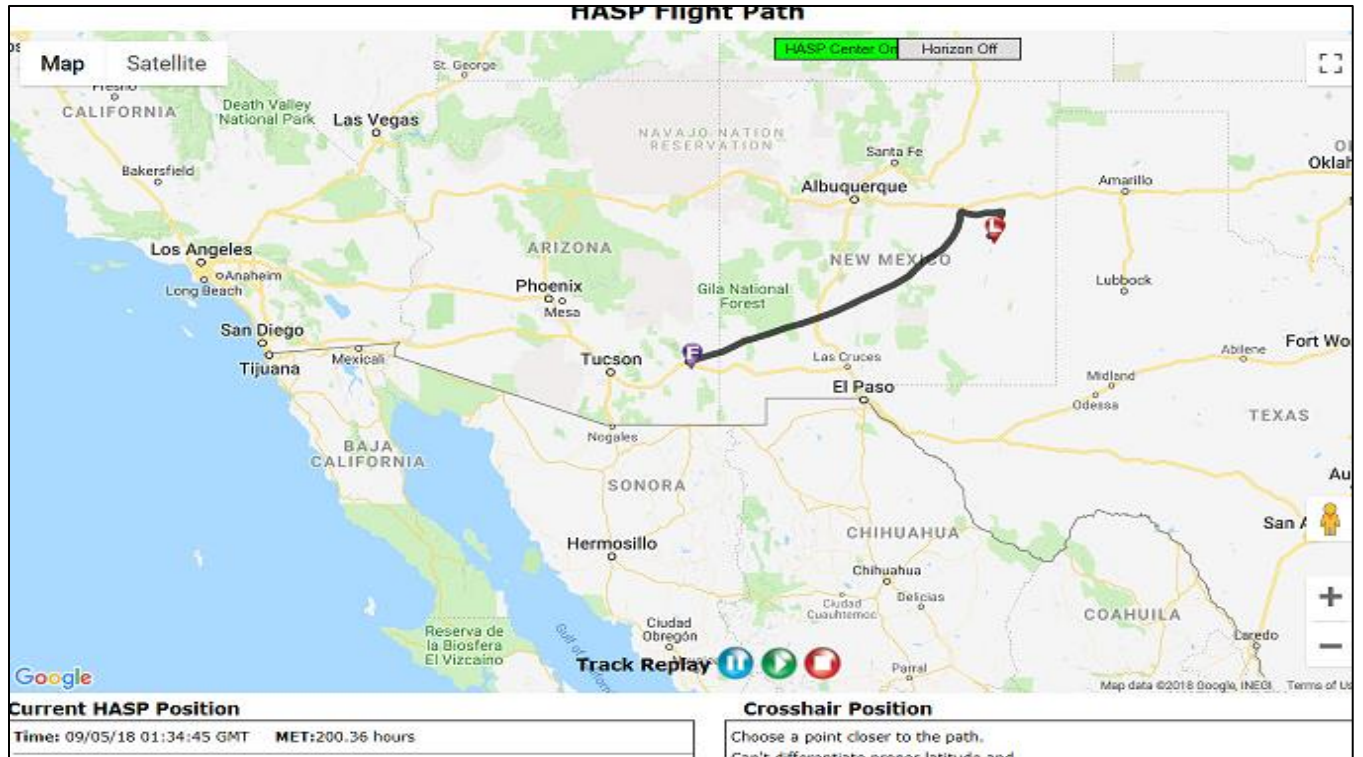


Fig.22 (c) Flight path of the balloon flight on the Google map

The HASP balloon flight was terminated and then impacted near Raso, AZ on September 5, 2018.

Fig. 23(a) to (d) shows the pictures of impact of HASP on the ground after termination. The impact of HASP on the ground was not perfectly vertical. Our payload got direct impact on ground. Our payload was mounted on corner of the gondola. That side was nosed into the turf pretty hard as shown in Fig. 23(a) and (b). We received the payload back with lot of mud on all sides of the payload (Fig. 23 (c) and (d)). About 514 grams of mud was removed from the payload.

We carefully removed the most of mud and dust particles. Then, we powered on the payload as shown in fig. 23 (e). We were surprised with joy that the payload was in working condition. We pulled the data and found that all sensors, heaters, temperature sensors, UV light sensors and GPS are in working conditions. In addition, there was no damage on the body of the payload. We concluded that our payload can work even after bad impact and immersed in to the wet mud too.

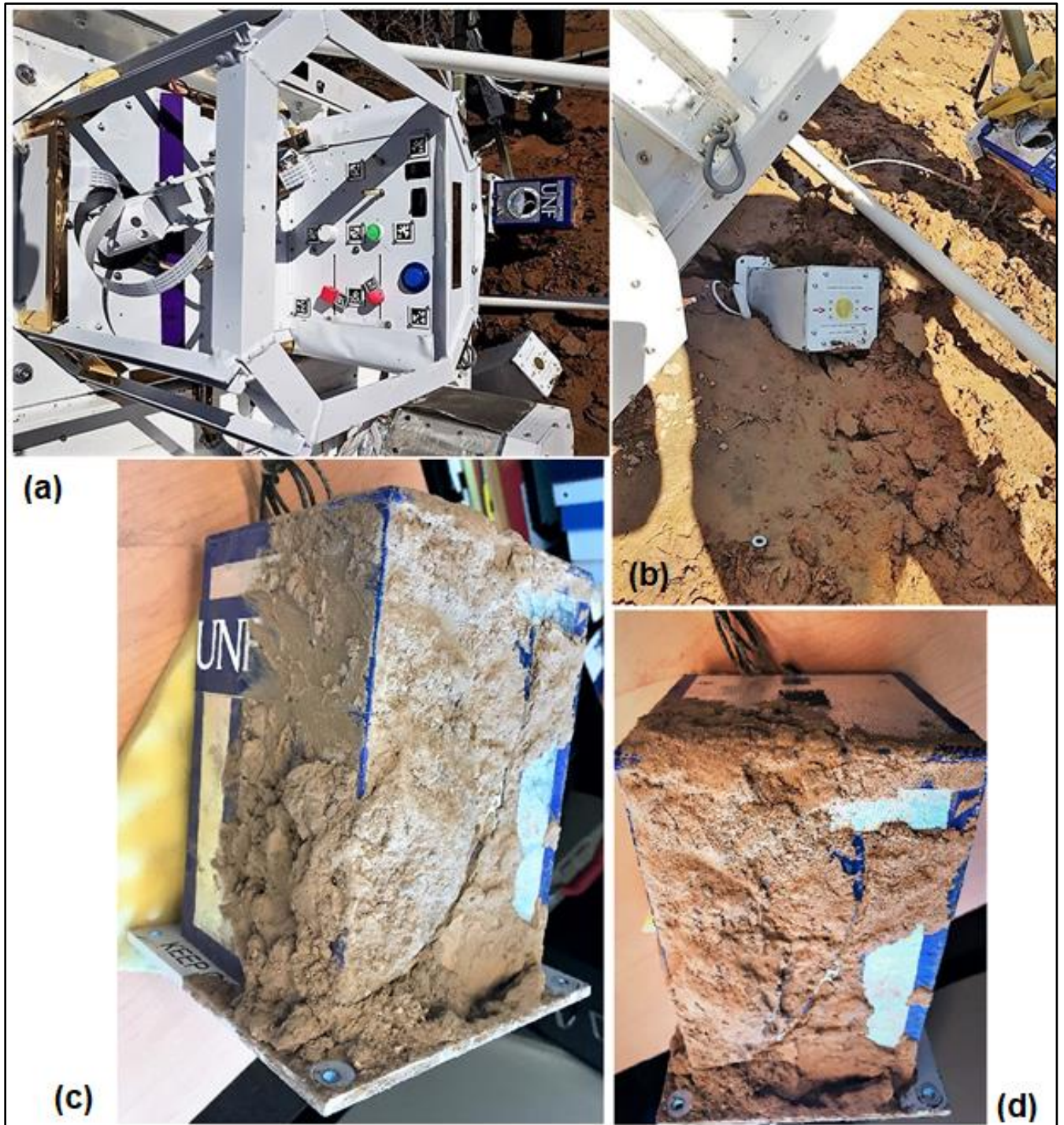


Fig. 23 Impact of HASP and UNF payload on the ground and mud on payload.



Fig. 23 (e) Testing of payload after carefully removing and cleaning of mud from the payload.

## 9. Results and Discussions:

### 9.1 How ozone profile measured in the Starosphere?

Fig. 24 shows various steps for the detection of ozone by the sensors payload during the flight.

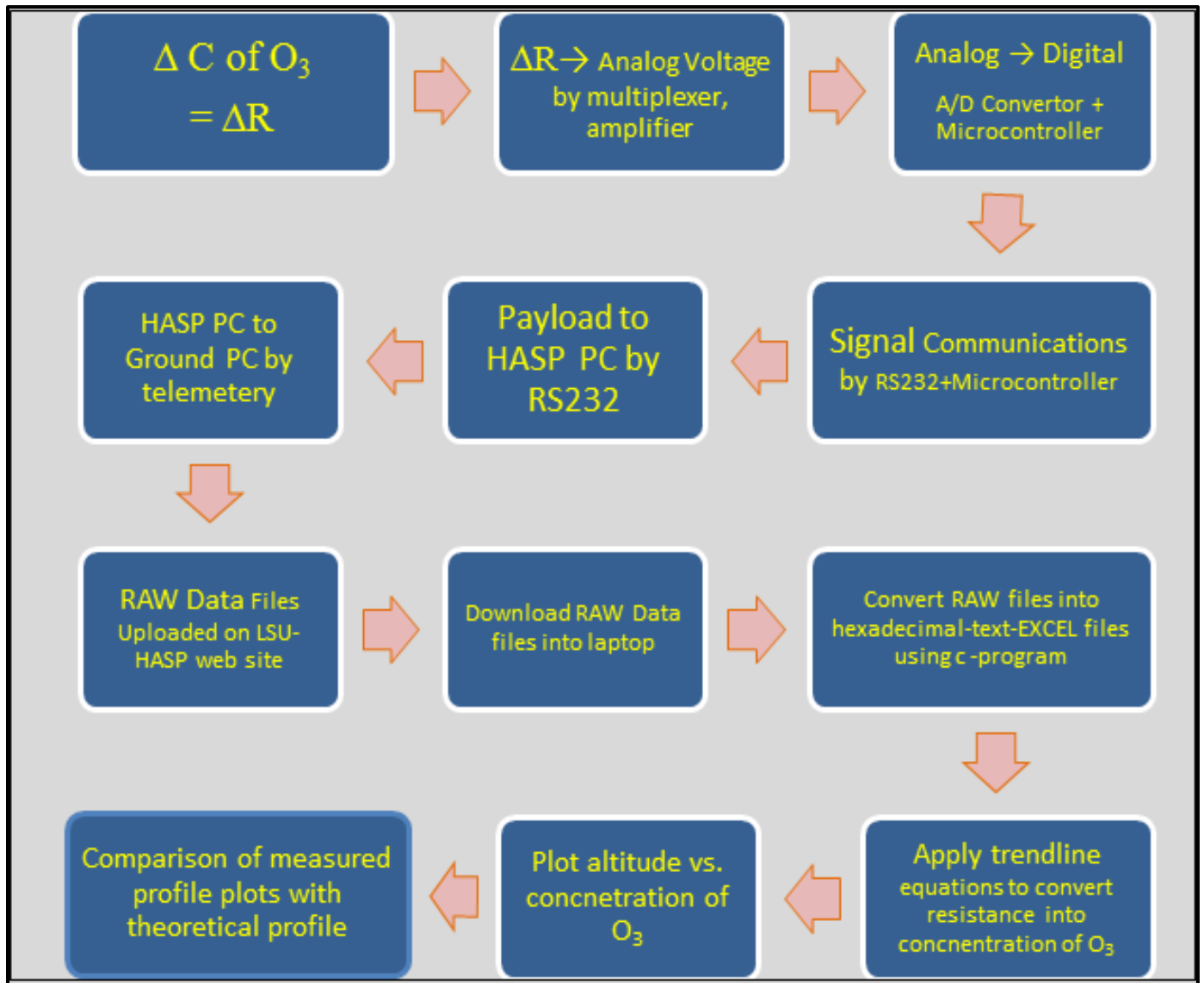


Fig.24 Steps for the detection of ozone by the payload

During the flight, UND-UNF sensors payload measured the ozone profile. The payload sent data files of 25 KB every 18 minutes during the flight time through the NASA-HASP computer and was uploaded on the HASP website. We downloaded all the RAW data files, and converted RAW files into one EXCEL file using the software program. It was found that the sensors, hardware and software worked very smoothly.

## 9.2 Uplinks commands

Uplink commands shown in table-4 for reset, switching the HASP GPS to UBLOX GPS, heater ON and heater OFF were applied for the flight.

Table-4 Uplink commands

Command	Hex Code	Description	Importance
RESET	7131	Reset System	Critical
HEATER_OVERRIDE_ON	7535	Turn Master Heater Switch Off. The main heater switch is disabled so no individual heaters will be able to turn ON.	Critical
HEATER_OVERRIDE_OFF	7636	Turn Master Heater Switch On (default). The main heater switch is enabled and thus each individual heater can turn ON or OFF as needed by the temperature controller.	Critical
UBLOX_STREAM	7939	Stream GPS via Embedded GPS (default)	Critical
HASP_STREAM	7A3A	Stream GPS via HASP GPS	Critical

	A	B	C	D	E
1		Status	Command Requested	Additional Comments	7/6/20
2					(DO NO
3	HASP Payload 01 - UMN	4		Getting moderately warm. Otherwise looking good	9/4/20
4	HASP Payload 02 - CC	4		Payload is functioning	9/4/201
5	HASP Payload 03 - FLC	4		Thanks	9/4/20
6	HASP Payload 04 - MU	4			9/4/201
7	HASP Payload 05 - UMD	5		science trigger received by payload, but the instrument fails to trigger. Loose connection suspect	9/4/201
8	HASP Payload 06 - SDSMT	1	sent x31x31	sent x31x31 again. Please confirm you still want this every hour and it's working	9/4/201
9	HASP Payload 07 - UNF/UND	4		Payload is working fine and data looks good.	9/4/20
10	HASP Payload 08 - SPJ	4		Payload still nominal	9/4/20
11	HASP Payload 09 - US@UK	1			9/4/20
12	HASP Payload 10 - UCB	4		Running pressurization cycles	9/4/201
13	HASP Payload 11 - DTCC	4		appreciated!	9/4/201
14	HASP Payload 12 - UH	4		just cruisin'	9/4/201
15	HASP Payload 13 - ARC	7	You are plugged in and should be working fine - Thanks a million :-)	Here remotely - Previous manual test ok. No telemetry available.	9/4/20
16					8/28/201
17	HASP Status	Just got word that the current trajectory of HASP is going in an unwanted direction and will potentially enter restricted airspace in the next two hours. We will meet with CSBF soon to get more details. The Durham Tech robot arm appears to be operating fine. Live video at <a href="http://laspace.lsu.edu/hasp/video.php">http://laspace.lsu.edu/hasp/video.php</a> . The YouTube HD video is quite impressive. <a href="https://www.youtube.com/watch?v=jIOBXdt62FA">https://www.youtube.com/watch?v=jIOBXdt62FA</a>			9/4/201
18					
19					
20					
21					
22					
23					
24					
25					
26					
27					
28					7/25/20

Fig. 25 Communication templet on Google.

During hang test at CSBF, Fort Sumner, NM and during the balloon flight, we used the Google account for communications with Mr. Doug Granger, HASP-LSU. The Google account templet is shown in fig. 25. We can inform about the payload status, receive the flight information and send request to uplink the command. The advantage of this method for communications is no need to use cell phone to call Mr. Doug Granger.

### 9.3 Balloon Flight Profile and Response of Pressure Sensor

Fig. 26 shows the HASP 2018 balloon flight profile. The altitude profile was measured by our payload GPS. Our UBLOX GPS worked very well during the flight and was not blocked at higher altitude. We did not need to switch to HASP GPS. The average altitude was around 36,800 m during the float. The float time was about 09 hours.

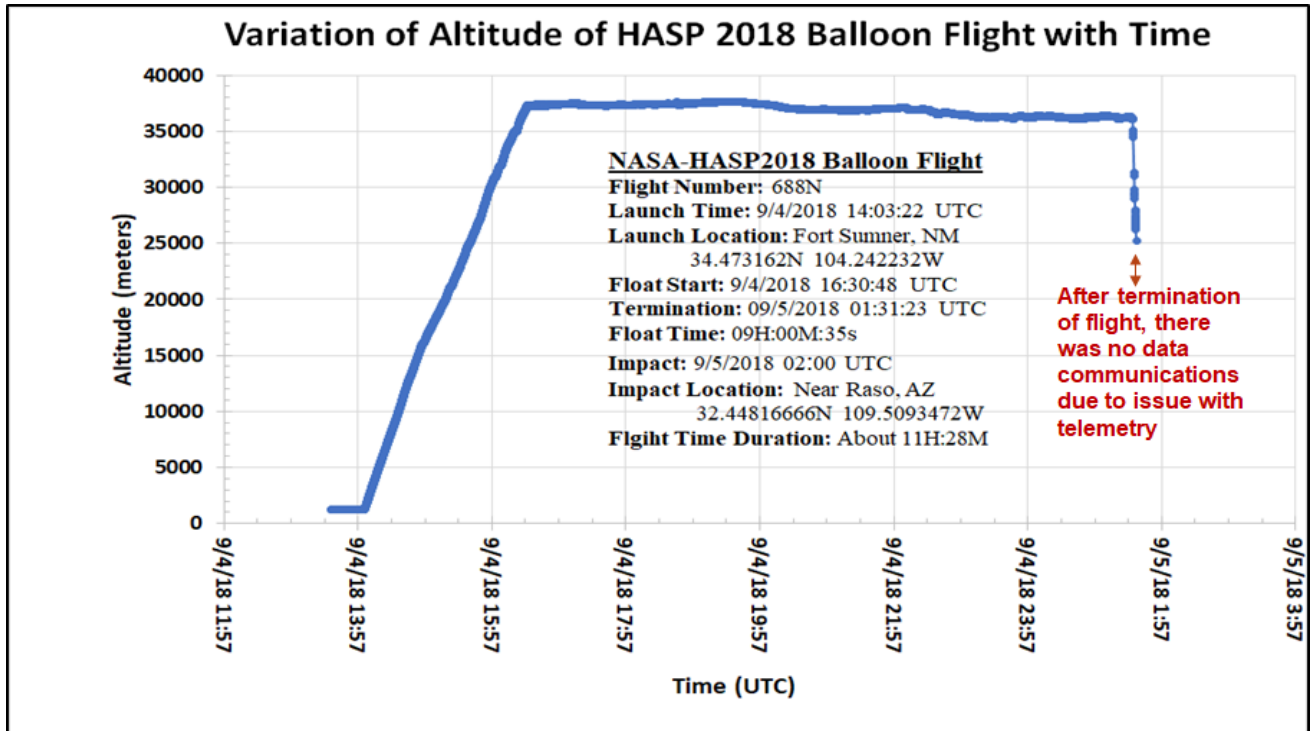


Fig.26 HASP2018 flight profile.

Fig.27 (a) shows the variation of pressure with the altitude during the flight. Pressure was measured by a pressure sensor mounted on the PCB of the payload. It was found that the pressure was decreased with increase of the altitude up about 15 km and then nearly saturate with increase of altitude up to the float. The saturation of pressure around 100 mbar was due to the technical limitation of our pressure sensor. We were not able to change it this year but will try to replace this pressure sensor with one having lower mbar range in the next balloon flight.

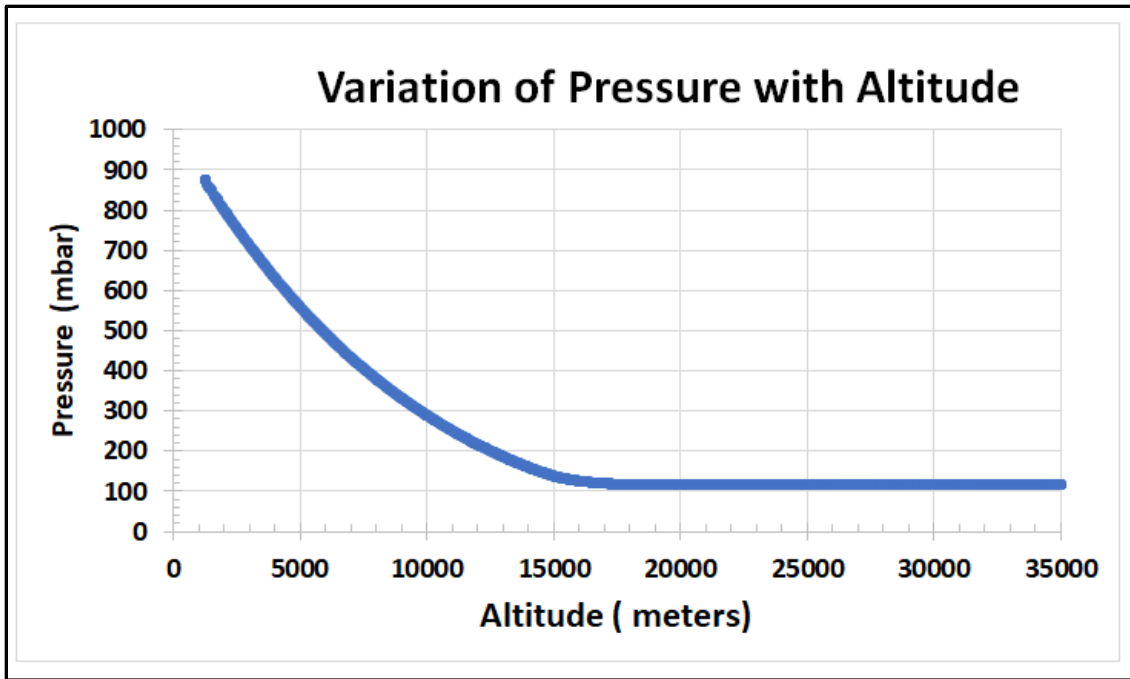


Fig.27 (a) Variation of pressure with the altitude.

Fig. 27 (b) shows the variation of pressure measured by the payload with the flight time (UTC). It shows change of pressure with time during ascending and float. We did not get the data after termination of the flight due to issue of HASP telemetry.

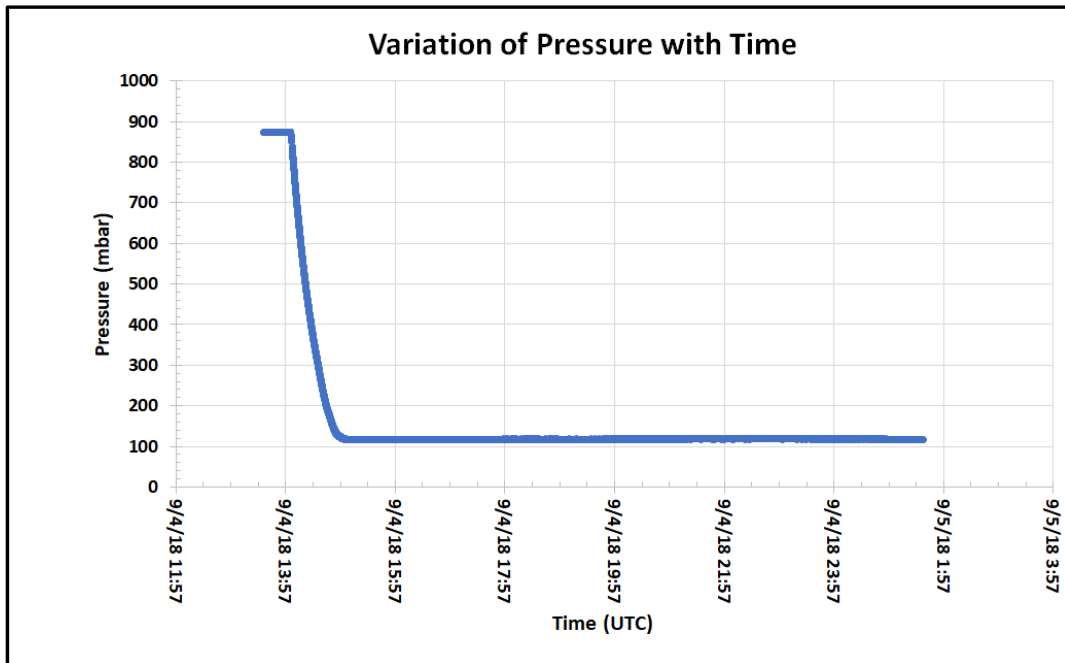


Fig.27 (b) Variation of pressure with the flight time.

#### 9.4 Power budget during the flight

Fig.28 shows the voltage applied to the payload during the flight. It was found that applied average voltage remain nearly constant about  $3300 \pm 25$  mV.

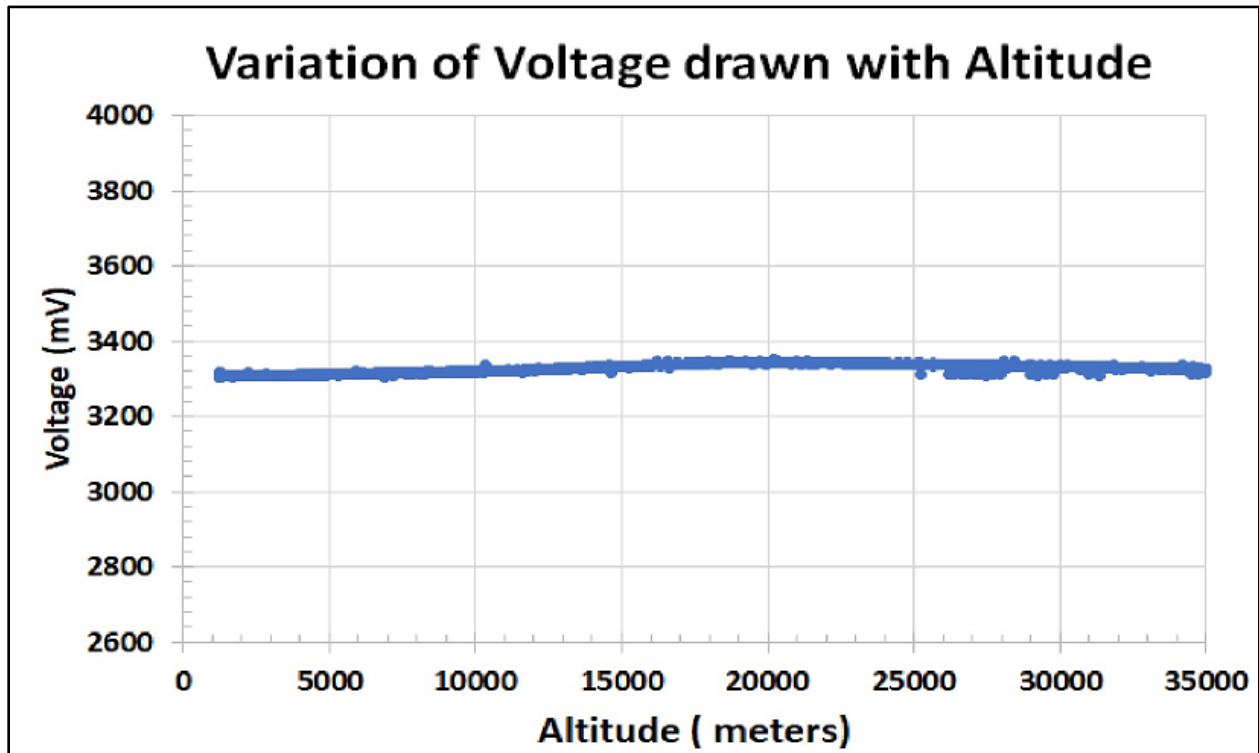


Fig.28 Voltage applied to the payload during the flight.

The current drawn by the payload during the flight is shown in fig. 29.

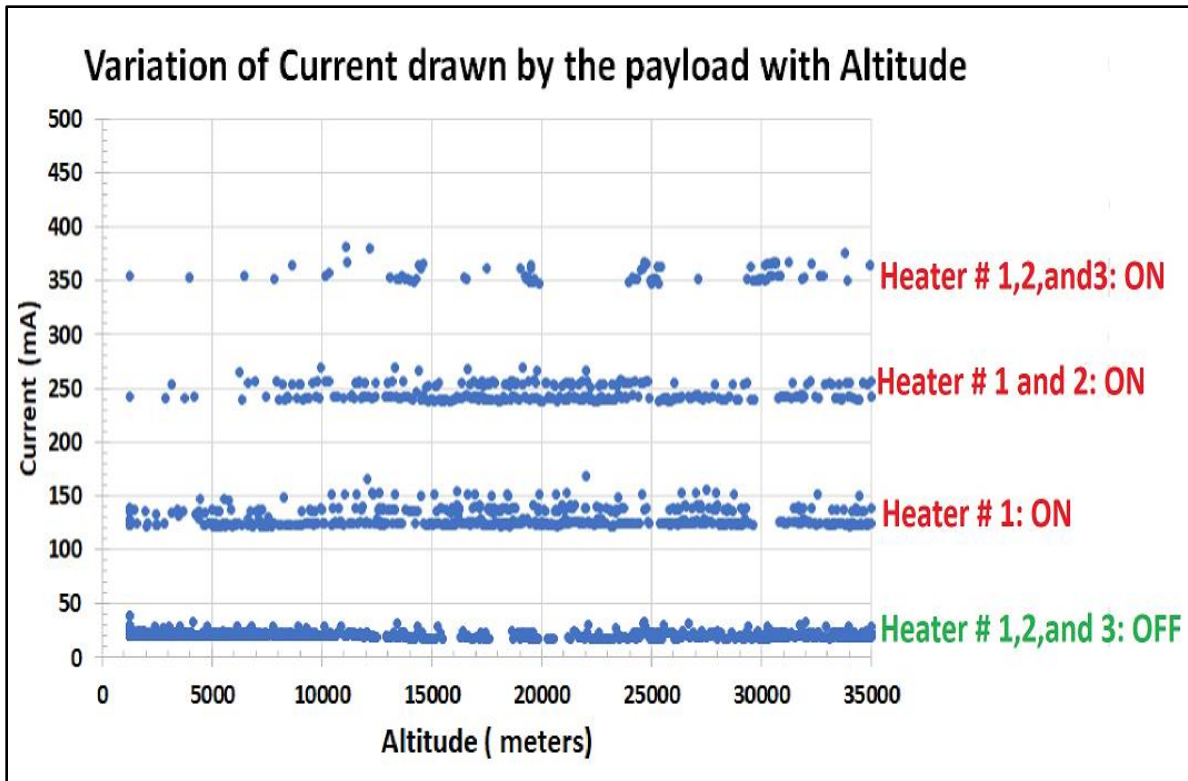


Fig.29 Current drawn by the payload during the flight.

The current drawn by the payload during the flight was

- (i) About  $35 \pm 6$  mA when all three heaters were off,
- (ii) About  $140 \pm 12$  mA when Heater #1 ON,
- (iii) About  $260 \pm 14$  mA when Heater # 1 and 2 ON and
- (iv) About  $360 \pm 15$  mA when all three heaters were ON.

The power budget was maintained under the upper limit of HASP requirement during the flight.

### 9.5 Thermal stability of the payload

The variation of temperature of ozone sensors box #1, 2 and 3 with altitude during the flight is shown in fig.30 (a) to (c), respectively. The temperature of sensors was controlled in the range of  $303 \pm 10$  K using an On-Off controller, a polyimide flexible heater (MINCO make) and a temperature sensor (TMP 36). Temperature of sensors was well controlled during the most of time of the balloon flight. In addition, the silver color thermal blanket applied to outer side of payload body and well-polished aluminum surface inside the payload kept isothermal condition for well thermal stability of the payload.

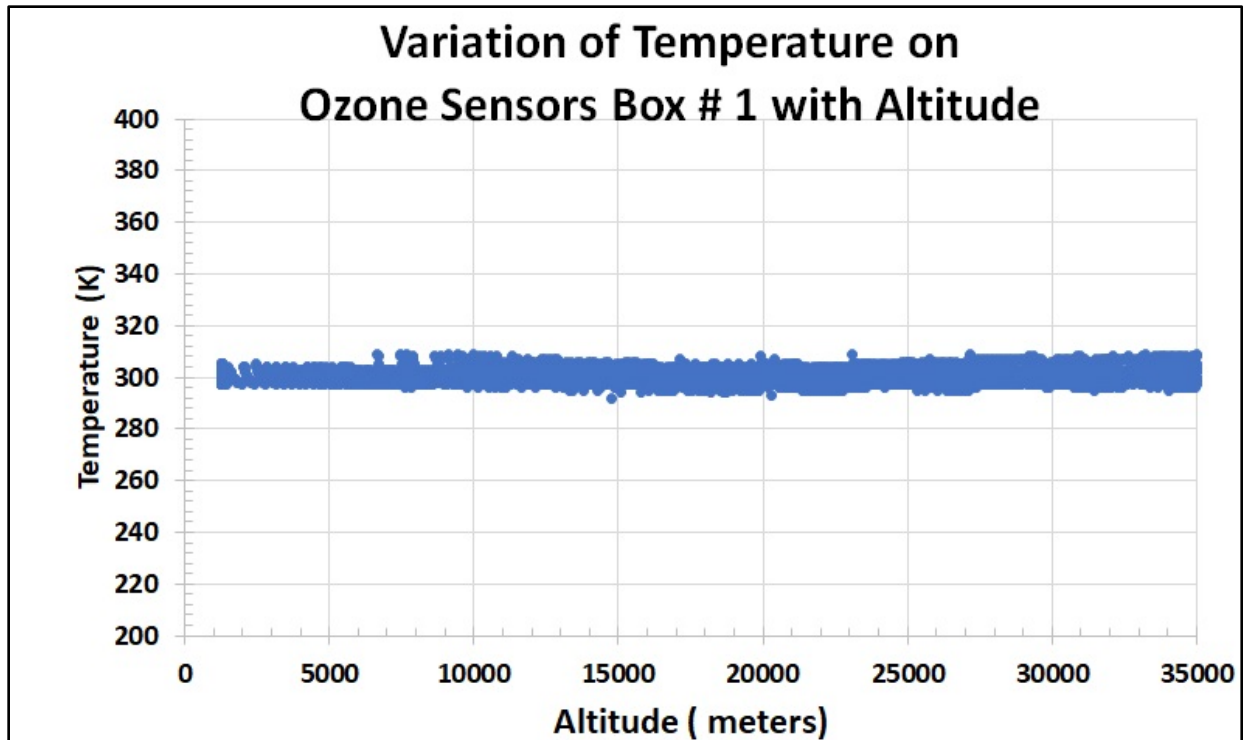


Fig.30 (a) Variation of temperature of ozone sensors in box#1 with the altitude.

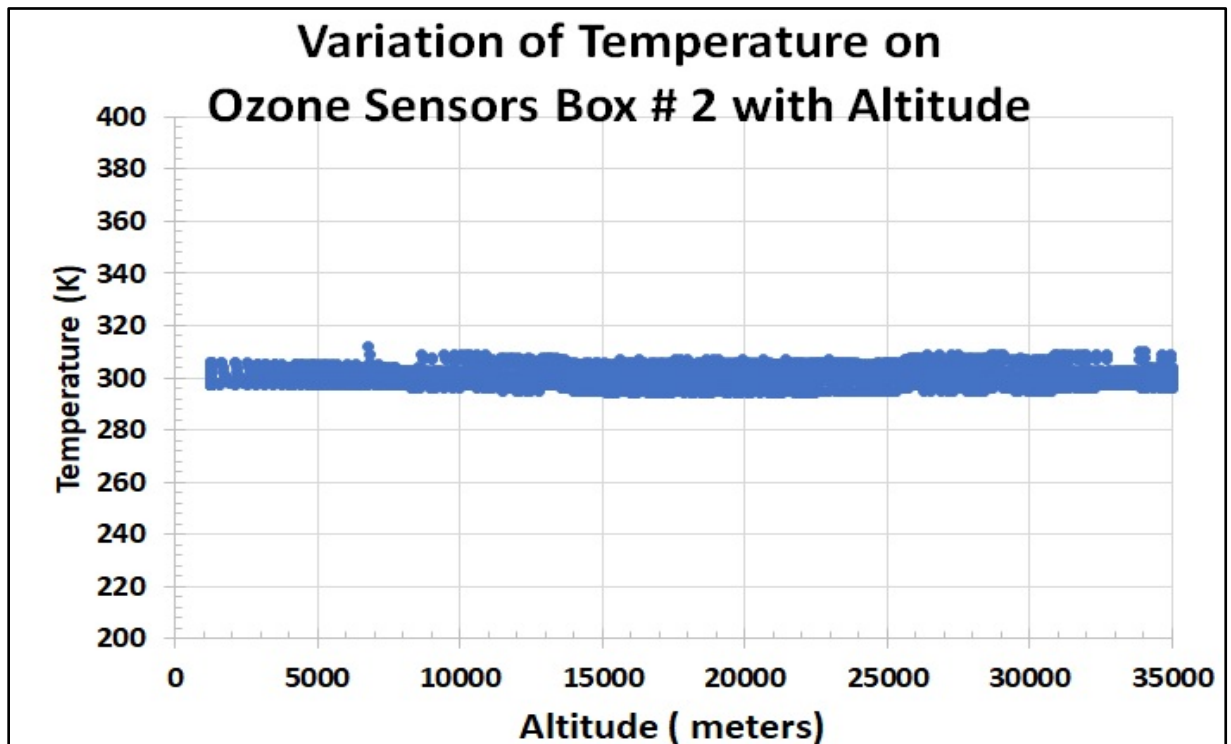


Fig.30 (b) Variation of temperature of ozone sensors in box#2 with the altitude.

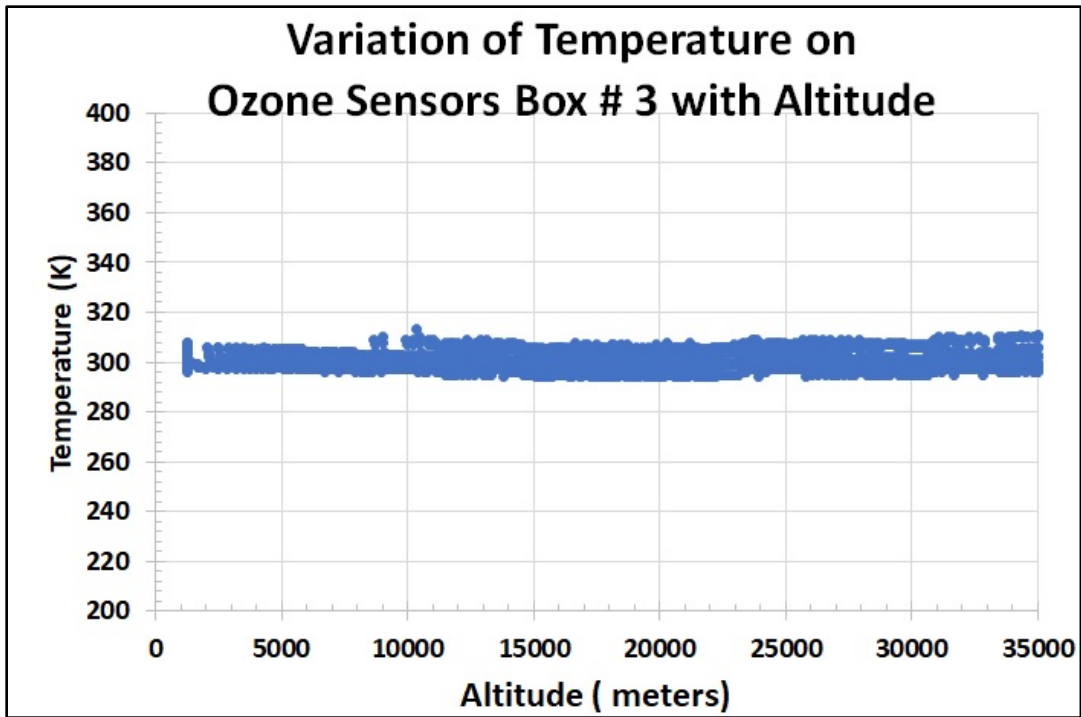


Fig.30 (c) Variation of temperature of ozone sensors in box#3 with the altitude.

Fig. 31 shows the comparison of measured average temperature on sensors in Box # 1, 2 and 3 with standard deviation as error bar. All three columns are overlapping each other within their standard deviation and hence no statistical significance difference between each sensors box.

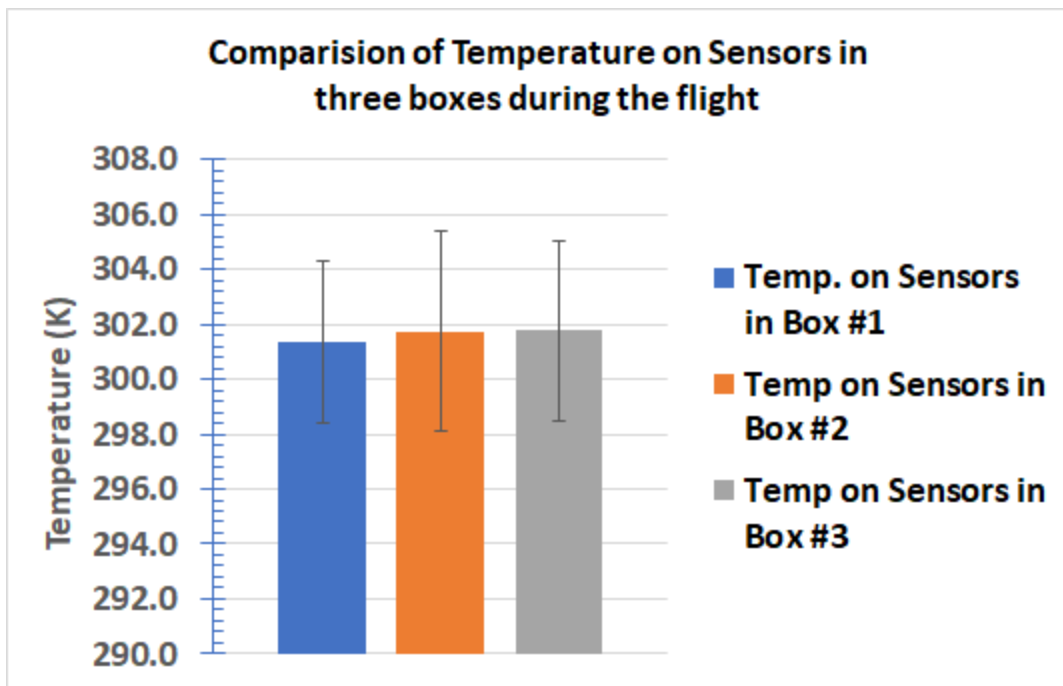


Fig.31 Comparison of temperature on sensors in three boxes during the flight.

Variation of temperature of ozone sensors in box#1, 2 and 3 with time (UTC) is shown in the fig. 32(a), (b) and (c), respectively. All three plots show the reasonable stability of temperature of ozone sensors in the box # 1, 2 and 3.

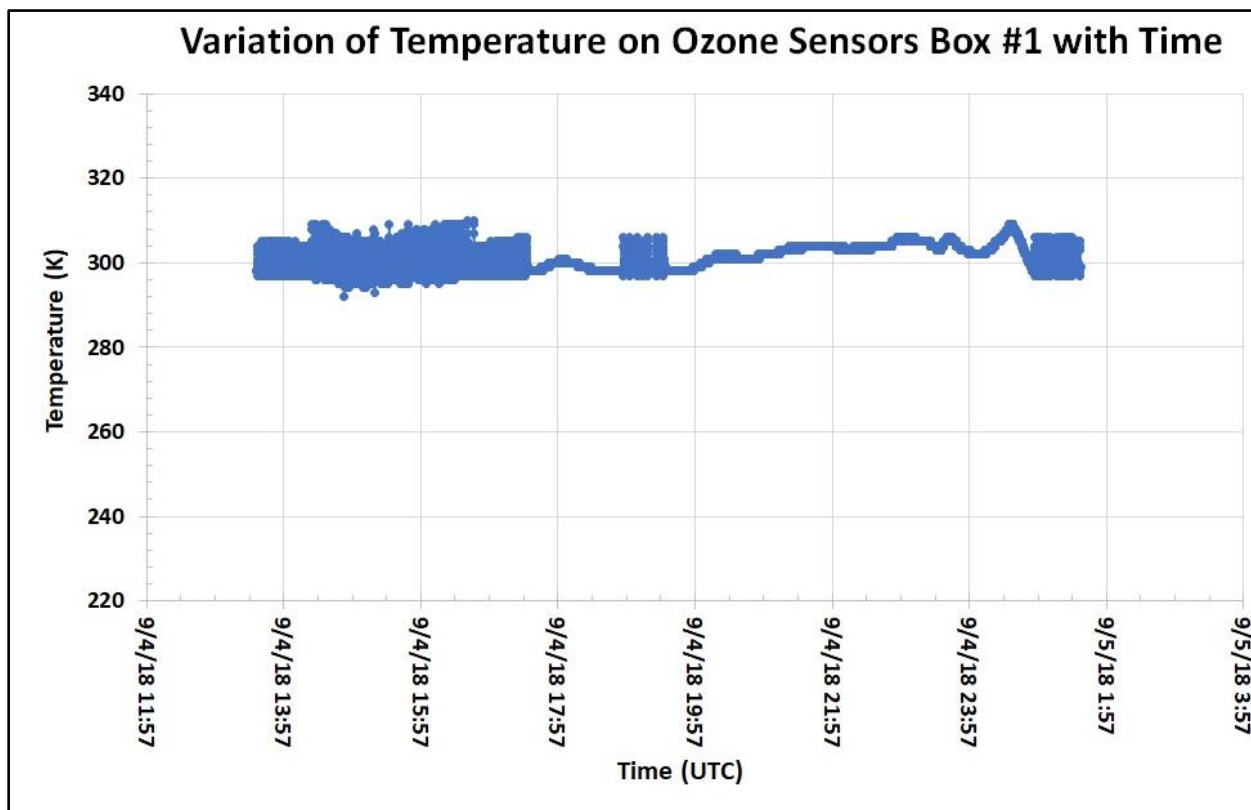


Fig.32 (a) Variation of temperature of ozone sensors in box#1 with time (UTC).

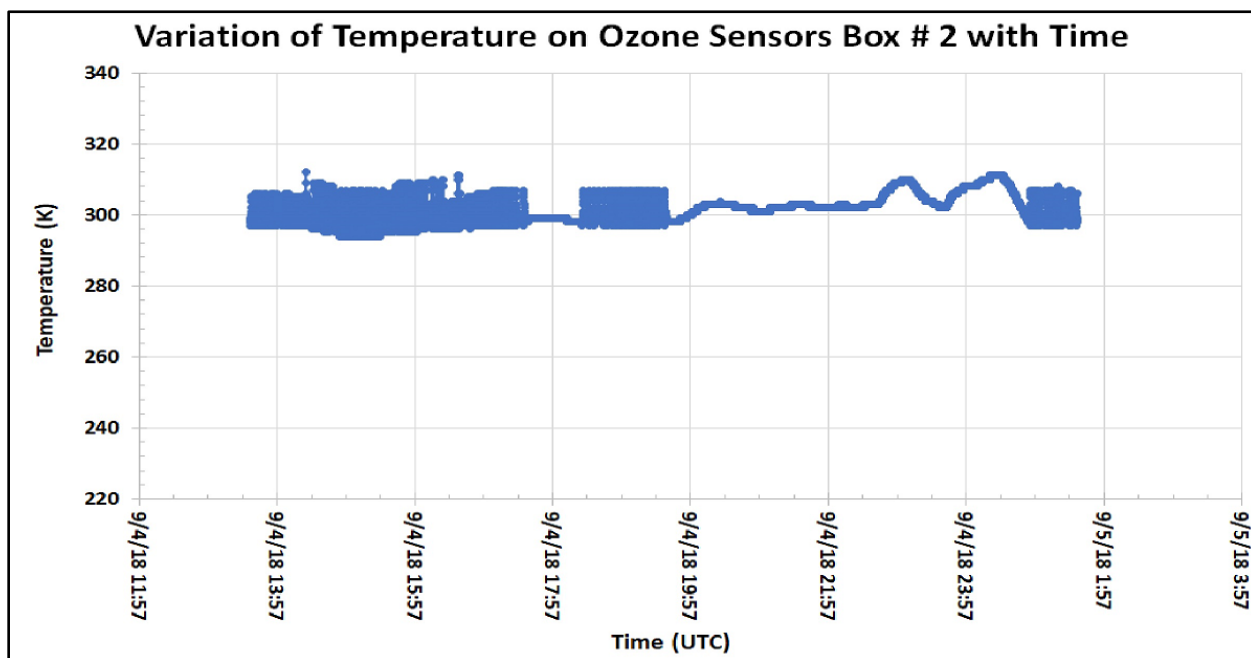


Fig.32 (b) Variation of temperature of ozone sensors in box#2 with time (UTC).

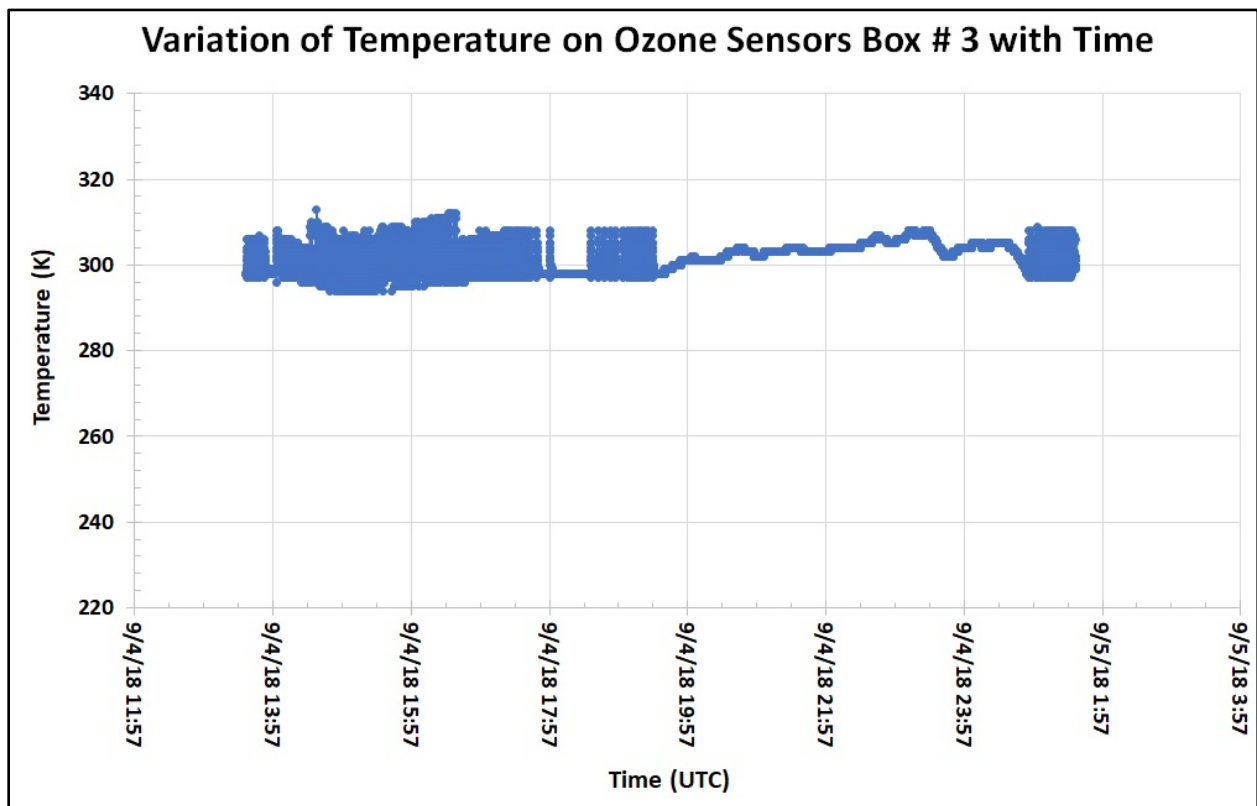


Fig.32 (c) Variation of temperature of ozone sensors in box#3 with time (UTC).

Fig. 32 (d) shows variation of ambient temperature outside of HASP with time. It was varied from about 197 to 300 K. We are thankful to Mr. Douglas Granger, HASP-LSU for sharing ambient temperature data.

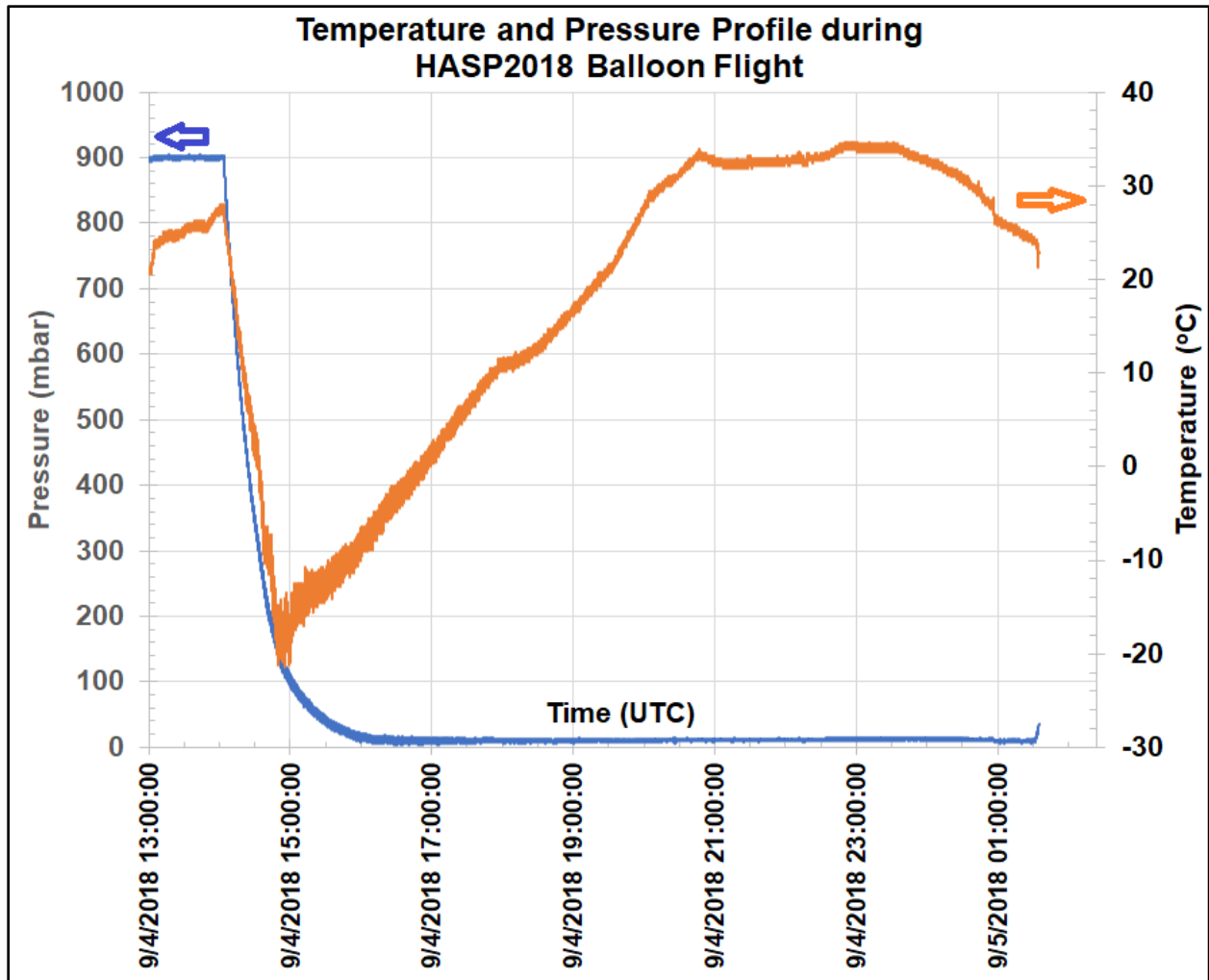


Fig. 32(d) Variation of ambient temperature outside of HASP  
(Data Courtesy: Mr. Doug Granger, HASP-LSU)

The temperature controller on sensors was maintained constant temperature in the range  $300 \pm 8$  K when temperature dropped down by turning on heater. We did not apply a solid state Peltier cooling device on the back side of sensors array to cool down sensors array when temperature increase higher than 310 K. We can add a Peltier cooling device on the back side of sensors array in future but it will certainly increase the power consumption and need to change the power budget. Dr. Patel had developed p-Sb<sub>2</sub>Te<sub>3</sub> - n- Bi<sub>2</sub>Te<sub>3</sub> thin film thermoelectric cooling Peltier device earlier [4].

### 9.6 Measurements of photovoltage profile during the flight

The variation of photovoltage generated by the photo diodes mounted on sensor box #1, 2 and 3 during the flight is shown in fig 33 (a), (b) and (c), respectively. It was observed that measured photovoltage was larger in the altitude range from 10,000 to 25,000 m. The larger photovoltage confirmed the presence of larger ultra violet Sun light. In the presence of that UV light, oxygen converted into ozone gas. The larger photovoltage confirmed the presence of ultra violet Sun light. In the presence of that UV light oxygen converted into ozone gas.

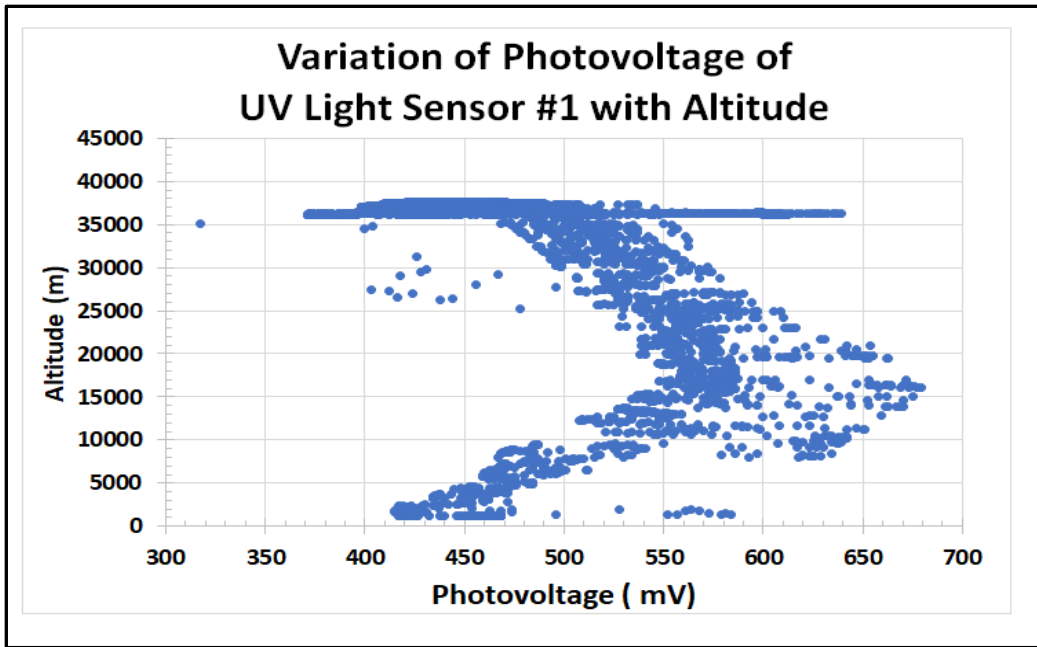


Fig.33 (a) Variation of photovoltage on sensor box -1 (S#1)

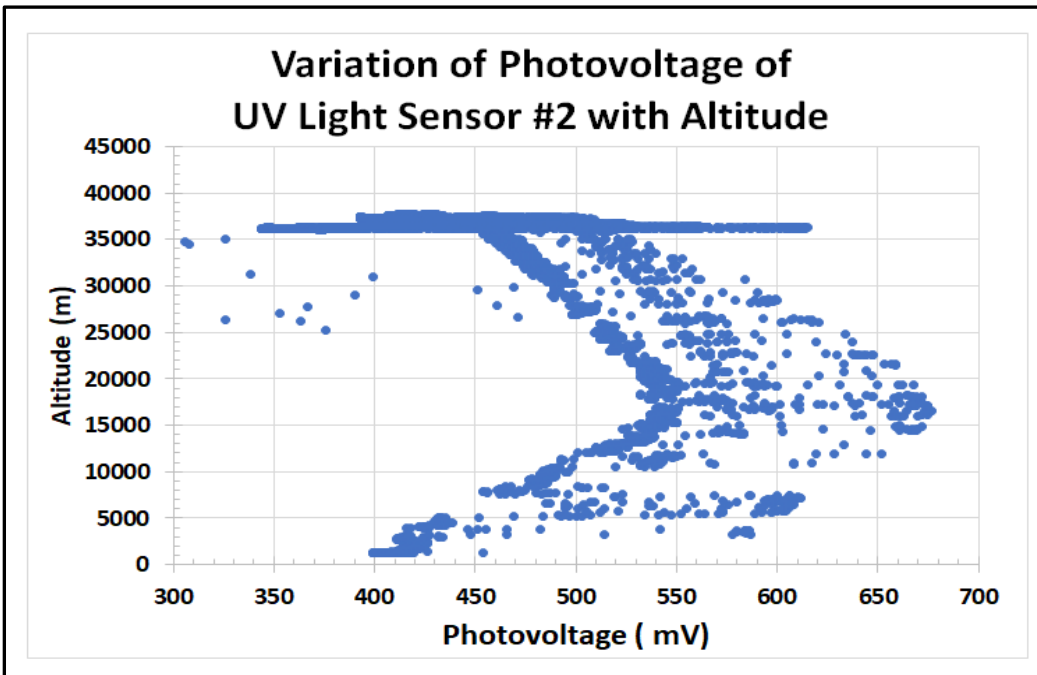


Fig.33 (b) Variation of photovoltage on sensor box-2 (S#2)

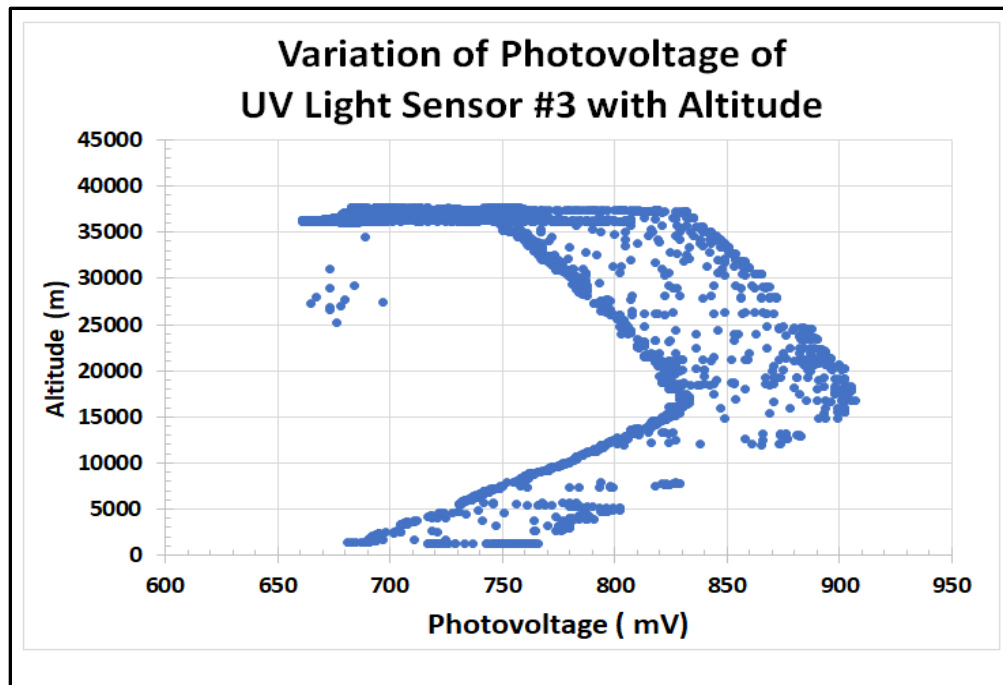


Fig.33 (c) Variation of photovoltage on sensor box -3 (S#3)

The variation of photovoltage generated by the photo diodes mounted on sensor box #1, 2 and 3 with the flight time (UTC) is shown in fig 34 (a), (b) and (c), respectively. All three photo sensors have nearly similar response. Photo sensor #3 has large magnitude of photovoltage due to higher sensitivity of compare to that of other two photo sensors # 1 and 2. Photo sensors #3 was new GaP (FGAP71) UV photodiode was purchased from [http://www.thorlabs.com/newgrouppage9.cfm?objectgroup\\_id=285&pn=FGAP71](http://www.thorlabs.com/newgrouppage9.cfm?objectgroup_id=285&pn=FGAP71)

**Three major zones** are shown in Fig. 33(a), (b) and (c) as

**(i) Ascending during day**

The photovoltage voltage was maximum and shown a peak in the middle to upper of stratosphere.

**(ii) Float during day**

The photovoltage was nearly stable but several small spikes during float in day time due to the balloon flight was traveling towards east direction.

**(iii) Float during sunset time and then termination**

The photovoltage was fluctuating with time and several large spikes during sunset time due to up and down of reflection of sunlight.

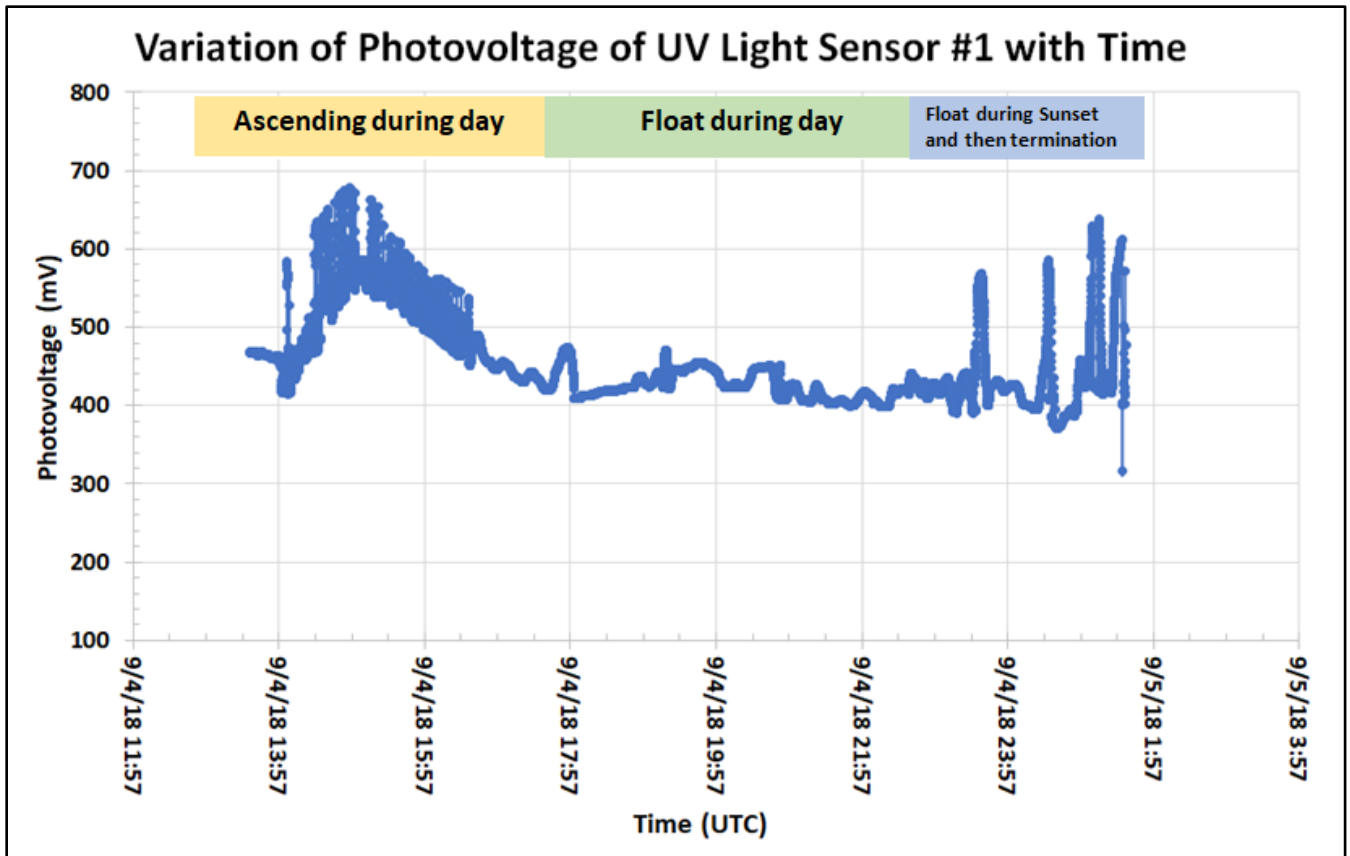


Fig.34 (a) Variation of photovoltage on sensor box#1 with time (UTC)

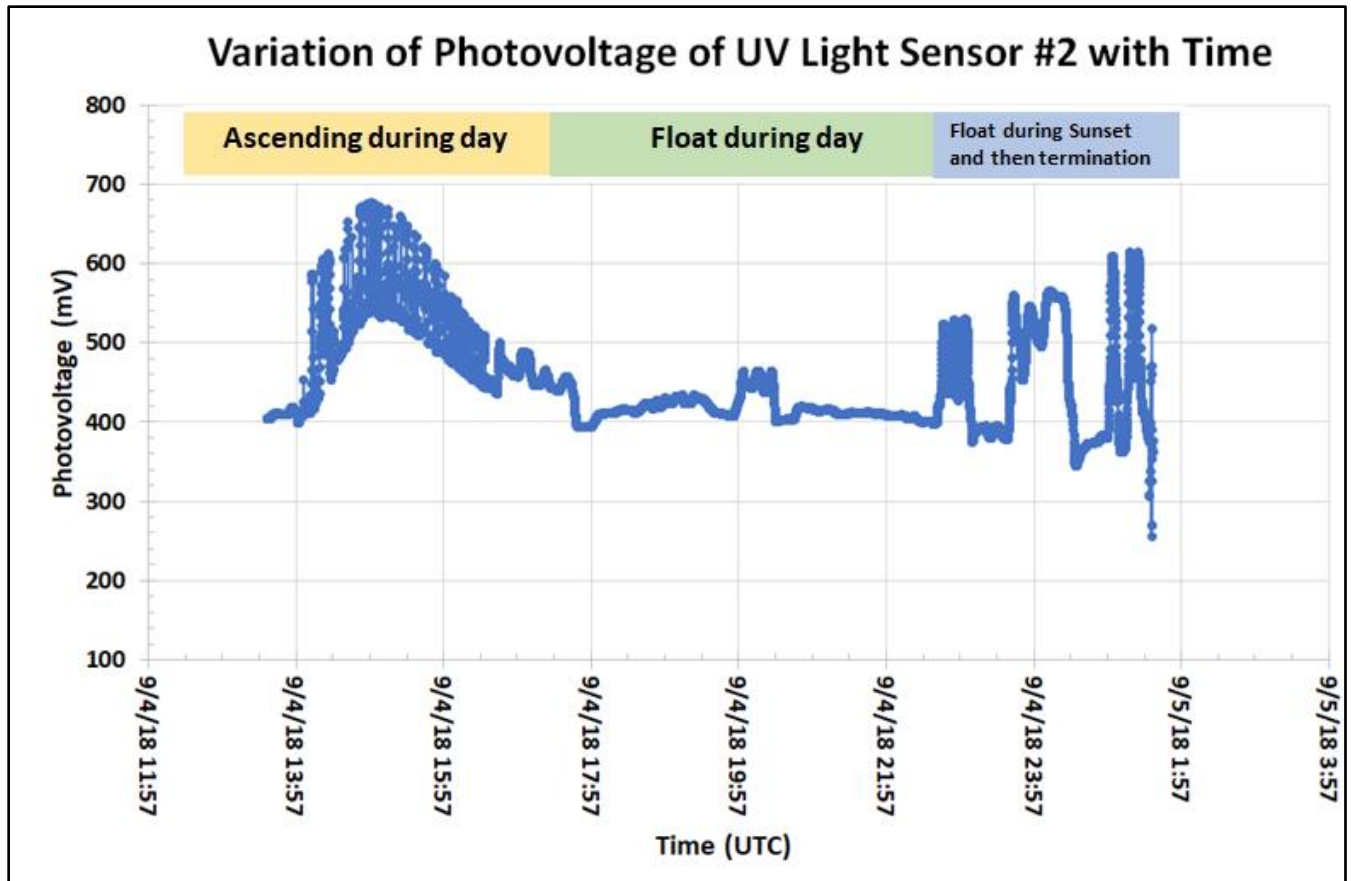


Fig.34 (b) Variation of photovoltage on sensor box#2 with time (UTC)

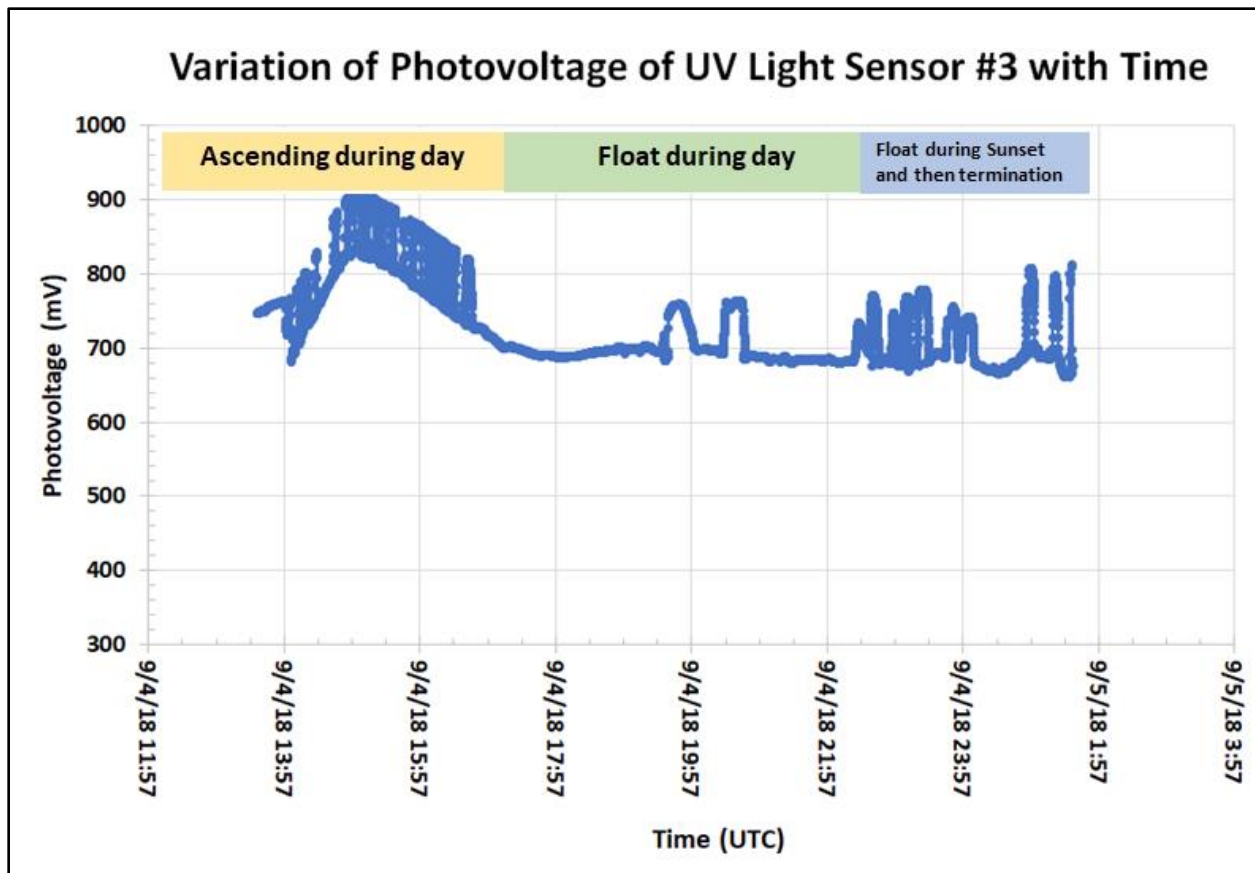


Fig.34 (c) Variation of photovoltage on sensor box#3 with time (UTC)

## 9.7 Discussion of Response of Gas Sensor Profile

Sensor # S1-5 was randomly picked for the discussion of response of ozone sensor with the entire altitude range of balloon flight. An array of eight ozone sensors of Box-S1 was made of improved version of nanocrystalline ITO thin films compare to our previous balloon flights. These sensors have better selectivity and sensitivity with ozone gas. Fig. 35 (a) shows the variation of resistance of ozone sensor S1#5 with time during entire flight, while fig.35 (b) shows the variation of concentration of ozone measured by sensor S1#5 with time during entire flight. Note that there was no data available immediate after termination of flight due to failure of HASP telemetry.

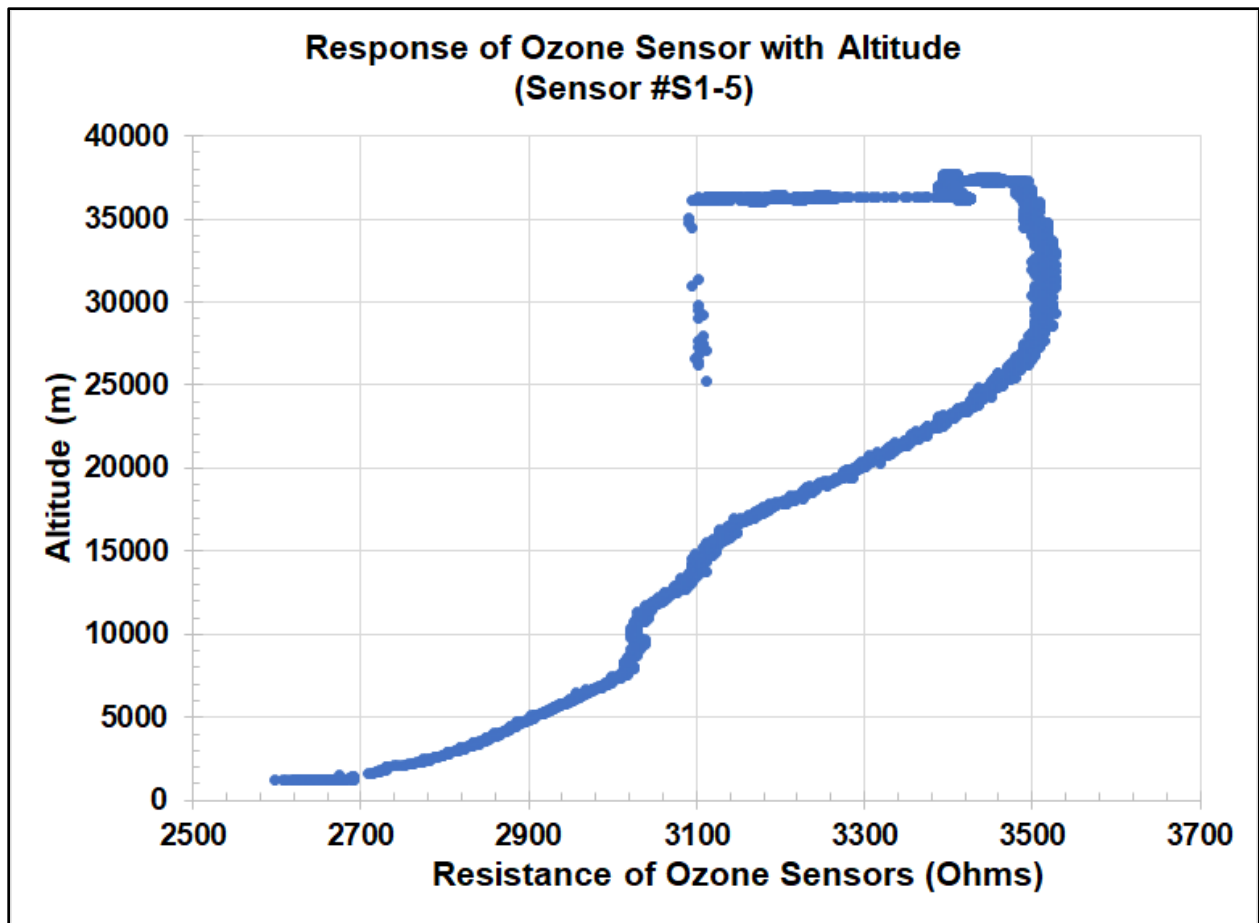


Fig. 35 (a) Variation of resistance of ozone sensor S1#5 with time during entire flight.

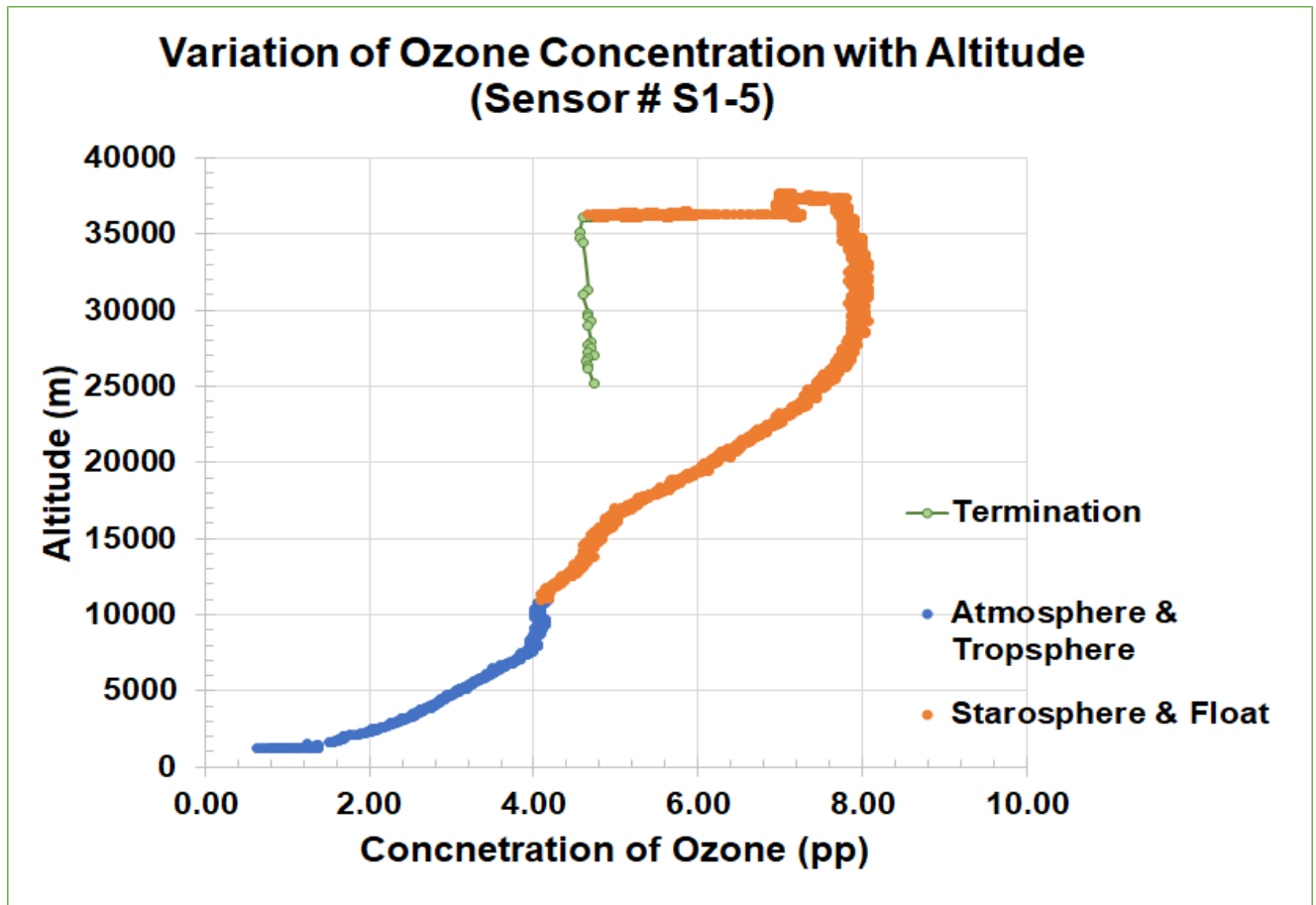


Fig.35 (b) Variation of concentration of ozone measured by sensor S1#4 with time during entire flight.

A small peak of ozone (blue color part in fig. 35 (b)) was observed during ascending of balloon flight at the altitude around 10,000 m. This range of altitude is from atmosphere to the troposphere. This small ozone peak is known as the bad ozone, which is mainly due to the generation of smog in the early morning due to pollutant gases from the automobile vehicles and industries. Due to low ambient temperature, pollutant gases were not able to disperse and diffuse. These pollutant gases and air particulates form the smog and hence form bad ozone. The bigger peak of ozone is observed at altitude above 10,000 to 37,000 m (orange color part in fig.35 (b)). This is due to the ozone in the stratosphere. This ozone is known as good ozone. In the presence of ultra violet light from Sun, oxygen converted into ozone gas. The concentration of ozone is higher in the middle to upper level of stratosphere in the presence of ultra violet light. Ozone is oxidizing gas and its concentration depends on amount of available Sun light. Upon adsorption of charge accepting molecules at the vacancy sites from ozone oxidizing gas, the electrons are effectively depleted from the conduction band of n-type Indium tin oxide (ITO) semiconductor sensor. Thus, this leads to an increase in the electrical resistance of n-type ITO gas sensor. During float of the balloon, the concentration of ozone should be constant, but it may vary due to variation of altitude, mixing ratio and availability of ultra violet rays from the sun during flight time. The concentration of ozone

decreased slowly during float and fluctuate several times due to dropping of altitude of balloon as well as less availability of UV light during sunset time and then starting of night time.

After termination of balloon from float at the end of sunset time or nearly night time, the payload again descending through the middle of stratosphere, then troposphere, and finally atmosphere. Due to failure of telemetry after termination of flight, we were not able to get any data during descending. We were not able to find any possibility of ozone peak due to nocturnal ozone or formation of diurnal variation.

Fig. 36 shows the variation of concentration of ozone measured by sensor# S1-5 with time during entire flight. It is found that measured ozone concentration is increased when measured photovoltage is also increased. Ozone concentration is found maximum about 8.00 ppm in the stratosphere. It was found that concentration of ozone fluctuating several times during sunset time due to stray radiation of light and reflection sunrays.

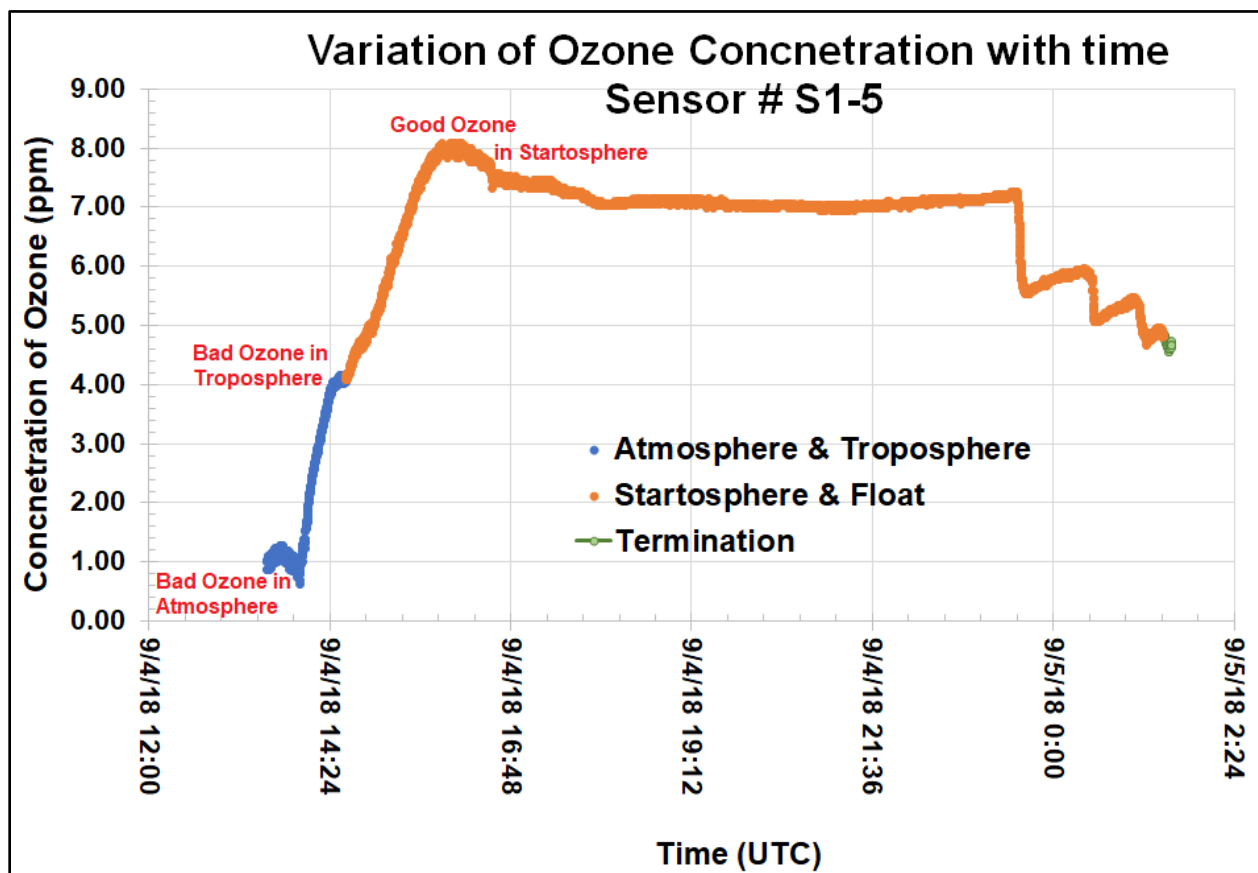


Fig 36 Variation of concentration of ozone of measured by ozone sensor #S1-5 with time.

Sensor S#2-4 also has similar response as sensor # S1-5. Variation of Variation of concentration of ozone of measured by ozone sensor # S2-4 with time is shown in fig. 37.

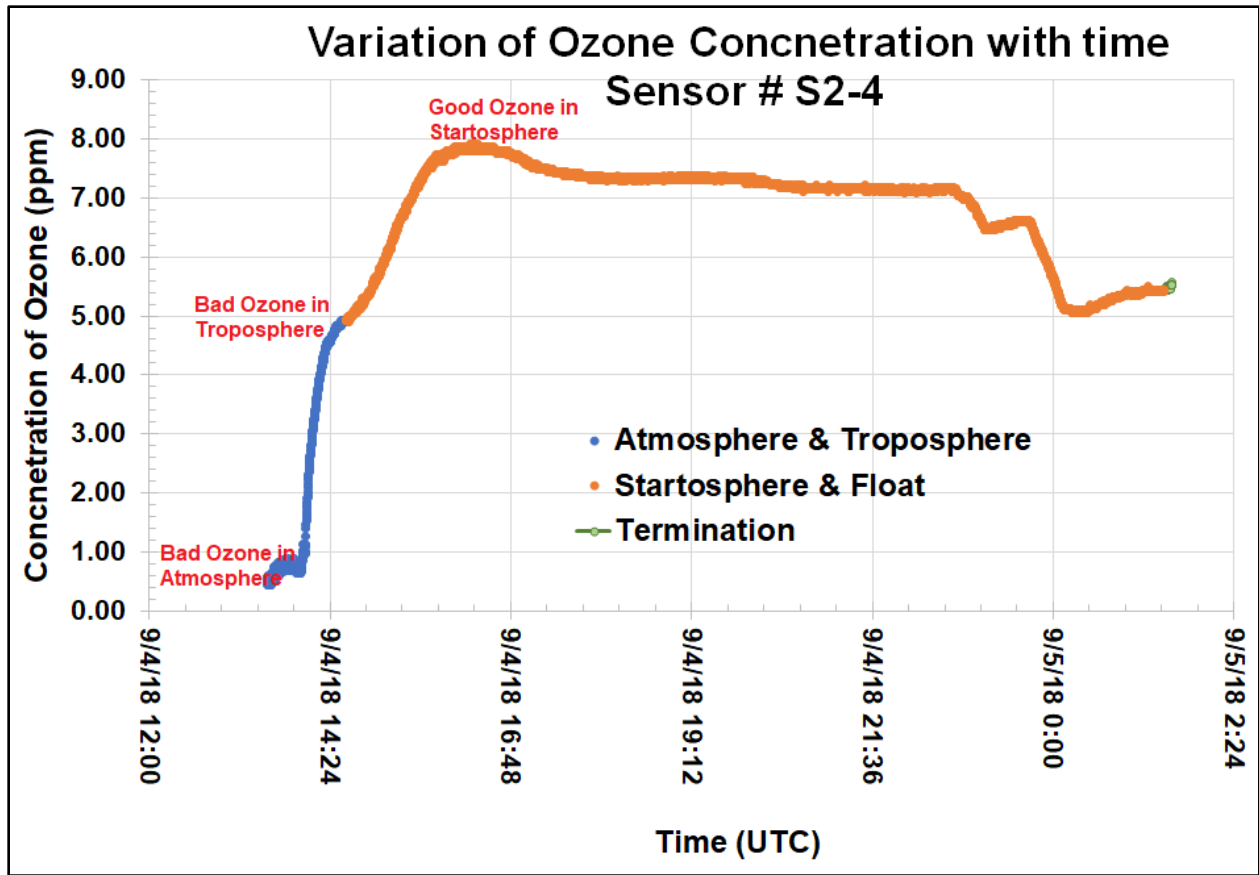


Fig 37 Variation of concentration of ozone of measured by ozone sensor #S2-4 with time

Response of other sensors in stratosphere was nearly similar to that of sensor #S1-5 and Sensor # S2-4.

### 9.8 Response of ozone sensors during the flight

Response of all eight ozone sensors of box #1 (S1) in the stratosphere are shown in Fig. 38 (a).

Response of all eight ozone sensors of box #2 (S2) in the stratosphere are shown in Fig. 38 (d).

Response of all eight ozone sensors of box #3 (S3) in the stratosphere are shown in Fig. 38 (f).

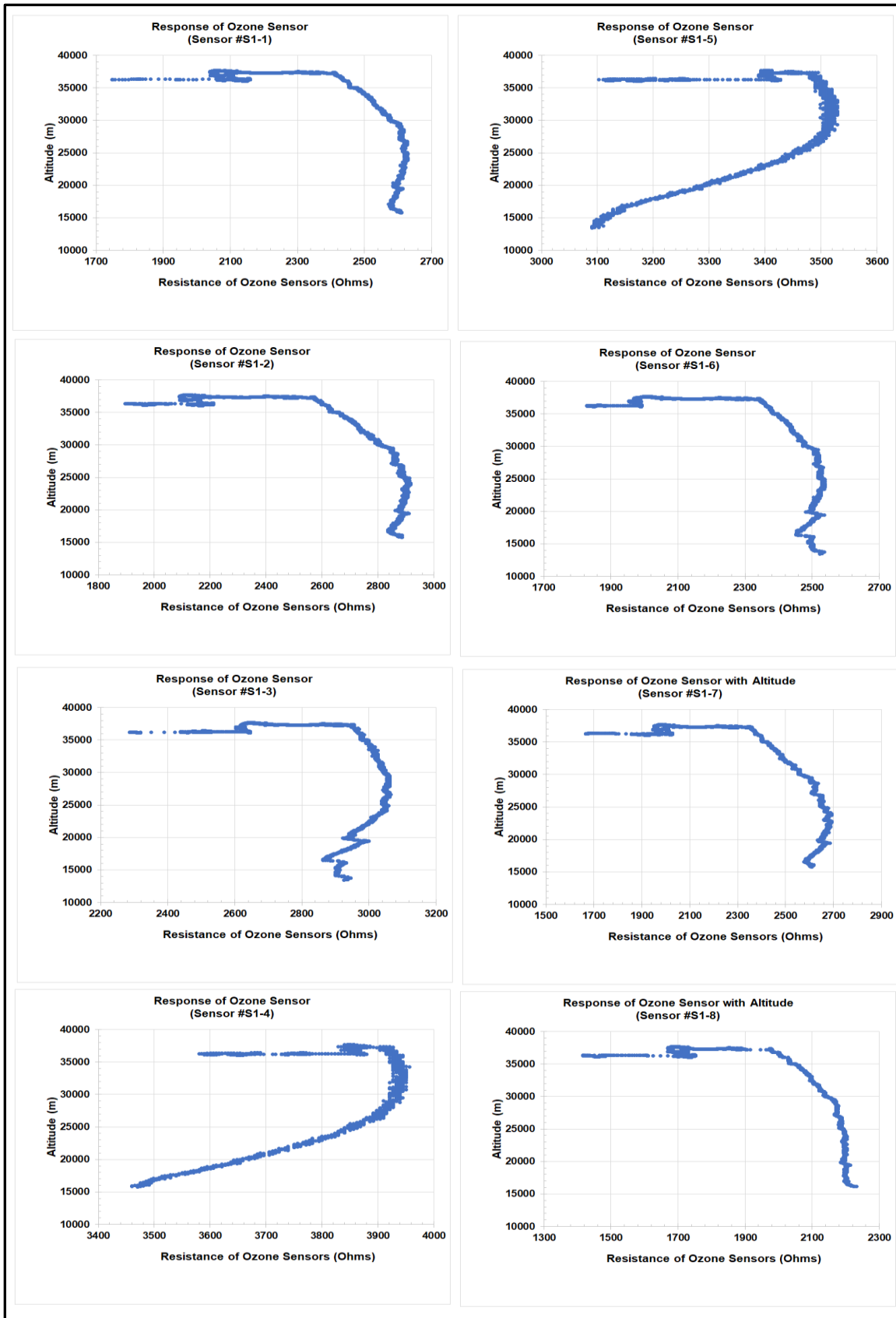


Fig.38 (a) Response of all ozone sensors of box #1 (S1) in the stratosphere altitude range

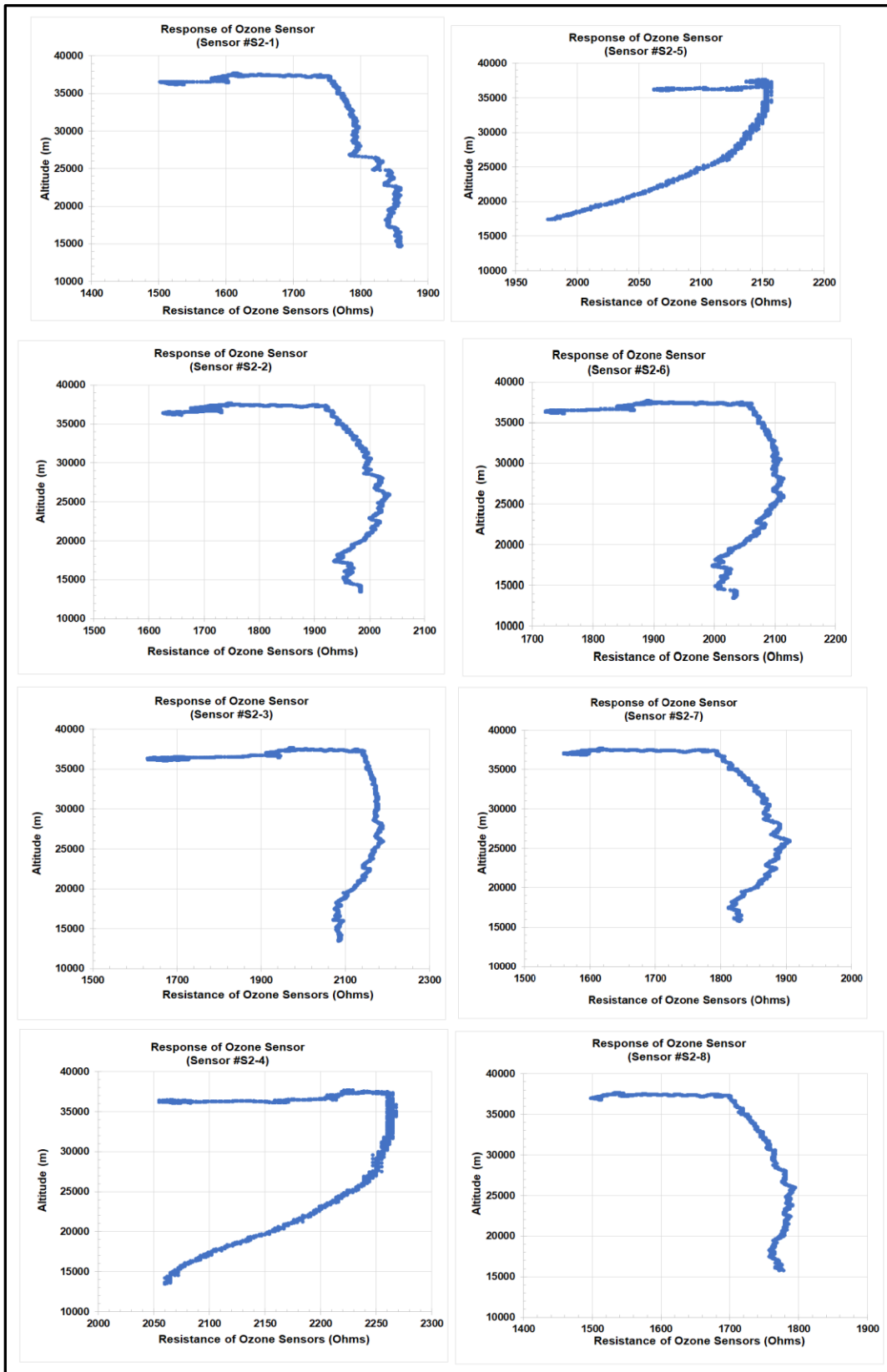


Fig.38 (b) Response of all ozone sensors of box #2 (S2) in the stratosphere altitude range

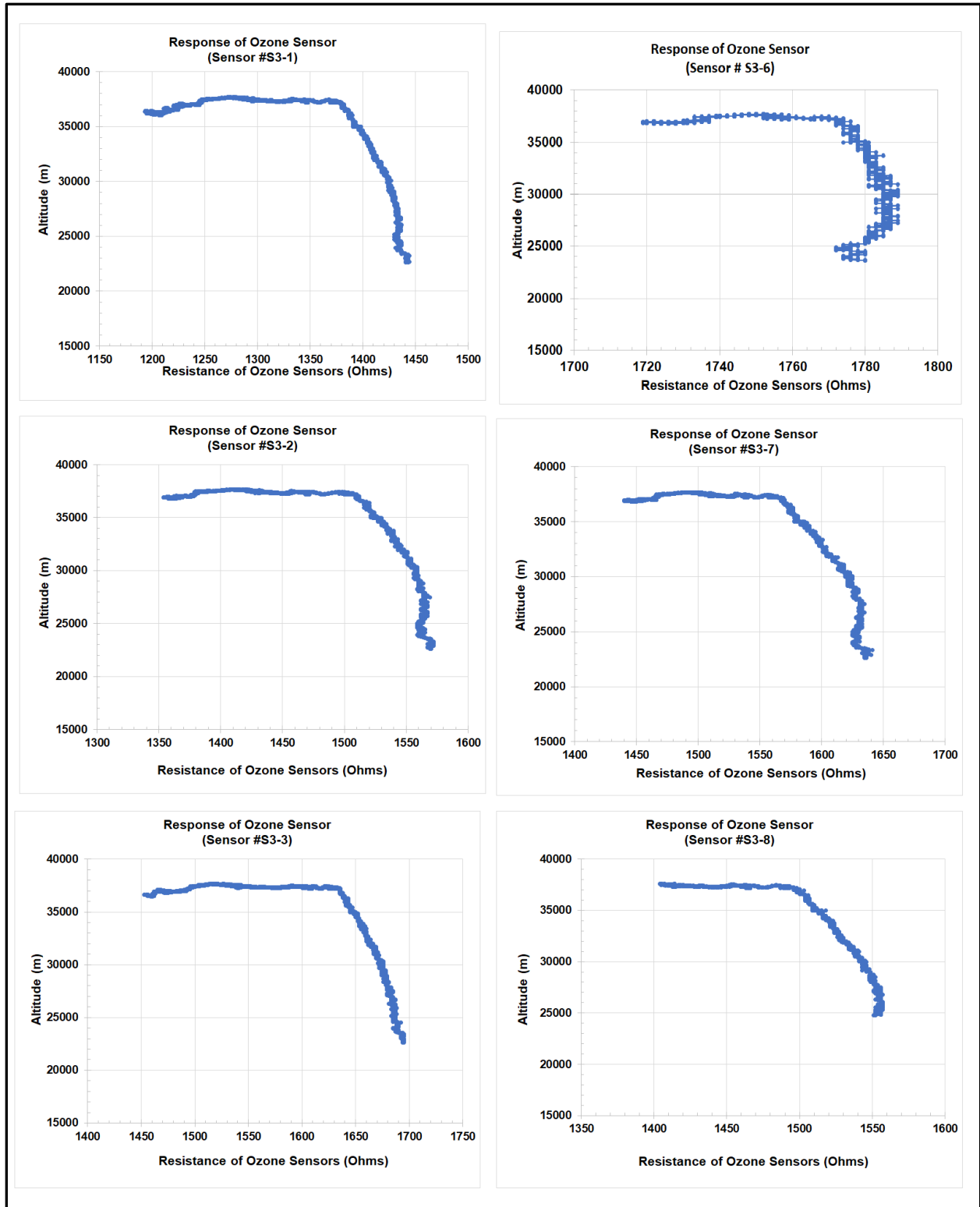


Fig.38 (c) Response of all ozone sensors of box #3 (S3) in the stratosphere altitude range

All sensors of the three boxes have shown the ozone peak in the stratosphere.

## 9.9 Measurements of ozone profile in the starosphere and comparison with the theoretical profile

We focused mainly on good ozone in stratosphere and hence measured the ozone profile in the stratosphere. Using calibration plots shown in fig. 7(a), (b), and (c), the trend line equation of plot of each sensor was applied to convert the resistance values of the sensors into concentration of ozone gas in ppm. Note that the calibration was made in the low pressure, which can be applied mainly to starosphere range. It may be different for atmosphere and troposphere data. The ozone concentration measured from 0 to 10.0 ppm may have slight different value of slope and y intercept due to experimental error due to the variation of sensors thickness, doping and oxidation and variation in chamber pressure due to minor leakage in the chamber with time.

The trend line equation of the calibration plot is given as:

$$y \text{ (sensor resistance, ohms)} = [m \text{ (slope)} \cdot x \text{ (concentration of ozone, ppm)}] + b \text{ (y intercept)}$$

$$\text{The concentration of ozone gas can be determined by: } x = (y - b) / m$$

The trendline equations for each sensors were listed in the following table-5.

Table-5 Trend line equations determined from the calibration plots shown in fig.7 (a), (b) and (c) of sensor box # S1, S2 and S3.

Ozone Sensor Box # S1				Ozone Sensor Box # S2				Ozone Sensor Box # S3			
Sensor Number	Slope (m)	y intercept (b)	Coreleation Coefficient (R <sup>2</sup> )	Sensor Number	Slope (m)	y intercept (b)	Coreleation Coefficient (R <sup>2</sup> )	Sensor Number	Slope (m)	y intercept (b)	Coreleation Coefficient (R <sup>2</sup> )
S1-1	129.57	1601.5	0.9999	S2-1	53.23	1429.1	0.9998	S3-1	33.80	1178.8	0.9993
S1-2	124.81	1902.5	0.9999	S2-2	50.19	1629.5	0.9999	S3-2	30.39	1324.7	0.9997
S1-3	15.40	2299.9	0.9999	S2-3	65.32	1649.1	0.9998	S3-3	34.43	1434.3	0.9996
S1-4	65.73	3224.2	0.9999	S2-4	25.44	2060.1	0.9993	S3-4	8.32	1711.6	0.9994
S1-5	54.49	3098.2	0.9996	S2-5	27.43	1950.1	0.9998	S3-5	21.49	1779.5	0.9993
S1-6	92.40	1798.8	0.9999	S2-6	47.70	1733.7	0.9998	S3-6	8.27	1719.5	0.9971
S1-7	125.53	1703.4	0.9998	S2-7	48.30	1519.0	0.9997	S3-7	28.74	1404.2	0.9993
S1-8	100.43	1398.3	0.9998	S2-8	40.40	1469.6	0.9998	S3-8	25.19	1354.8	0.9999

With these equation parameters, we obtained the following the ozone profile plots shown in fig.39 (a), (b) and (c):

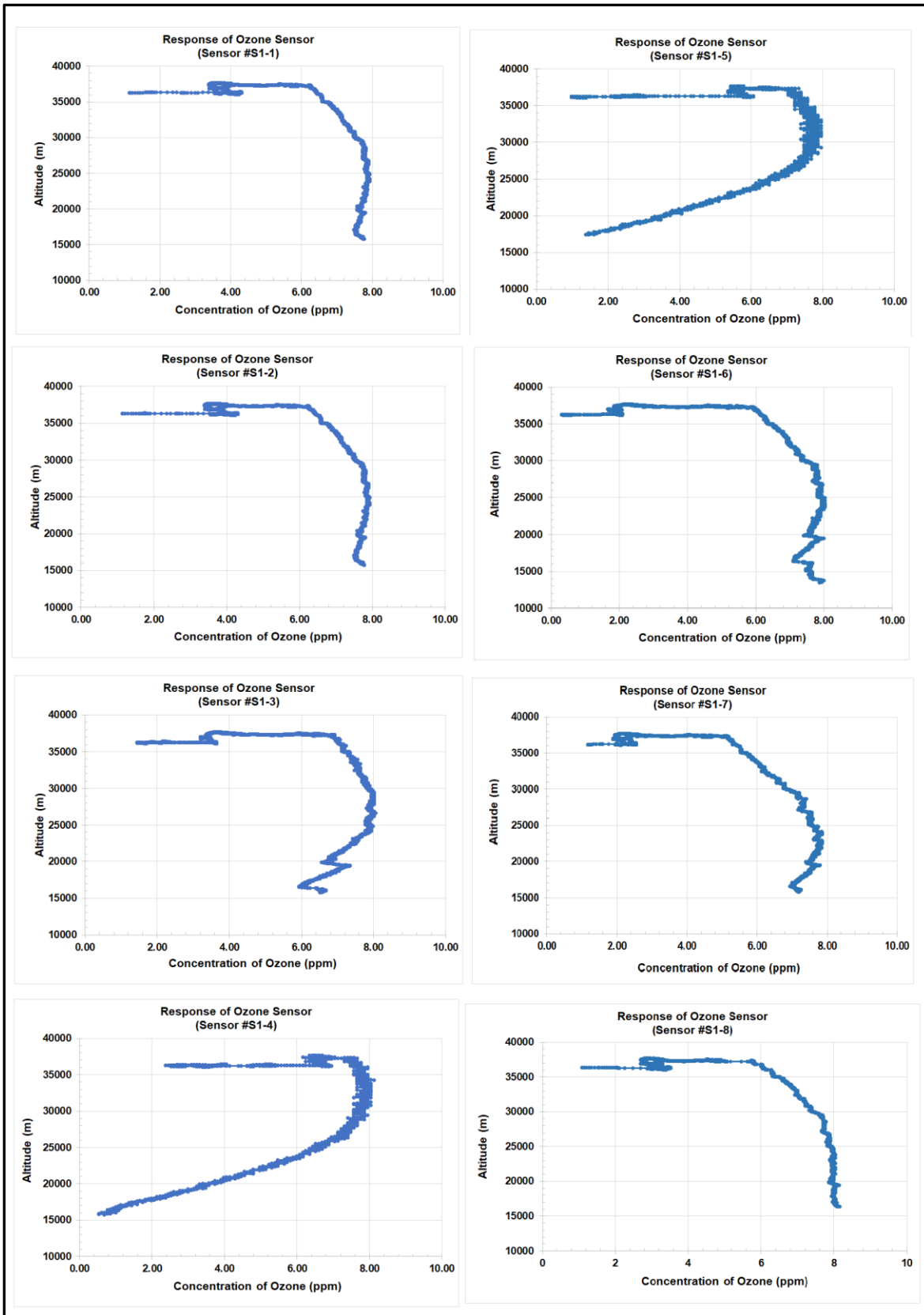


Fig. 39 (a) Ozone profile measured by sensors # S1-1 to S1-8.

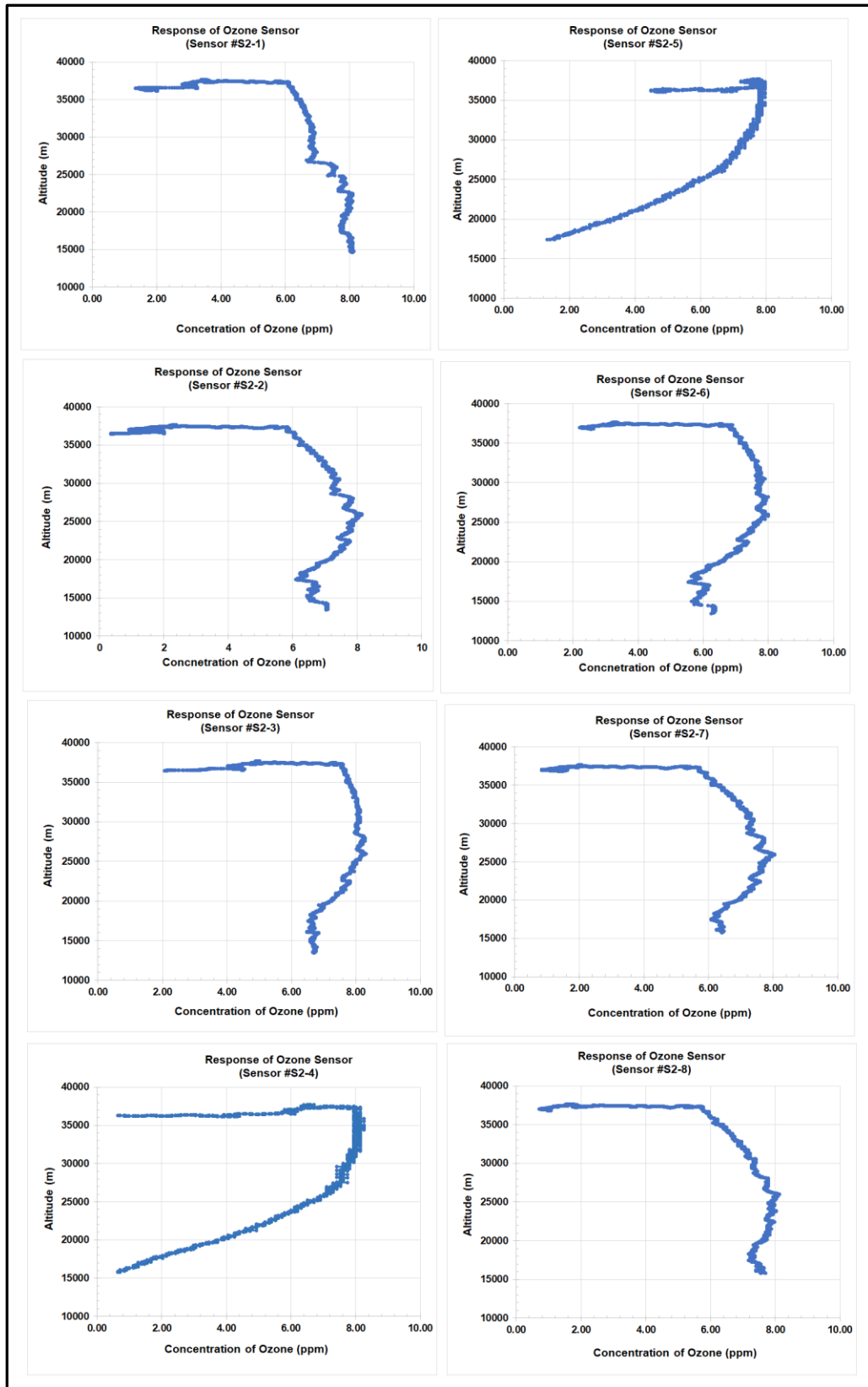


Fig. 39 (b) Ozone profile measured by sensors # S2-1 to S2-8.

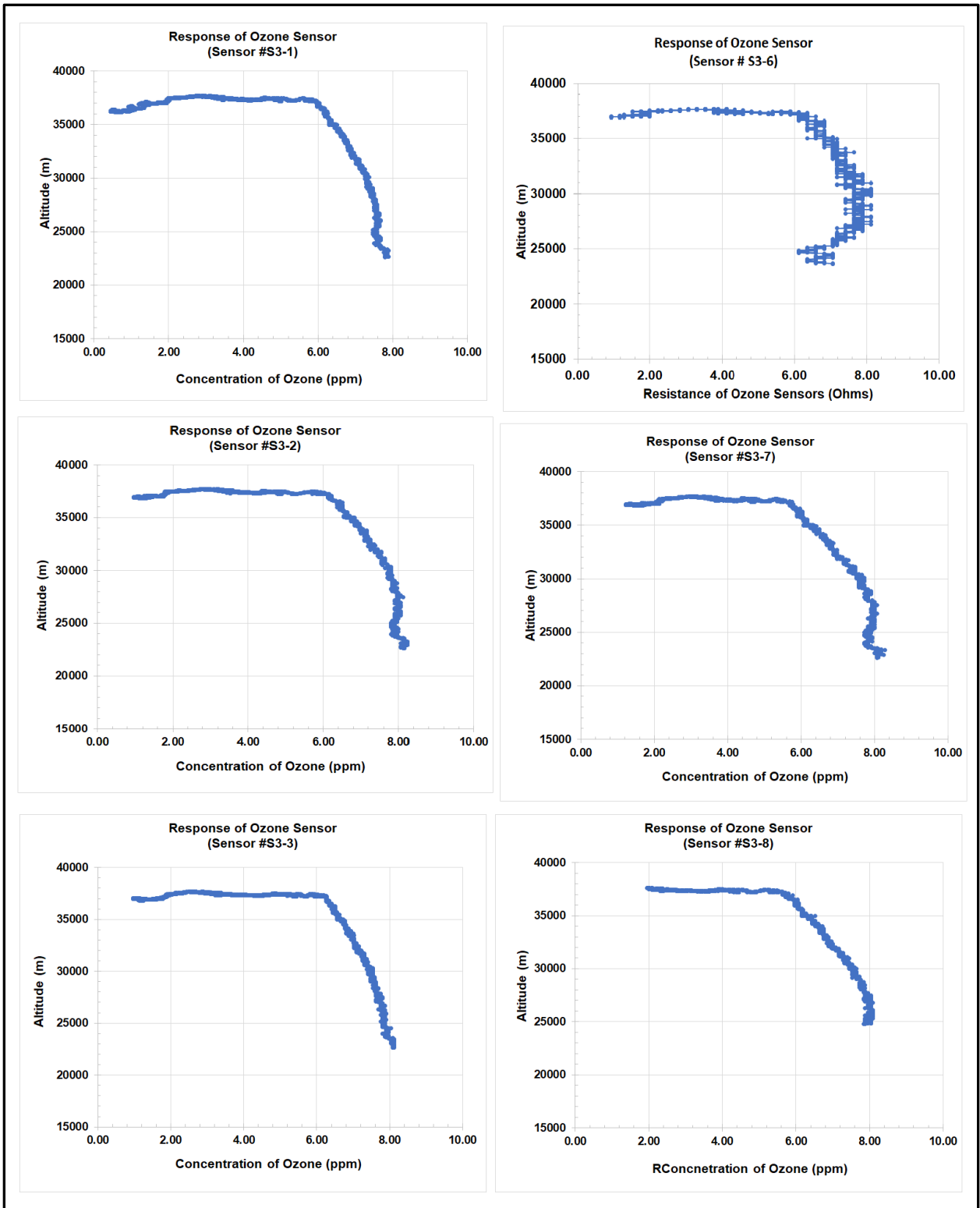


Fig. 39 (c) Ozone profile measured by sensors # S3-1, 2, 3, 6, 7 and 8

The nature of ozone profiles measured by ozone sensors box # S1, S2 and S3 are nearly matched with the theoretically profile measured and quoted by various research groups, which are shown

in Fig. 40(a) to (d) for the comparison purpose. The measured value of maximum concentration of ozone was observed about  $8.00 \pm 0.20$  ppm, which is very close to the expected values reported earlier. We will find out some theoretical calculation method to generate theoretical data for comparison.

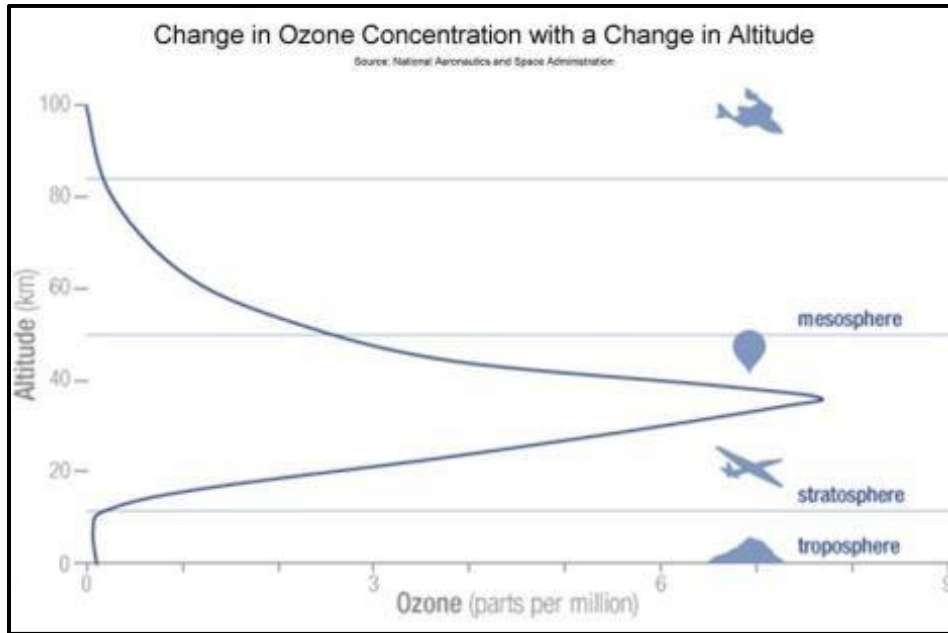


Fig.40 (a) Change in ozone concentration with a change in altitude.

Picture Courtesy : <http://sites.gsu.edu/geog1112/lab-2-part-2/>

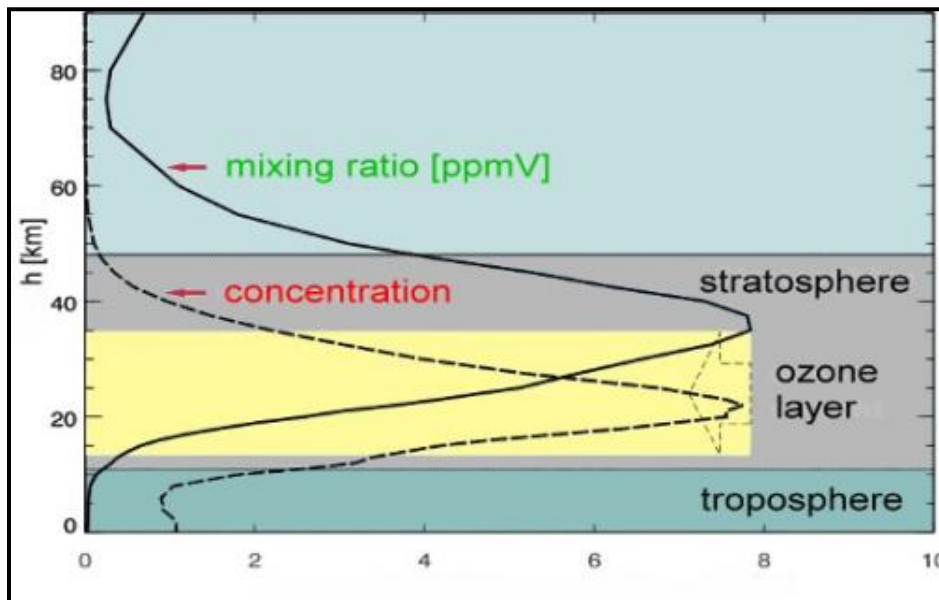


Fig.40 (b) Theoretical ozone profile in stratosphere

Picture Courtesy : <http://www.atmosphere.mpg.de/enid/1yy.html>

(ppmv = parts per million by volume = volume mixing ratio)

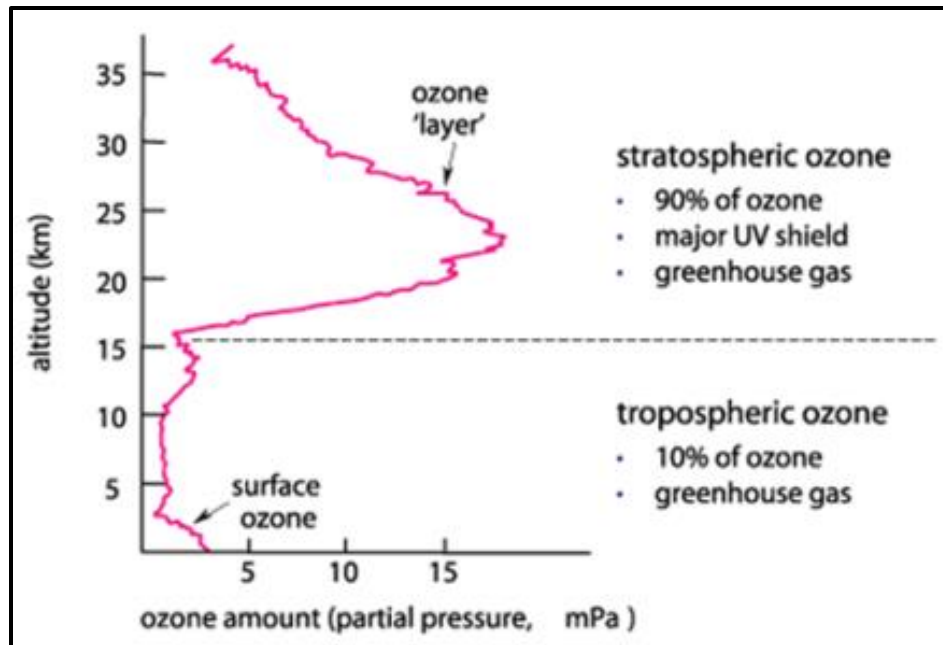


Fig.40(c) Ozone in the atmosphere with its impact

<http://www.environment.gov.au/soe/2001/publications/theme-reports/atmosphere/atmosphere03-1.html>

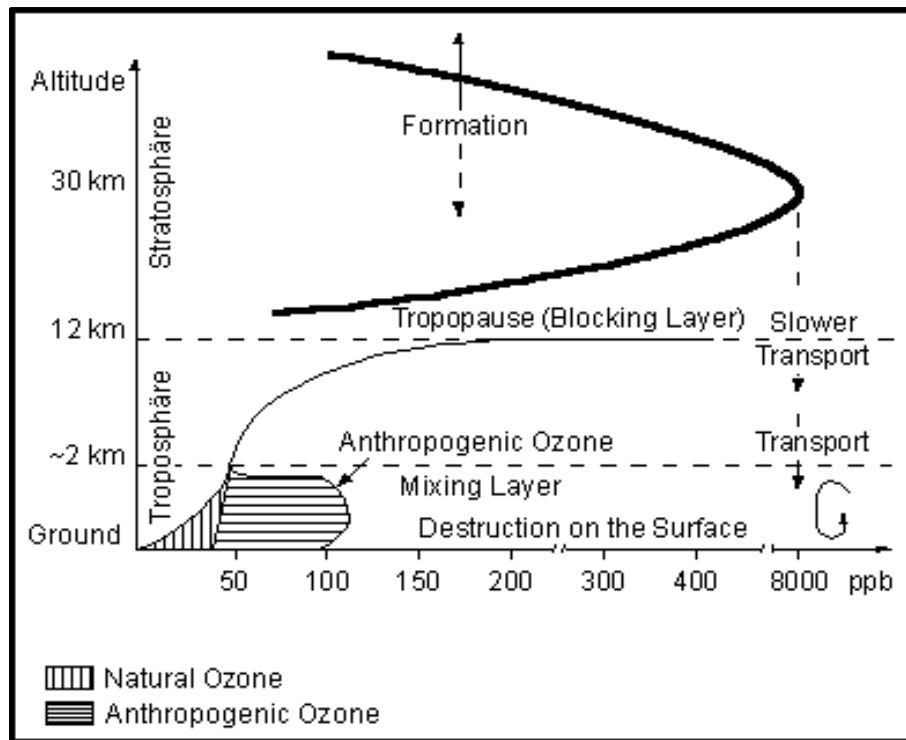


Fig.40 (d) Ozone profile

Courtesy : [http://www.stadtentwicklung.berlin.de/umwelt/umweltatlas/ed306\\_01.htm](http://www.stadtentwicklung.berlin.de/umwelt/umweltatlas/ed306_01.htm)

## 10. Problems, failure analysis and future

- (1) Our nanocrystalline ozone gas sensors (Box # S1, S2 and S3) worked well for measurement of ozone profile. We made new composite of ITO+SnO<sub>2</sub> to enhance detection of ozone in the stratosphere as well as smog in atmosphere / troposphere. Sensors of box #3 worked satisfactory. We will continue to improve the performance of sensors by changing materials, composition, and fabrication parameters of sensors.
- (2) We have focused on measurements of good ozone in the stratosphere. In addition, we have also focused on measurements of bad ozone in atmosphere and troposphere. Measurements of bad ozone is equally important as good ozone. We were also interested to explore any possible observation of nocturnal ozone maxima.
- (3) We did not get much information and data about bad ozone due to (i) launching of balloon was delayed few times from early morning to late morning. As result, smog in atmosphere and troposphere were disperse out in the presence of sunlight, and (ii) not able to get data immediately after termination of flight due to failure of HASP telemetry.
- (4) Pressure sensor was saturated at 110 mbar. We found that that pressure sensor can work only up to 110 mbar. We planned to replace it by new pressure sensor in the next flight.
- (5) Our payload got direct impact on ground and fully immersed in the wet mud. Some of mud was entered into the payload from minor gap between payload body and HASP plate. We need to change design and add water proof sealant or rubber gasket between payload body and HASP plate.
- (6) We are working on development and fabrication of nano sensors using an electron beam lithography technique ([www.raith.com](http://www.raith.com)) attached with scanning electron microscope. We are interested to examine the performance of nano sensors. We will accelerate our work and we may try it in the next HASP 2019 balloon flight.

## 11. Conclusions

- (i) The payload worked very well during the flight. We got very good data during the flight.
- (ii) Our science objectives of all sensors were successfully tested and scientifically verified for measurement of good ozone in stratosphere. We will further improve the performance of our gas sensors and payload during next HASP2019 flight.
- (iii) The improved nanocrystalline ITO thin film gas sensors (Box#1) and nanocomposite ZnO+ITO thin film gas sensors fabricated (Box#2) by the UNF team have good selectivity with ozone gas and worked well during entire flight period and measured the

ozone profile of the stratosphere. Nanocomposite ITO+SnO<sub>2</sub> thin film gas sensors (Box#3) have satisfactory response with ozone in stratosphere. We still need to improve the performance of box#3 S3 sensors.

- (iv) Light sensor proved the presences of UV light, which are responsible to generate more ozone gas by converting oxygen into ozone.
- (v) Improved temperature control circuit and software program gave better stability of temperature of sensors during entire flight period. No need to reset or change the commands during the flight.
- (vi) Our UBLOX GPS worked well without any issue of blocking data.
- (vii) New modified JAVA based software handles all sensors data and faster conversion of RAW file into EXCEL file for quick view of the plots and also makes the real-time monitoring the plots using LabVIEW.
- (viii) After receiving payload back, we cleaned all mud from the payload and dried the payload. Then, tested the payload, circuit and all sensors. We found the payload is working in good condition even though the payload was emerged in the wet mud.
- (ix) We will focus again to measure bad ozone in atmosphere and troposphere in addition to good ozone in stratosphere in the next HASP2019 flight.
- (x) UNF team is interested to make further improve sensors payload and seeking another opportunity for the HASP 2019 flight.

## 12. References

- [1] Perry J. Samson, “Nocturnal Ozone Maxima”  
Atmospheric Environment, Vol.12 (1978) 951-955.
- [2] A. Mavrakis, H. Flocas, E. Mavromatidis, G. Kallos, G. Theoharatos and A. Christides, “A Case of Nighttime High Ozone Concentration over the Greater Athens Area”, Meteorologische Zeitschrift, Vol. 19, No.1 (2010) 035-045.
- [3] R. San Jose, A. Stohl, K. Karatzas, T. Bohler, P. James and J.L. Perez,  
“A Modelling Study of an Extraordinary Night Time Ozone Episode over Madrid Domain”. Environmental Modelling & Software 20 (2005) 587-593.
- [4] Thermoelectric cooling effect in a p-Sb<sub>2</sub>Te<sub>3</sub>-n-Bi<sub>2</sub>Te<sub>3</sub> thin film thermocouple  
N. G. Patel and P.G. Patel  
Solid State Electronics, Vol 35, No.9 (1992) 1269-1272 (UK)

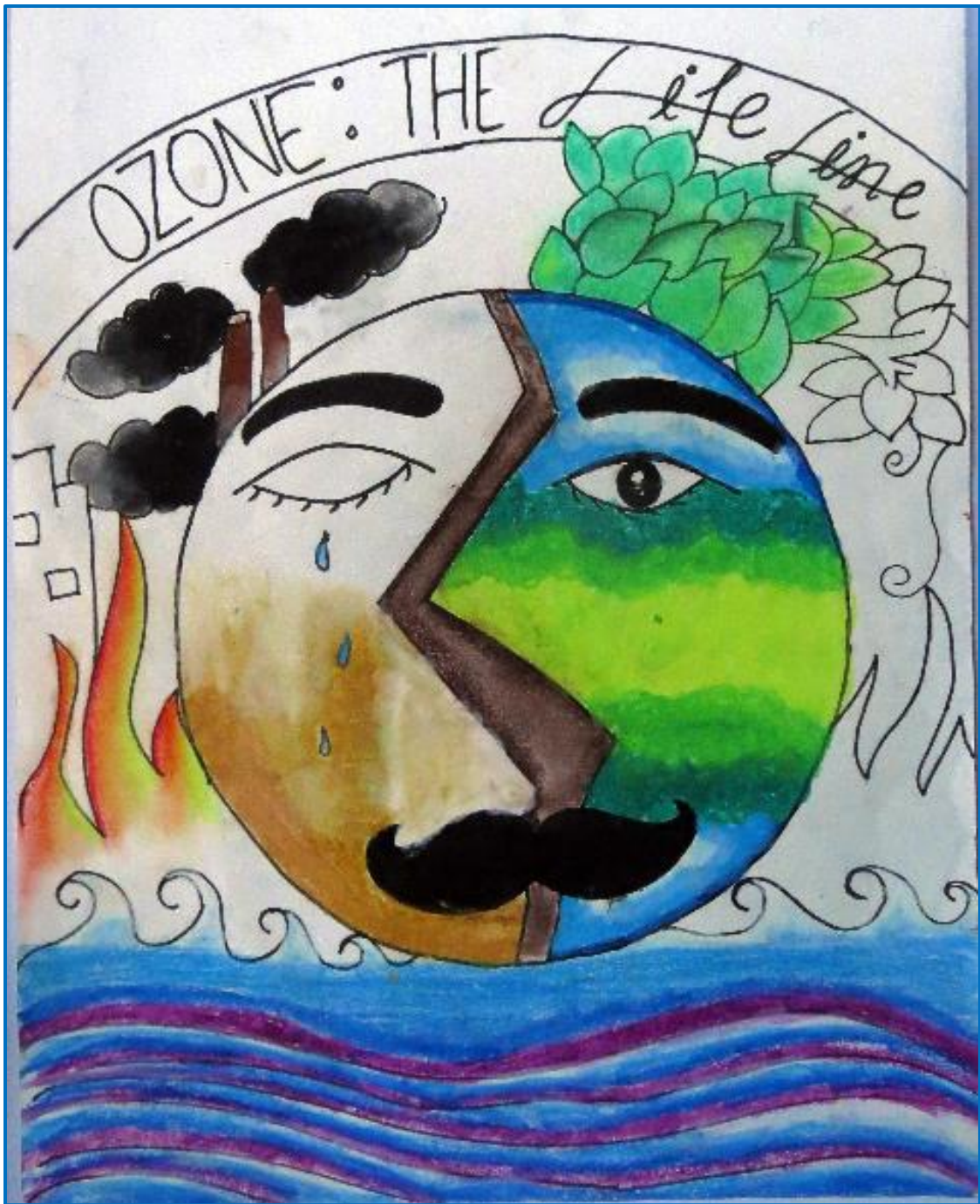
## 13. Acknowledgements

We are very grateful to

- (i) Dr. Gregory Guzik and Mr. Doug Granger HASP-LSU for their continuous help, cooperation and encouragement. We also appreciate help of Mr. Doug Granger for sharing temperature data and pictures. We also thankful to Mr. Anthony Ficklin and Mr. Joshua Collins for their cooperation during the thermal vacuum test.
- (ii) Columbia Scientific Balloon Facilities (CSBF)-NASA and Orbital ATK, Palestine TX and CSBF, Fort Sumner, NM, and their team.
- (iii) Florida Space Grant Consortium for providing the support to UNF team.
- (iv) Dr Jaydeep Mukherjee, Director, Florida Space Grant Consortium (FSGC) for his valuable help and encouragement.
- (v) Websites links mentioned in this report for using their pictures and references to explain the science of this report. Our intention is not to violate any copyright, but purposes of education and research training.

## 14. Presentation of Research work.

- (1) Jesse Lard and Dr. Nirmal Patel presented talk on “**Measurements of Good Ozone and Bad Ozone Using Ozone Sensor Payload on HASP 2018 Flight**” at Florida Space Grant Consortium Advisory Board meeting held at University of North Florida, Jacksonville on October 18, 2018.
- (2) A research poster on “**Measurements of Good Ozone and Bad Ozone Using Ozone Sensor Payload on HASP 2018 Flight**” will be presented at UNF –Science Departments poster session on October 26, 2018. This poster will be presented by Joseph Ward and Trevor Roger, new students for HASP 2019.
- (3) **An abstract on “Ozone Sensors Payload on NASA- High Altitude Student Platform (HASP) Balloon Flights**” by Nirmalkumar G. Patel, Jesse Lard and Ronald Fevig has been accepted for poster presentation at AGU (American Geophysical Union) fall 2018 meeting at Washington D.C. Abstract number is 437208.



-----